SECTION A

JOURNAL OF RESEARCH

of the NATIONAL BUREAU OF STANDARDS

JNBAAR 79A (4), 541–608 (July-Aug. 1975)

U.S. DEPARTMENT OF COMMERCE / National Bureau of Standards

Physics and Chemistry

Journal of Research

of the

National Bureau of Standards

A. Physics and Chemistry

July–Aug. • 1975

VOLUME • 79A

NUMBER • 4

Editor: C. W. Beckett

Associate Editor: D. D. Wagman

Publication dates:
Feb. 1, Apr. 1, June 1, Aug. 1, Oct. 1, Dec. 1, 1975

J. Res. Nat. Bur. Stand. (U.S.), A

JOURNAL OF RESEARCH

The National Bureau of Standards Journal of Research reports research and development in the fields of activity shown at right. Also included from time to time are survey articles on topics closely related to the Bureau's scientific and technical program.

The Journal is published in two separate sections as follows:

A. Physics and Chemistry

Contains papers of interest primarily to scientists working in these fields. Issued six times a year. Annual subscription: domestic, $17.00; foreign, $21.25. Single copy, varies.

B. Mathematical Sciences

Presents studies and compilations designed mainly for the mathematician and the theoretical physicist. Issued quarterly. Annual subscription: domestic, $9.00; foreign, $11.25. Single copy $2.25.

The National Bureau of Standards[1] was established by an act of Congress March 3, 1901. The Bureau's overall goal is to strengthen and advance the Nation's science and technology and facilitate their effective application for public benefit. To this end, the Bureau conducts research and provides: (1) a basis for the Nation's physical measurement system, (2) scientific and technological services for industry and government, (3) a technical basis for equity in trade, and (4) technical services to promote public safety. The Bureau consists of the Institute for Basic Standards, the Institute for Materials Research, the Institute for Applied Technology, the Institute for Computer Sciences and Technology, and the Office for Information Programs.

THE INSTITUTE FOR BASIC STANDARDS provides the central basis within the United States of a complete and consistent system of physical measurement; coordinates that system with measurement systems of other nations; and furnishes essential services leading to accurate and uniform physical measurements throughout the Nation's scientific community, industry, and commerce. The Institute consists of a Center for Radiation Research, an Office of Measurement Services and the following divisions:

Applied Mathematics — Electricity — Mechanics — Heat — Optical Physics — Nuclear Sciences[2] — Applied Radiation[2] — Quantum Electronics[3] — Electromagnetics[3] — Time and Frequency[3] — Laboratory Astrophysics[3] — Cryogenics[3].

THE INSTITUTE FOR MATERIALS RESEARCH conducts materials research leading to improved methods of measurement, standards, and data on the properties of well-characterized materials needed by industry, commerce, educational institutions, and Government; provides advisory and research services to other Government agencies; and develops, produces, and distributes standard reference materials. The Institute consists of the Office of Standard Reference Materials and the following divisions:

Analytical Chemistry — Polymers — Metallurgy — Inorganic Materials — Reactor Radiation — Physical Chemistry.

THE INSTITUTE FOR APPLIED TECHNOLOGY provides technical services to promote the use of available technology and to facilitate technological innovation in industry and Government; cooperates with public and private organizations leading to the development of technological standards (including mandatory safety standards), codes and methods of test; and provides technical advice and services to Government agencies upon request. The Institute consists of a Center for Building Technology and the following divisions and offices:

Engineering and Product Standards — Weights and Measures — Invention and Innovation — Product Evaluation Technology — Electronic Technology — Technical Analysis — Measurement Engineering — Structures, Materials, and Life Safety[4] — Building Environment[4] — Technical Evaluation and Application[4] — Fire Technology.

THE INSTITUTE FOR COMPUTER SCIENCES AND TECHNOLOGY conducts research and provides technical services designed to aid Government agencies in improving cost effectiveness in the conduct of their programs through the selection, acquisition, and effective utilization of automatic data processing equipment; and serves as the principal focus within the executive branch for the development of Federal standards for automatic data processing equipment, techniques, and computer languages. The Institute consists of the following divisions:

Computer Services — Systems and Software — Computer Systems Engineering — Information Technology.

THE OFFICE FOR INFORMATION PROGRAMS promotes optimum dissemination and accessibility of scientific information generated within NBS and other agencies of the Federal Government; promotes the development of the National Standard Reference Data System and a system of information analysis centers dealing with the broader aspects of the National Measurement System; provides appropriate services to ensure that the NBS staff has optimum accessibility to the scientific information of the world. The Office consists of the following organizational units:

Office of Standard Reference Data — Office of Information Activities — Office of Technical Publications — Library — Office of International Relations.

[1] Headquarters and Laboratories at Gaithersburg, Maryland, unless otherwise noted; mailing address Washington, D.C. 20234.
[2] Part of the Center for Radiation Research.
[3] Located at Boulder, Colorado 80302.
[4] Part of the Center for Building Technology.

U.S. DEPARTMENT OF COMMERCE
Rogers C. B. Morton, Secretary
NATIONAL BUREAU OF STANDARDS
Ernest Ambler, Acting Director

Order all publications from the Superintendent of Documents
U.S. Government Printing Office, Washington, D.C. 20402.

The Secretary of Commerce has determined that the publication of this periodical is necessary in the transaction of the public business required by law of this Department. Use of funds for printing this periodical has been approved by the Director of the Office of Management and Budget through June 30, 1976.

JOURNAL OF RESEARCH of the National Bureau of Standards—A Physics and Chemistry
Vol. 79A, No. 4, July–August 1975

Radiance Temperature (at 653 nm) of Iron at Its Melting Point

A. Cezairliyan and J. L. McClure

Institute for Materials Research, National Bureau of Standards, Washington, D.C. 20234

(April 21, 1975)

Radiance temperature (at 653nm) of iron at its melting point was measured using a subsecond-duration pulse heating technique. Specimens in the form of strips with initially different surface roughnesses were used. The results do not indicate any dependence of radiance temperature (at the melting point) on initial surface or system operational conditions. The average radiance temperature (at 653 nm) at the melting point for 13 specimens is 1670 K on IPTS–68, with a standard deviation of 0.8 K and a maximum absolute deviation of 1.7 K. The total error in the radiance temperature is estimated to be not more than ±6 K.

Key words: High-speed measurements; high temperature; iron; melting; normal spectral emittance; radiance temperature.

1. Introduction

A subsecond-duration pulse heating technique was used earlier to measure the radiance temperature [1] of niobium [1],[2] zirconium [2], and molybdenum [3] at their respective melting points. It was found that the radiance temperature was constant during the initial melting period and was reproducible for different specimens of the same substance. In the present study, the same technique is used to measure the radiance temperature of iron at its melting point.

The method is based on rapid resistive self-heating of the specimen from room temperature to its melting point in less than one second by the passage of an electrical current pulse through it; and on measuring specimen radiance temperature (at the rate of 1200 temperatures per second) with a high-speed photoelectric pyrometer [4]. The radiance measurements were performed at 653 nm which corresponds to the effective wavelength of the pyrometer's interference filter. The bandwidth of the filter was 10 nm. The circular area viewed by the pyrometer was 0.2 mm in diameter. Details regarding the construction and operation of the measurement system are given in earlier publications [5, 6].

2. Measurements

The measurements of the radiance temperature (at 653 nm) of iron (99.95% pure) at its melting point were performed on 13 specimens in the form of strips. The manufacturer's typical analysis indicated the presence of the following impurities in ppm by weight: O, 34; C, 30; Na, 10; P, 20; S, 30; Cr, 30; Co, 100; Ni, 150. The total amount of all other detected elements was less than 60 ppm, each element being below 10 ppm limit. The nominal dimensions of the strips were: length, 51 mm; width, 3.2 mm and thickness, 0.25 mm. Before the experiments, specimen surface was treated using abrasive; three different grades of abrasive were used yielding three different surface roughnesses (ranging from approximately 0.2 to 0.5 μm in RMS value) for different specimens. In some experiments, specimens with "as received" surface conditions (approximately 0.1 μ in roughness) were also used. Heat treatment was applied to one of the specimens prior to melting by pulse heating it to approximately 1500 K for ten times. At the end of this procedure, the specimen surface showed rough irregularities which resulted from going through the $\alpha \rightarrow \gamma$ crystallographic transformation.

All the experiments were performed with the specimen in an argon environment at atmospheric pressure. The heating rate for different specimens was in the range 1200 $K \cdot s^{-1}$ to 4300 $K \cdot s^{-1}$, corresponding to specimen heating periods (from room temperature to its melting point) in the range 0.15 to 0.5 s.

Radiance temperature of iron at its melting point for the 13 specimens and other pertinent results are reported in table 1. All temperatures reported in this paper are based on the International Practical Temperature Scale of 1968 [7]. Variation of the radiance temperature as a function of time near and at the melting point is shown in figure 1 for two typical experiments representing two specimens with different initial surface and heat treatment conditions. The magnitude of the spike before the melting plateau for one of the specimens is probably related to the

[1] Radiance temperature[6] (sometimes referred to as brightness temperature) is the apparent temperature of the specimen surface corresponding to the effective wavelength of the measuring pyrometer.

[2] Figures in brackets indicate the literature references at the end of this paper.

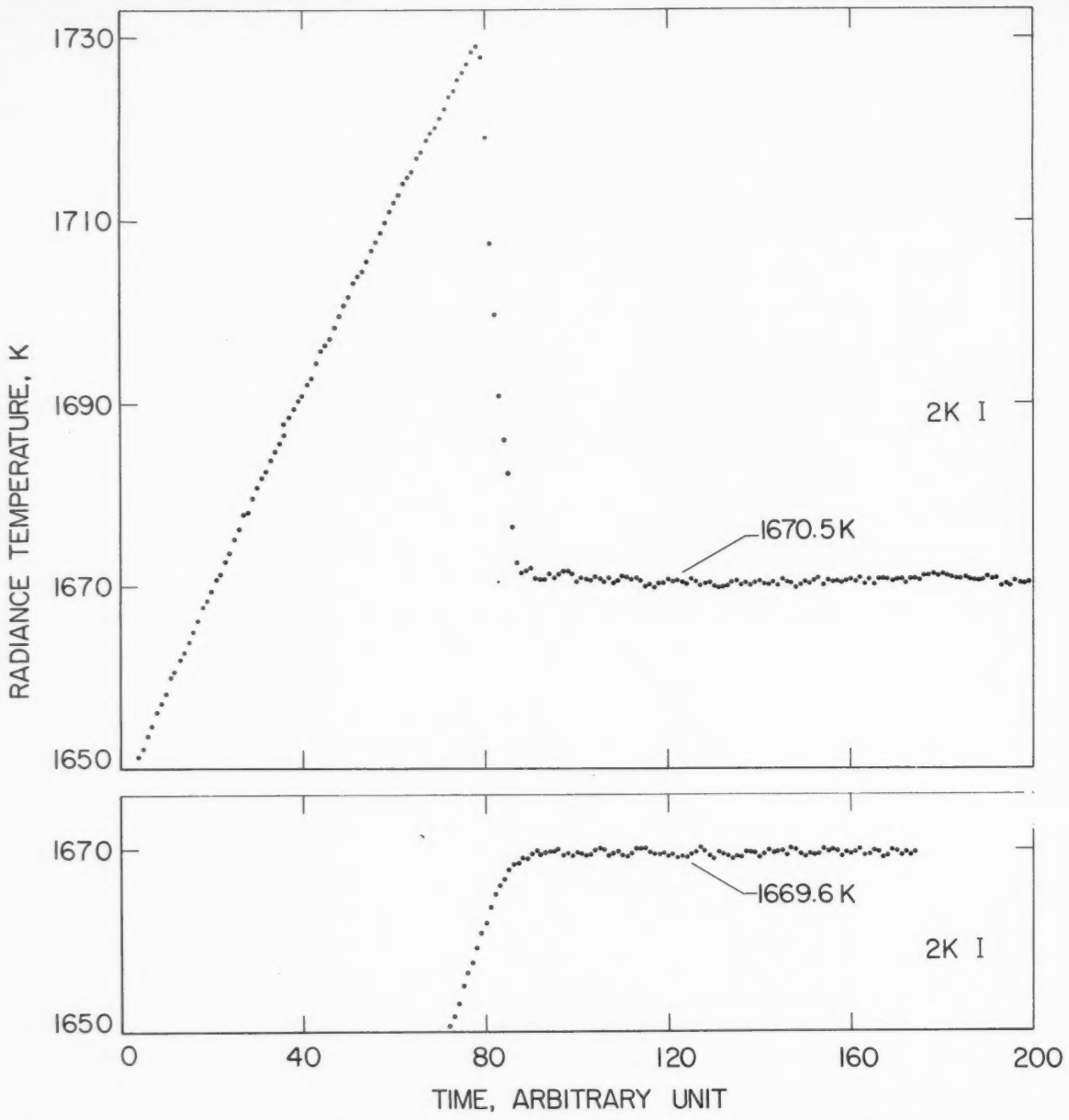

FIGURE 1. *Variation of radiance temperature (at 653nm) of iron as a function of time near and at its melting point for two typical experiments (1 time unit = 0.833 ms).*

The upper curve corresponds to the experiment in which the specimen (number 13) was heat treated prior to melting by pulse heating it for ten times to approximately 1500 K – above its $\alpha \rightarrow \gamma$ transformation point – which created an irregular and rough surface. The high values before the plateau are indicative of the differences in the normal spectral emittance of the solid and liquid phases. The lower curve corresponds to the experiment in which the specimen (number 3) had a smooth surface prior to melting as indicated by the absence of a spike before the plateau.

degree of initial surface roughness of the specimen. However, regardless of the differences in the initial conditions, radiance temperature at the melting plateau is approximately the same for the two specimens. It may be seen from table 1 that this argument is also satisfied by the other specimens.

A single value for the radiance temperature at the plateau for each specimen was obtained by averaging the temperatures at the plateau. The number of temperatures used for averaging ranged from 42 to 119, depending both on the melting rate and on the behavior of the specimen during melting. The standard deviation

of an individual temperature from the average was in the range 0.3 to 0.4 K for all the experiments. Similar values (for standard deviation) were obtained when fitting the temperature data corresponding to the premelting period to a quadratic function in time. This indicates that during melting no undesirable effects took place, such as vibration of the specimen, development of hot spots in the specimen and random changes in the specimen surface conditions.

To determine the trend of measured temperatures at the plateau, temperatures for each experiment were fitted to a linear function in time using the least squares method. The slopes of the linear function do not show any significant bias with respect to sign. The detailed results are reported in table 1. The temperature difference between the beginning and the end of the plateau (corresponding to the slope in the plateau) is in the range 0 to 0.4 K. The standard deviation of an individual temperature from the linear function was approximately the same as the standard deviation obtained by direct averaging of the temperatures.

The average radiance temperature at the melting point for the 13 iron specimens was 1670.3 K with a standard deviation of 0.8 K and a maximum absolute deviation of 1.7 K. The results are presented in figure 2.

A detailed analysis of the sources and magnitudes of the errors in the measurements using the present system is given in an earlier publication [5]. In a more recent publication [3], the specific errors in radiance temperature measurements are summarized. Based on these, it is estimated that the total error (random and systematic) in the radiance temperature of iron at its melting point is not more than 6 K. This includes an uncertainty of about 1 K in the melting point due to the impurities in the specimen.

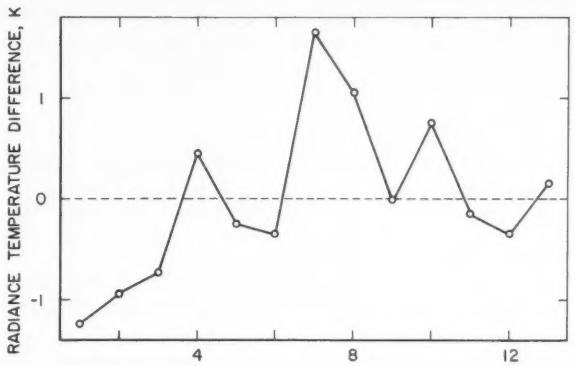

FIGURE 2. *Difference of radiance temperature (at the melting point of iron, at 653 nm) for individual experiments from their average value of 1670.3 K (represented by the "zero" line).*

It may be concluded that the radiance temperature (at 653 nm) of iron at its melting point is 1670 ± 6 K.

3. Discussion

The pulse heating technique used in this study has demonstrated the capability of measuring radiance temperature of metals during their initial melting

TABLE 1. *Summary of measurements of radiance temperature (at 653 nm) of iron during melting*

Specimen number [a]	Surface roughness [b]	Premelting period		Melting period				
		Heating rate [c]	Standard deviation [d]	Number of temperatures [e]	Slope at plateau [f]	Plateau temp. difference [g]	Radiance temperature [h]	Standard deviation [i]
		K · s^{-1}	K		K · s^{-1}	K	K	K
1	B	1200	0.3	109	0	0	1669.1	0.4
2	C	1500	.4	49	3.7	0.2	1669.4	.3
3	A	1800	.4	83	0	0	1669.6	.4
4	B	2000	.3	99	3.6	0.3	1670.8	.4
5	D	1900	.3	93	−2.9	−0.2	1670.1	.4
6	A	1900	.3	44	−12.1	−0.4	1670.0	.4
7	C	1700	.3	93	0	0	1672.0	.4
8	C	2800	.4	63	−4.2	−0.2	1671.4	.4
9	B	3000	.4	56	−8.4	−0.4	1670.3	.4
10	D	3000	.4	46	7.4	0.3	1671.1	.3
11	D	4300	.3	58	9.4	0.4	1670.2	.3
12	A	4300	.4	42	−4.7	−0.2	1670.0	.3
13	E	1500	.4	119	−2.5	−0.2	1670.5	.4

[a] Also represents the experiments in chronological order.

[b] The notations used for surface conditions correspond to the following typical roughnesses in μm: A, 0.1; B, 0.2; C, 0.4; D, 0.5. Surface "A" designates the specimen under "as received" condition. Surface "E" designates the specimen after heat treating it to about 1500 K.

[c] Heating rate evaluated at a temperature approximately 10 K below the melting point.

[d] Represents standard deviation of an individual temperature as computed from the difference between the measured value and that from the smooth temperature versus time function (quadratic) obtained by the least squares method. Data extend approximately 100 K below the melting point.

[e] Number of temperatures used in averaging the results at the plateau to obtain an average value for the radiance temperature at the melting point of the specimen.

[f] Derivative of the temperature versus time function obtained by fitting the temperature data at the plateau to a linear function in time using the least squares method.

[g] Maximum radiance temperature difference between the beginning and the end of the plateau based on the linear temperature versus time function.

[h] The average (for a specimen) of measured radiance temperatures at the plateau.

[i] Standard deviation of an individual temperature as computed from the difference between the measured value and that from the average plateau radiance temperature.

period. It may be noted, however, that with the present system, it was not possible to follow the entire melting process because the specimen collapsed and opened the main electrical circuit prior to the completion of melting.

The present results have shown the constancy and reproducibility of the radiance temperature of iron at its melting point for a number of specimens with different initial surface conditions. This substantiates similar earlier results on other metals: niobium [1], zirconium [2] and molybdenum [3].

Bonnell et al. [8] have reported a value of 1671 K for the radiance temperature (at 645 nm) of iron at its melting point. Since the wavelength dependence of the radiance temperature for iron at its melting point is not known, it is not possible to compare exactly the result of Bonnell et al. with that of the present work. However, an estimated value of about 0.25 $K \cdot nm^{-1}$ for the wavelength dependence of the radiance temperature obtained from an extrapolation of the lower temperature (1600 to 1800 K) results [9] adjusts the radiance temperature value from 1671 K (at 645 nm) to 1669 K (at 653 nm). This is about 1 K lower than the result of the present work.

Considering 1808 K for the melting point of iron [10] and 1670 K for the radiance temperature at the melting point, a value of 0.365 is obtained for the normal spectral emittance (at 653 nm) of iron at its melting point. The values reported in the literature are: 0.36 at 660 nm [11] and 0.37 at 650 nm [12].

In conclusion, the results of the present work in addition to earlier results on niobium, zirconium and molybdenum suggests the possibility of using the radiance temperature at the melting point of selected metals for secondary calibration and checking of optical temperature measuring equipment in high temperature systems. However, the final assessment will require additional accurate work on the same and other metals.

4. References

[1] Cezairliyan, A., Radiance temperature of niobium at its melting point. J. Res. Nat. Bur. Stand. (U.S.), **77A** (Phys. and Chem.), No. 3, 333–339 (May–June 1973).

[2] Cezairliyan, A. and Righini, F., Measurement of melting point, radiance temperature (at the melting point), and electrical resistivity (above 2100 K) of zirconium by a pulse heating method. Rev. Int. Hautes Tempér. et Réfract. In press.

[3] Cezairliyan, A., Coslovi, L., Righini, F., and Rosso, A., Radiance temperature of molybdenum at its melting point. Proceedings of the European Conference on Temperature Measurement. In press.

[4] Foley, G. M., High-speed optical pyrometer. Rev. Sci. Instr., **41,** No. 6, 827–834 (June 1970).

[5] Cezairliyan, A., Morse, M. S., Berman, H. A., and Beckett, C. W., High-speed (subsecond) measurement of heat capacity, electrical resistivity, and thermal radiation properties of molybdenum in the range 1900–2800 K. J. Res. Nat. Bur. Stand. (U.S.), **74A** (Phys. and Chem.), No. 1, 65–92 (Jan.–Feb. 1970).

[6] Cezairliyan, A., Design and operational characteristics of a high-speed (millisecond) system for the measurement of thermophysical properties at high temperatures. J. Res. Nat. Bur. Stand. (U.S.), **75C** (Eng. and Instr.), No. 1, 7–18 (Jan.–March 1971).

[7] International Committee for Weights and Measures. The International Practical Temperature Scale of 1968. Metrologia **5,** No. 2, 35–44 (April 1969).

[8] Bonell, D. W., Traverton, J. A., Valerga, A. J., and Margrave, J. L., The emissivities of liquid metals at their fusion temperatures in Temperature—Its Measurement and Control in Science and Industry, H. H. Plumb, ed., Vol. 4, Part 1 (ISA, Pittsburgh, 1972), pp. 483–487.

[9] Touloukian, Y. S. and DeWitt, D. P., Thermal Radiative Properties, Vol. 7 of Thermophysical Properties of Matter (IFI/Plenum, New York, 1970).

[10] Cezairliyan, A. and McClure, J. L., Thermophysical measurements on iron above 1500 K using a transient (subsecond) technique. J. Res. Nat. Bur. Stand. (U.S.), **78A** (Phys. and Chem.), No. 1, 1–4 (Jan.–Feb. 1974).

[11] Bidwell, C. C., Radiation from solid and molten iron. Phys. Rev., **3,** No. 6, 439–449 (1914).

[12] Burgess, G. K. and Waltenberg, R. G., The emissivity of metals and oxides, Nat. Bur. Stand. Bull., **11,** 591–605 (1915).

(Paper 79A4–856)

JOURNAL OF RESEARCH of the National Bureau of Standards—A. Physics and Chemistry
Vol. 79A, No. 4, July–August 1975

Precision Measurements of the Dimensional Stability of Four Mirror Materials

B. Justice*

Institute for Basic Standards, National Bureau of Standards, Washington, D.C. 20234

(April 11, 1975)

There are several glasses and glass-ceramics available today which have low coefficients of thermal expansion—some near zero. For this reason they often serve as substrates for massive mirrors in orbit. In order for such a mirror to enjoy a lifetime of 5 years or more of diffraction-limited service, the substrate must be dimensionally stable and thereby preserve the original figure.

Early in 1967, it was decided that the National Bureau of Standards and Corning Glass Works would undertake a joint effort to measure the lengths of small samples of such materials over a period of years. These measurements were completed in 1971.

The average length changes in parts per million of the four materials[1] selected are as follows:

Corning Code 9623 a glass ceramic	−0.30
Corning Code 7971 a titanium silicate	−0.37
Corning Code 7940 a vitreous silica	−0.47
Corning Code 9622 a glass-ceramic	−1.03.

Key words: Dimensional stability; glass; glass-ceramic; interferometry.

1. Technique

The glass gauge blocks are 1″ × 1⅜″ × ⅜″. They were wrung to optical flats at the beginning of the study and never removed. The Zeiss gauge block interferometer at NBS was used with the 5461 Å line of Hg 198. The fringe patterns from the top of the sample and from the optical flat on either side relative to a reference flat were recorded on high speed 35 mm film. It was assumed to be unlikely that the order of interference, 93,000 or so, would change as much as one. Thus we recorded only the fractional displacement of the block fringes relative to the platen fringes.

The negatives were scanned three times by a microdensitometer. The data were smoothed by computer, fringe centers computed, and the fractional displacement at the gauging point calculated.

The interferogram contains 5 to 8 fringes on the gauge block and an equal number on either side from the base flat. All of this occupies a 6 mm circle on the 35 mm film. Usually four negatives (two from each of 2 consecutive days) are averaged to obtain a block length. The observed length is corrected for ambient conditions to 20 °C, 760 mm Hg and 10 mm of water vapor. The fringes are $\cos^2$ Fizeau fringes.

The original experiment called for three sets of 12 samples each from each of four materials, for a total of 144 samples. For a number of reasons, we ended up with 94 acceptable survivors and these are reported on here. Some of these samples were exposed to pressure cycling or temperature cycling as described later.

The term "length" in this report refers to the optical length of the gauge block. It includes the physical length, the thickness of the wringing film, and any contribution due to a difference between the phase change upon reflection from the sample and the phase change from the platen. All platens were made of Corning Code 7940 material, a vitreous silica.

2. Precision

There are many factors which affect our precision. There are also several improvements we could make in the technique—looking back at the experiment. However, we feel that the limiting precision on good blocks over a long period of time—using this technique as is—is about $6\sigma = 30$ millifringes, or slightly over 0.3 ppm.

Precision is affected by the flatness and parallelism of the blocks and platens; by the accuracy of the corrections for atmospheric pressure, temperature, and humidity; by the placement of fringes by the operator and nature over the years; by the fidelity of the photographic record; by the precision we can attain in

*The author performed this work while he was an Industrial Research Associate at the National Bureau of Standards; Present address: Corning Glass Works, Research and Development Laboratory, Technical Staffs Division, Corning, New York 14830.

[1]The mirror materials are identified by brand name and code number to specify precisely what was measured. This identification does not imply a product endorsement by the National Bureau of Standards.

extracting the data from the film; and by the quality of the computer algorithm which converts these data to physical lengths. Some of these areas are discussed below in detail.

The average difference between pairs of negatives made in quick succession for the 1-year data was less than 0.010 fringe. For the latest 3-year data, this increased to 0.016 fringe, due apparently to poorer image contrast.

A set of 11 negatives, which was exposed September 16 and November 4, 1968, has been used to establish the precision of the technique and the permanence of the photographic information. These same negatives have been measured on five separate occasions. The second and third times were 6 and 29 months after the first, respectively. The fourth and fifth times were on a single day about 31 months after the first, so that the negatives remained in alinement in the microdensitometer for both runs.

The average spread for the first three runs is about 0.005 fringe; for all five runs, it is about 0.0075 fringe, and for the two consecutive runs on 4–26–72, it is less than 0.003 fringe.

Three scans are made in the x direction at three different y locations. The central sample scan has two symmetric platen scans just 2.3 mm full scale (0.46 mm on the negative) from either edge of the sample. If any x scan is repeated without any adjustments being made, the fringe locations repeat to 0.001 fringe. The fringe separation was 600 to 1200 μm. Intensity every 8 μm was recorded. Recording every two micrometers did not improve the precision enough to justify the expense of handling four times as much data.

Since the image of the block is only 2000 μm in width, an error of 25 μm in alinement will produce an error of 0.003 fringe with an out of parallel of 0.25 fringe, across the 9500 μm ($^3/_8$″) face.

The data are as follows:

Displacement in Fringe Fractions for Card 104

Film No.	Date Measured				
	9–30–69	3–20–70	2–16–72	4–26–72A	4–26–72B
1	0.8444	0.8411	0.8423	0.8469	0.8441
2	.8422	.8417	.8432	.8471	.8435
3	.7077	.7070	.7035	.7093	.7113
4	.7098	.7151	.7148	.7160	.7177
5	.0913	.0856	.0866	.0900	.0922
6	.0919	.0893	.0896	.0905	.0937
7	.7314	.7362	.7300	.7330	.7309
8	.7444	.7427	.7379	.7458	.7430
9	.2961	.2866	.2959	.2987	.3014
10	.2894	.2836	.2869	.2900	.2939
11	.3053	.3015	.3044	.3070	.3044
Avg	.5140	.5119	.5123	.5158	.5160
Deviation from Grand mean	0.0000	−0.0021	−0.0017	+0.0018	+0.0020

It is apparent that 1 and 2, 3, and 4 etc. are repeat negatives of the same block.

Two of the three microdensitometer scans are on the base flat along either side of the gauge block. The third is halfway between, down the center of the block. The computer reports all fringe and crosshair positions detected. It also reports halfwidths and intensities. The program, however, uses only two of the block fringes and the next surrounding pairs of platen fringes.

The program might well have been written to be more informative by putting to use all of the incidental data. As an example, table 1 shows the intervals in micrometers between successive pairs of the six fringes detected on film 1 of card 104 for the five runs described before.

TABLE 1. *Precision of Fringe Placement for Film 1 on Card 104*

Left Platen Scan						
9–30–69	913	913	903	959	950	927.6
3–20–70	908	915	897	966	947	926.6
2–16–72	912	912	908	959	942	926.6
4–26–72	907	915	909	954	948	926.6
4–26–72	905	915	909	954	949	926.4
	909	914	905	958	947	926.8
Sample Scan						
9–30–69	973	975	955	989	969	972.2
3–20–70	964	974	955	985	974	970.4
2–16–72	971	971	957	987	968	970.8
4–26–72	965	974	958	984	973	970.8
4–26–72	964	975	958	984	973	970.8
	967	974	957	986	971	971.0
Right Platen Scan						
9–30–69	933	876	938	946	955	929.6
3–20–70	931	874	939	943	957	928.8
2–16–72	941	875	938	943	947	928.8
4–26–72	931	875	942	940	955	928.6
4–26–72	930	875	943	938	956	928.4
	933	874	940	942	954	928.8

Several conclusions can be drawn about the sample and the flat, as they were in the fall of 1968. The conclusions are based upon those points of the surfaces intersected by the three densitometer scans.

For example:

(1) The left platen surface lacks about 0.002 fringe of being parallel to the right platen surface, in the areas scanned.

(2) The sample surface is about 0.047 fringe out of parallel with the platen surface.

(3) The three surfaces have localized areas out of flat by as much as 0.057 fringe, 0.030 fringe and 0.085 fringe respectively.

(4) The Kodak 2485 film[2] with an Estar base must

[2]Certain commercial products are identified in order to adequately specify the experimental procedure. In no case does such identification imply recommendation or endorsement by the National Bureau of Standards nor does it imply that the products identified are necessarily the best available for the purpose.

itself be dimensionally stable over the 31 months, to within a few parts per thousand.

(5) The sample surface is more nearly flat than the platen surfaces. The average deviation from a least-squares straight line is only four parts in 970, for the sample surface.

(6) The average discrepancy in fringe location for two successive runs is about ⅔ micrometer.

3. Environments

A set usually consists of nine 1-inch gauge blocks (⅜″ × 1⅜″) wrung to a Corning Code 7940 optical flat. The Corning Code 9622 experienced ambient conditions only. The three other materials also had additional sets which were subjected to uniaxial compression cycling, parallel to the gauging direction, from 0 to about 14.1 Kg/cm², or to temperature cycling from −2° to +52° Celsius. The time required for either cycle was 1 h. A series of 1, 10, 100, and 1,000 total cycles was used. These forced environments were all completed between the 60-day and 365-day data. Except for this total 1,000 hours, all other storage was in the same well-controlled room with the "ambient" samples. Ambient humidity during the measurements had values ranging from 22 to 62% R.H.

4. Summary of Data

All but some of the earliest data consist of the average of four interferograms, two from each of two usually consecutive days. Zero time was the day of the first measurement. The other reported dates are near the 1 month, 6 months, 1-, 2-, and 3-year intervals. See tables 2 through 5. These data were normalized by reporting the deviation of each block about its mean for 3 years (3.1–3.4) in millifringes. A value of 50, for example, is equivalent to 0.050 fringe, or about 0.54 microinch.

Listed below is a summary from tables 2 through 5, which ranks these four materials in order of decreasing stability. The shrinkage figures in parentheses are the values obtained if one averages the first two data points, which were less than 60 days apart. Shrinkage ranges from about ¼ to 1 nm per mm (¼ to 1 microinch per inch) over 3+ year period.

TABLE 2. *Individual Length Changes in Millifringes*

Corning Code 9623, Pressure

Days	0	53	156	373	772	1238	Δ
Sample:							
A–2–7*	−1	0	−14	5	13	−4	−3
8*	−9	2	−33	10	22	8	17
9*	−7	−9	−4	10	17	−5	2
11*	3	−1	−10	−6	14	3	0
12*	8	9	−22	0	9	−1	−9
13*	9	−1	−4	6	3	−10	−19
15*	−13	−5	−4	17	8	0	13
16*	25	20	−31	1	−8	−9	−34
17	30	30	−19	0	−4	−34	−64
Average	5	5	−16	5	8	−6	−11

TABLE 2. *Individual Length Changes in Millifringes*—Continued

Corning Code 9623, Temperature

Days	0	43	126	374	735	1189	Δ
Sample:							
A–3–7*	16	5	−5	−14	−7	8	−8
8*	19	13	11	−2	−21	−21	−40
9	79	34	−8	−38	−35	−34	−113
12	31	37	−8	−10	−20	−29	−60
13	44	33	−16	−21	−12	−27	−71
15*	19	11	−21	1	−1	−11	−30
16*	14	40	−3	−18	−17	−15	−29
17	58	60	−2	−21	−30	−62	−120
Average	35	29	−7	−15	−18	−24	−59

Corning Code 9623, Ambient

Days	0	34	215	366	732	1208	Δ
Sample:							
A–1–7*	8	14	−6	5	−18	0	−8
8*	24	6	0	−7	−10	−11	−35
9*	8	−4	−7	19	5	−21	−29
12	24	7	14	2	−20	−28	−52
13*	9	6	11	16	−33	−6	−15
15*	−24	−2	−1	22	7	0	24
16	28	16	−3	22	−43	−22	−50
17*	10	3	−12	22	−27	4	−6
Average	11	6	0	13	−17	−11	−22

Corning Code 9623, Ambient

Days	0–40	120 190	245 310	375	730	1125	Δ
Sample:							
A–2–6*	−6	−14	−5	3	23	−3	3
10*	5	−16	11	15	20	−36	−41
A–1–6*	4	−4	−2	9	−1	−3	−7
10*	−3	−17	5	3	9	2	5
14*	13	−19	−5	6	2	1	−12
A–3–6*	22	−11	−9	5	10	−17	−39
10	38	−4	−2	1	7	−39	−77
14*	14	−6	4	−6	−3	−3	−17
Average	11	−11	−1	5	8	−12	−23

TABLE 3. *Individual length changes in millifringes*

Corning Code 7971, Pressure

Days	0–6	45	118	372	730	1192	Δ
Sample:							
D–2–7*	35	18	6	−27	−31	−3	−38
11	33	12	9	−14	−22	−15	−48
13*	17	20	4	−7	−23	−11	−28
15*	−6	11	−6	18	−5	−9	−3
16	31	50	14	−21	−43	−30	−61
Average	22	22	5	−10	−25	−14	−36

TABLE 3. *Individual length changes in millifringes*—Continued

Corning Code 7971, Temperature

Days	0	42	117	367	833	1182	Δ
Sample:							
D–3–7*.....	−4	0	1	−5	−7	14	18
8*.....	−12	1	−12	6	−3	20	32
9*.....	3	4	−1	9	2	−14	−17
11*.....	10	5	−14	7	4	−10	−20
Average.....	−1	2	−6	4	−1	2	+3

Corning Code 7971, Ambient

Days	0	48	157	280	370	732	1195	Δ
Sample:								
D–1–7*.....	15	20	−11	−6	−9	−15	7	−8
8*.....	19	9	0	−5	−2	−8	−10	−29
9.....	60	18	0	3	−17	−25	−38	−98
12.....	60	17	−5	−15	−18	−19	−17	−77
13.....	42	0	0	−7	−15	−7	−10	−52
15.....	70	3	−6	−10	−15	−14	−25	−95
17.....	69	9	−12	0	−26	−19	−18	−87
Average.....	48	11	−5	−6	−15	−14	−16	−64

Corning Code 7971, Ambient

Days	0–40	120 190	245 310	375	730	1125	Δ
Sample:							
D–2–6*.....	10	−2	3	−4	2	−9	−19
10.....	32	−5	−9	2	3	−22	−54
14.....	4	4	23	54	−35	−50	−54
D–1–6*.....	14	−9	−3	10	0	−13	−27
10.....	30	−2	7	2	−7	−28	−58
D–3–6*.....	8	−8	6	−13	5	5	−3
10*.....	−13	8	8	24	−5	−22	−9
14*.....	−25	−37	25	17	23	−5	20
Average.....	8	−6	8	12	−1	−18	−26

TABLE 4. *Individual length changes in millifringes*—Continued

Corning Code 7940, Temperature

Days	0	34	132	372	739	1213	Δ
Sample:							
C–4–7.....	28	36	19	−23	−33	−26	−54
9*.....	23	23	7	−16	−16	−20	−43
11*.....	−17	30	5	0	−10	−5	12
13.....	21	33	−13	−7	−7	−26	−47
15*.....	16	32	−8	−9	−7	−23	−39
17.....	45	47	20	−3	−51	−59	−104
Average.....	19	33	5	−10	−21	−26	−45

Corning Code 7940, Ambient

Days	0–18	49′	162	370	734	1215	Δ
Sample:							
C–2–7*.....	1	3	−2	15	−17	0	−1
8*.....	36	9	−3	−12	−41	11	−25
11.....	31	29	−1	−19	−28	−13	−44
12.....	23	41	5	1	−41	−27	−50
13*.....	8	2	−12	33	−22	−11	−19
15*.....	15	34	−8	7	−23	−23	−38
16*.....	6	2	2	14	−21	−3	−9
17.....	27	37	−15	4	−33	−19	−46
Average.....	18	20	−4	5	−28	−11	−29

Corning Code 7940, Ambient

Days	0–40	120 190	245 310	375	730	1125	Δ
Sample:							
C–2–6*.....	6	7	−8	3	1	−6	−12
10*.....	23	−11	2	8	−4	−18	−41
C–3–10.....	22	9	3	−10	20	−45	−67
14.....	39	0	−14	−10	7	−24	−63
C–4–6.....	24	−5	8	7	−2	−29	−53
10*.....	−10	−13	17	12	5	−9	1
Average.....	17	−2	1	2	4	−22	−39

TABLE 4. *Individual length changes in millifringes*

Corning Code 7940, Pressure

Days	0	31	129	371	730	1182	Δ
Sample:							
C–3–7.....	44	29	−17	−19	−18	−19	−63
8.....	69	59	−40	−34	−31	−23	−92
9.....	66	42	−37	−29	−35	−9	−75
11.....	36	29	−41	−2	−10	−9	−45
12.....	91	62	−10	−44	−63	−38	−129
13*.....	35	31	−29	−10	−34	5	−30
15.....	31	32	−1	−7	−33	−20	−51
16*.....	6	0	11	−11	−20	14	8
Average.....	47	36	−21	−20	−31	−12	−59

TABLE 5. *Individual Length Changes in Millifringes*

Corning Code 9622, Ambient

Days	0–18	42–124	270	381	487′	685	1125	Δ
Sample:								
E–1–7.....	50	30	12	6	−20	−20	−55	−105
8.....	51	25	13	4	−15	−28	−47	−98
9.....	51	31	12	−5	−18	−26	−45	−96
11.....	54	39	14	4	−26	−36	−51	−105
12.....	48	27	23	2	−23	−30	−44	−92
13.....	56	17	−8	16	−18	−19	−42	−98
15.....	60	12	5	10	−24	−42	−23	−83
16.....	52	19	9	10	−23	−21	−46	−98
17.....	51	8	5	−4	−11	−18	−34	−85
Average.....	53	23	9	5	−20	−27	−43	−96

	Number of Samples	Average Total Change in Millifringes	Range of Individuals	% <40mf	% >80mf
Corning Code 9623.....	33	−28 (−24)	+24 to −120	76	6
Corning Code 7971.....	24	−34 (−29)	+32 to −98	58	12
Corning Code 7940.....	28	−44 (−41)	+12 to −129	46	11
Corning Code 9622.....	9	−96 (−81)	−81 to −150	0	100

The Code 9622 shows the greatest average shrinkage but indicates extremely uniform and more nearly predictable performance. Figure 1 shows the average deviation of the nine blocks about their means as a function of time. The average individual variation about the average is only ±12 mf. The curve is based upon shrinkage in any year being 58 percent of the previous year's shrinkage.

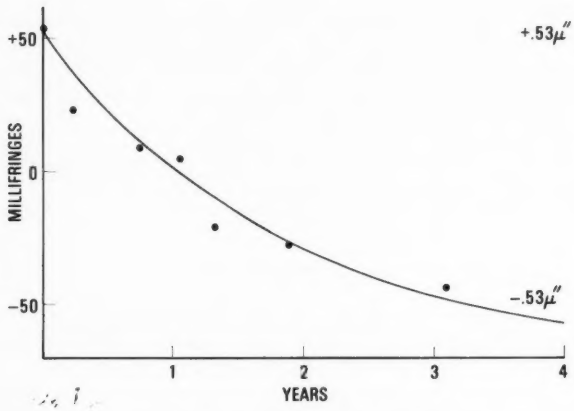

FIGURE 1. *Code 9622—average length versus time.*

In tables 2 through 5, the Δ column is simply the 3-year value minus the time zero value. The asterisks denote those samples whose Δ is about 40 mf or less. Of the 94 samples, 52 are in this category of being quite stable. However, 32 of these have a Δ of 20 mf or less. These samples, therefore, exhibit dimensional stability to something less than 0.07 ppm/year. Sixteen of these 32 blocks are Corning Code 9623 glass-ceramic.

5. Conclusions

The conclusions to be drawn are:

(1) About half of these samples exhibit length stability at least as good as 0.4 ppm for 3 years. About 40 percent are better than 0.3 ppm, about the precision of the experiment.

(2) Other samples, notably Code 9622 material, may shrink as much as 1 ppm in 3 years.

6. Statistical Analysis

A two-part, statistical analysis of the data was made by standard techniques. The first part was a test of the contributions made by barometric pressure, temperature and humidity to the observed variation in length. If one measures these three atomospheric parameters exactly and corrects precisely for optical path and thermal expansion, then there would be no significant contribution to the observed length.

In many instances, however, this was not the case. The following table lists the confidence level at which we can say that barometric pressure, or temperature, or humidity explains a significant portion of the variance in length. (Cases less than 90% confident are not included).

	Baro. Press.	Temp.	Humidity
9623 (pressure environment)..	90%	95%	99%
7940 (pressure environment)..	90%		
9623 (temp. cycling).....		95%	
7940 (temp. cycling).....		90%	
7940 (ambient).....			90%
7971 (ambient).....	99%		
9622 (ambient).....			[a] 89%

[a] Code 9622 showed a large time-dependent shrinkage. These values fit several mathematical equations quite well. The residuals from the best-fitting curve—i.e., subtracting out the time-dependent length change—were then tested in the same manner for contributions by barometric pressure, temperature, and humidity. At the 89 percent level of confidence, humidity was making a significant contribution to this residual length variance. The equation of the form $\Delta L = ae^{-bt}$ accounted for 88.1 percent of the length variation with time.

There appears to be neither a consistent measurement error, nor a fixed correction error. There is, however, adequate suspicion to encourage one to make such measurements in vacuum. In this way, all of the pressure, humidity, and temperature contributions to the refractive index would be eliminated—only a very slight (for these materials) thermal expansion effect would remain.

The second part of the statistical analysis was an analysis of variance with change in length as the dependent variable, and material, environment, side finish, and orientation, as the independent variables.

6.1. Material

At the 99.4 percent level of significance there is a difference among the four materials. When the Code 9622 glass-ceramic is excluded, this drops to 77.5 percent—that is probably no significant difference.

6.2. Code 7971 Titanium Silicate

At the 92.4 percent level of significance, using data

from all environments and all side finishes, there is a difference due to the orientation of the gauging dimension in the original boule of glass. Those with the gauging dimension parallel to the axis of the boule showed the greatest shrinkage.

This significance may be appearing higher than it really is, due to moderate interaction between side finish and environment which showed up on a two-way analysis of variance. When orientation was tested, using only data from an ambient environment and acid relieved side finish, the significance dropped to 79.1 percent.

6.3. Code 9623 Glass-Ceramic

At the 99.7 percent level of significance, there is a difference due to side finish, that is, some of the blocks had the nongauging surfaces polished, or acid relieved, or left as ground. The polished samples showed greatest shrinkage.

At the 98.9 percent level of significance, there is a difference due to environment. The temperature cycling environment showed the greatest shrinkage.

6.4. Code 7940 Vitreous Silica

Orientation, side finish, and environment had no significant effect upon the dimensional stability of Code 7940 glass.

6.5. Code 9622 Glass-Ceramic

Only orientation could be tested and it proved to be probably not significant—79.2 percent level.

The original experiment was not designed to fully characterize the effects of the numerous variations of finish, environment, and orientation. The majority of samples were acid-relieved and stored at ambient temperature. This left very few samples, due to economic considerations, in the other possible combinations. For this reason, and because of the apparent interaction between some of the variables, the summary just given might better be used with some degree of caution.

I am indebted to many people at the National Bureau of Standards, but the work would not have gotten done without the unfailing assistance of Clyde Tucker, who patiently shot and reshot many thousands of interferograms.

(Paper 79A4–857)

JOURNAL OF RESEARCH of National Bureau of Standards—A. Physics and Chemistry
Vol. 79A, No. 4, July–August 1975

A Correlation for the Second Interaction Virial Coefficients and Enhancement Factors for Moist Air*

R. W. Hyland

Institute for Basic Standards, National Bureau of Standards, Washington, D.C. 20234

(March 28, 1975)

Experimental measurements of the enhancement factors for mixtures of water vapor and CO_2-free air have been made at −20, −10, and +70 °C. The results, coupled with previous experimental enhancement data, have been used to calculate the second interaction virial coefficients, B_{aw}, for water vapor air mixtures from −50 to +90 °C. Within this temperature range, an error analysis shows that the uncertainties in B_{aw} are between 6 and 10 percent. The calculated B_{aw} values are used in deriving enhancement factors at 10 °C intervals for $-50 < t < 90$ °C, at varying pressure intervals from 0.25 to 100 bar. The associated uncertainties are shown as a function of pressure and temperature. The enhancement factors are extrapolated to −80 °C.

Key words: Enhancement factor; equation of state; interaction virial coefficients; moist air; saturated air; second virial coefficients; virial coefficients.

1. Introduction

The objective of this paper is to take limited experimental data on the saturated water vapor content of CO_2-free air and develop a sound basis for predicting this saturated content over wide ranges of temperature and pressure. The approach is through the virial equation of state, and follows the methods outlined previously by Hyland and Wexler [1, 2],[1] where they reported experimental results for the range $30 \leq t \leq 50$ °C. In this paper the experimental range is extended to include $-20 \leq t \leq 70$ °C, and the results used to obtain both the second interaction virial coefficients, B_{aw}, for air-water vapor mixtures, and enhancement factors, defined below, over the temperature range $-50 \leq t \leq 90$ °C.

The experiments require the saturation of CO_2-free air at known conditions of pressure and temperature. The water vapor is then separated from the air, and the mole fractions of each component determined. The enhancement factor for the particular pressure and temperature of saturation may be expressed by

$$f = \frac{x_w P}{e_s} = \frac{(1-x_a)P}{e_s} \qquad (1)$$

where f = the enhancement factor.

x_a, x_w = the mole fractions of air and water vapor in the saturated mixture.

P = total pressure above the surface of the condensed phase (water or ice).

e_s = the pure phase saturation vapor pressure of water substance at the temperature of saturation.

$x_w P$ = the effective water vapor pressure at the given pressure and temperature of saturation.

The determination of an empirical relationship for f as a function of pressure and temperature is impractical because of the large number of experiments involved. We therefore chose to use the theoretical equation of [2], given as eq (A–4) in the appendix to this paper. This equation yields enhancement factors, providing all required virial coefficients are known with sufficient accuracy. This was the case for all virial coefficients within our range of interest except B_{aw}. Our approach was to perform a limited number of enhancement factor measurements, and, by inverting eq (A–4) into a quadratic for B_{aw}, to calculate B_{aw} at each experimental point. The values obtained at each temperature were averaged, and the temperature dependence of the averages estimated by least-squares fitting them with the Lennard-Jones (12–6) potential function, resulting in the values found in table 4 of this paper. All of the information necessary for using eq (A–4) was then in hand, and the enhancement factors given in table 8 were obtained.

2. Experimental Method and Results at −20, −10, and +70 °C

Commercially supplied, compressed air, with impurity characteristics as described in [1], is passed

*This work sponsored in part by ERDA, Sandia Laboratories, Primary Standards Laboratory, Albuquerque, N. Mex. 87115.

[1] Figures in brackets indicate literature references at the end of this paper.

through a unit which lowers the CO_2 content to a level near 2 ppm. The air is then saturated by passage over the surface of either water or ice. Pressure and temperature within the saturator are monitored. The water vapor is subsequently removed from the air stream, and the mass of water vapor and associated dry air determined. One obtains the water vapor mole fraction from the mass ratio, and the pure phase saturation vapor pressure from the saturator temperature. Combining these with the saturator pressure in eq (1) determines the enhancement factor at the saturator P, T condition.

Several such experiments are done along an isotherm. Since B_{aw} is a function of temperature only, each experiment should yield the same value, providing a check on whether or not the apparatus is performing properly, and whether the equation relating B_{aw} to f (the inverse of eq (A–4) in this paper) is valid at the given conditions.

The details of the methods for experiments above 0 °C, including our new point at +70 °C, are found in [1, 2]. The 70 °C data and results are in table 2 of this paper.

The saturating apparatus of [1, 2] is unsuitable for use at temperatures below 0 °C. Instead, for our points at −20 and −10 °C, the low-frost point generator of Greenspan [3] was used. Air samples were prepared by first evacuating containers, then back-filling them through a CO_2-removal unit in series with a coil immersed in a bath at roughly −78 °C. The air pressure during filling increased monotonically from about 1 to 125 bar. The process provided containers of dry, low-CO_2 content (2–5 ppm) air. In the course of an experiment, the air mass passing through the saturator was found by weighing the air containers before and after the experiment on a modified, higher-capacity version of a balance described by Russell in [4]. The water mass was determined with the usual gravimetric drying train [5].

The experimental results at −10 and −20 °C are given in table 2, while table 3 summarizes the results obtained previously at 30, 40, and 50 °C.

All experimental results are referred to the International Practical Temperature Scale of 1948 (6). In table 4, above −20 °C, it makes no difference whether the given temperatures are considered to be on IPTS–48 or IPTS–68 (7). At −20, −30, and −40 °C, B_{aw} becomes more negative by 0.01 cm³/mol, and at −50 °C, 0.02 cm³/mol, if one considers the given values to be on the 1948 scale and converts to the 1968 scale. In table 8, to the number of reported places, the temperatures can be considered to represent either temperature scale.

3. Data Reduction

We first derive values of B_{aw} from enhancement data. The necessary equations have been discussed in refs. [1, 2]. However, the derivation of eq (12) of [2] is incorrect as presented, and the proper derivation is outlined in the appendix to this paper. Also summarized in the appendix are equations in which no changes have been made. Presented here are equations and constants which differ from those used in [1, 2]. These differences are associated with the wider temperature ranges considered. Also, the molecular weight of air containing 2–5 ppm CO_2 was recalculated, based on the proposal by Harrison [8] that the sum of the CO_2 and oxygen volume percentage is constant at 20.979. The molecular weight ratio of water to air becomes 0.622062, differing slightly from the value used in [1, 2].

3.1. Specific Volume of Hexagonal Ice I

The specific volume of hexagonal ice I, used in the calculation of B_{aw} from experimental enhancement data at temperatures below 0 °C, was formulated by first considering the specific volume data of Ginnings and Corruccini [9], along with a correlation of data on the linear expansion of ice from Jukob and Erk [10], Powell [11], Butkovich [12], Dantl [13], and LaPlaca and Post [14], resulting in

$$V_{P_a,T} = 1.074351 - 0.867004 \cdot 10^{-4}\, T + 0.656565 \cdot 10^{-6}\, T^2 - 0.430316 \cdot 10^{-9}\, T^3 \quad (2)$$

where $V_{P_a,T}$ is the specific volume of ice at one standard atmosphere and at absolute temperature T.

Equation (2) is used in our correlation of Leadbetter's values [15] of the adiabatic compressibility of hexagonal ice I, to yield

$$V_{P,T} = V_{P_a,T}\,[1 - (8.875 + 0.0165T)(P - 1.01325) \cdot 10^{-6}] \quad (3)$$

where the pressure unit is bars.[2]

3.2. Expressions for B_{aa}, C_{aaa}, and C_{aaw}

Equations (4), (5), and (6), below, were obtained by fitting, using the method of least squares, a wider range of data of Sengers et al. [16], Hilsenrath et al. [17], and Mason and Monchick [18] than was done in [2]. Polynomial equations were used for the fits. The data fitted here covers the nominal temperature range from −50 to +110 °C. The standard deviations of the fits do not, of course, reflect the overall uncertainties in the parameters.

$$B_{aa}(t) = -13.5110 + 0.24311t - 0.10846 \cdot 10^{-2} t^2 + 0.42504 \cdot 10^{-5} t^3 - 0.81851 \cdot 10^{-8} t^4 \text{ cm}^3/\text{mol}; \quad \sigma_{\text{fit}} = 0.023 \quad (4)$$

$$C_{aaa}(t) = 1314.2 - 0.89988t - 0.30474 \cdot 10^{-2} t^2 + 0.42015 \cdot 10^{-4} t^3 - 0.40869 \cdot 10^{-6} t^4 + 0.43810 \cdot 10^{-8} t^5 - 0.20677 \cdot 10^{-8} t^6 \text{cm}^6/\text{mol}^2; \quad \sigma_{\text{fit}} = 0.157 \quad (5)$$

$$C_{aaw}(t) = 860.82 - 2.4454t + 0.94106 \cdot 10^{-2} t^2 + 0.14909 \cdot 10^{-4} t^3 - 0.59389 \cdot 10^{-6} t^4 + 0.30265 \cdot 10^{-8} t^5 \text{ cm}^6/\text{mol}^2; \quad \sigma_{\text{fit}} = 0.353 \quad (6)$$

The temperature, t, is degrees Celsius.

[2] 1 bar = 10^5 pascals.

3.3. Expressions for the Henry's Law "Constants"

The correlation of the Henry's "constant", k, for air, from 0 to 100 °C, is based in part on the "constants" for nitrogen, as was done for the 0 to 50 °C range of [2].

For atmospheric nitrogen, correlations were obtained from the data of [19, 20, 21], and, for nitrogen at pressures of 50 and 100 atmospheres, from the data of [22] as reported in Dorsey [21], and from [23].

The 50- and 100-atmosphere air curves were obtained by requiring the same percentage differences between the 1- and 50-atmosphere curves and the 50- and 100-atmosphere curves as the corresponding differences for nitrogen.

The results, using bars as the pressure units, were fitted to the polynomial

$$10^6 k = \sum_{i=0}^{n} C_i t^i \qquad (7)$$

where $n=4$ or 5, yielding the coefficients in table 1. The units of k are mole fraction/bar.

There seems to be no high pressure data for solubility of air in ice. At all temperatures less than 0 °C, the Henry's "constant" for water at 0 °C and 1 bar is used. The resulting systematic error estimate, given as 10 percent in [2], has been increased to 20 percent, introducing a maximum uncertainty on the order of 0.2 percent into the calculated value of B_{aw}.

TABLE 1. *Coefficients to equation (7)*

i	Pressure, bars		
	1	50	100
0	23.5199	21.6663	19.7652
1	−0.60277	−0.54460	−0.47424
2	$.11518 \cdot 10^{1}$	$.93580 \cdot 10^{-2}$	$.81569 \cdot 10^{-2}$
3	$-.12556 \cdot 10^{-3}$	$-.75473 \cdot 10^{-4}$	$.67051 \cdot 10^{-4}$
4	$.74217 \cdot 10^{-6}$	$.24146 \cdot 10^{-6}$	$.22157 \cdot 10^{-6}$
5	$.17765 \cdot 10^{-8}$	—	—

3.4. Saturation Vapor Pressure Over Ice

The expression for the saturation vapor pressure of ice is that given by Goff, in [24]. At −10 and −20 °C, the estimated systematic uncertainty is 0.1 percent in the predicted vapor pressure.

Goff's equation is

$$\log_{10}(e_i) = -9.096936\,[273.16/(T-1)] - 3.56654 \log_{10}(273.16/T) + 0.876817\,(1-T/273.16) + 0.786118 \qquad (8)$$

where e_i = saturation vapor pressure of pure ice, millibar

T = absolute temperature, kelvins.

This equation does not give the identical value of e_s at the triple point as that of water used above 0 °C (see [25], but the difference, 1×10^{-4} mbar, is negligible in the context of this paper.

3.5. Theoretical Smoothing Function for B_{aw}

In order to obtain an equation for the interpolation and extrapolation of B_{aw} versus t, the Lennard-Jones (12–6) potential was fitted to the mean, experimentally based values of B_{aw} found in tables 2 and 3, yielding the calculated values of table 4. The potential parameters are $b_o = 51.994$ cm³/mol, and $\epsilon/k = 143.513$ K. The data are not randomly distributed about the predicted curve; however, within the error limits assigned in section 5.2, this is not significant.

The analysis of Hanley and Klein [26] shows that, given a LJ (12–6) fit to data within the region where the reduced temperature T^* is between approximately 2.0 and 10.0, any two- or three-parameter function can be fitted equally well to the data. Furthermore, in this situation, extrapolation much beyond the experimental

TABLE 2. *Summary of experimental conditions and results*

Saturation temp. °C	Saturation vap. press. mb	Total press. bar	Mole fraction water vapor	Enhancement factor [a]	Interaction virial coeff. cm³/mol	Normalized [b] inter. vir. coefficient cm³/mol
t	e_s	P	x_w	f	B_{aw}	B_{aw}
70.0067	311.7533	24.0502	0.013640	1.0523	−16.59	−16.61
70.0007	311.6726	29.5089	.011258	1.0659	−18.25	−18.25
69.9952	311.5984	32.8965	.010172	1.0739	−17.84	−17.83
69.9991	311.6510	34.9783	.0096093	1.0785	−18.18	−18.18
					Mean =	−17.72
					std. dev. of mean =	0.38
−10.0043	2.595475	19.9975	.00014031	1.0857	−40.47	−40.46
−10.0000	2.596456	29.0621	.00010028	1.1268	−41.17	−41.17
					Mean =	−40.82
					std. dev. of mean =	0.35
−20.0125	1.03023	19.9953	.000056020	1.0873	−43.29	−43.29

[a] $f = x_w P/e_s$

[b] By noting the slope of B_{aw} versus t, one adjusts the values of the previous column to correspond to exactly 70, −10, or −20 °C.

region, particularly toward lower temperatures, may be hazardous.

For our experiments, $1.76 < T^* < 2.40$, with two of the six points being below $T^* = 2.0$. We verified that (9–6) and (24–6) potential fits produced, to well within experimental accuracies, the same results as the (12–6) fit from at least −50 to +90 °C, then dropped them from further consideration. The extrapolations probably could be extended upwards by another 20 or 30 °C with little change in the accuracy. However, because of the potential hazards of extrapolating downwards, we feel that assigning errors below −50 °C would be meaningless.

TABLE 3. *Mean values and uncertainties of the experimental NBS virial coefficients at 30, 40, and 50 °C* [2]

t	$\bar{B}_{aw}^{(a)}$	$\bar{\sigma}^b$	Systematic error	$3\sigma +$ syst.
°C	cm³/mol	*Percent*	*Percent*	*Percent*
30	−29.2	0.6	4	5.8
40	−26.3	.7	4	6.1
50	−23.6	1.4	6	10.2

[a] From [2].
[b] $\bar{\sigma}$ = standard deviation of the mean value of $\bar{B}_{aw}$.

TABLE 4. *Results of fits to* B_{aw}[a]

t	B_{aw}, from I.J(12–6) cm³/mol	B_{aw}, from eq (9) cm³/mol
°C		
−50	−58.0	−58.0
−40	−53.0	−52.9
−30	−48.4	−48.4
−20	−44.2	−44.2
−10	−40.4	−40.5
0	−37.0	−37.0
+10	−33.8	−33.8
20	−30.9	−30.9
30	−28.2	−28.2
40	−25.7	−25.6
50	−23.3	−23.3
60	−21.2	−21.2
70	−19.2	−19.2
80	−17.3	−17.3
90	−15.5	−15.5

[a] From I.J (12–6) fit to data of tables 2 and 3, $b_o = 51.9941$ cm³/mol and $\epsilon/k = 143.513$ K.

In most cases it would be easier to use a polynomial representation of B_{aw} versus t, rather than to interpolate tables of Lennard-Jones values. Accordingly, the values predicted from the Lennard-Jones fit (column 2 of table 4), using the method of least squares, were fitted to a polynomial function of Celsius temperature, resulting in the equation

$$-B_{aw} = 36.98928 - 0.331705t + 0.139035 \cdot 10^{-2}t^2 - 0.574154 \cdot 10^{-5}t^3 + 0.326513 \cdot 10^{-7}t^4 - 0.142805 \cdot 10^{-9}t^5 \text{ cm}^3/\text{mol}, \quad (9)$$

valid for $-50 < t < 90$ °C. The values predicted by eq (9) are given in the final column of table 4.

The maximum difference between the rounded values of eq (9) and the Lennard-Jones values, is seen to be 0.1 cm³/mol. Equation (9) supercedes eq (37) of [2].

4. Uncertainties in B_{aw}

In this section are presented, first, a discussion of the uncertainties in the experimentally-based values of B_{aw}, and second, a discussion of the uncertainties in the predicted values.

4.1. Uncertainties in the Experimentally Derived Values

a. Contribution from Measured Quantities

At 70 °C, the systematic uncertainties from the measured quantities may all be placed into the measured enhancement factor, as was done in [2]. The systematic uncertainty in the measured enhancement factor is 0.07 percent just as it was for the 30, 40, and 50 °C values of [1]. This includes all but inconsequential effects from pressure, temperature (and through it, the saturation vapor pressure), and mole fraction of water vapor (as determined from the measured mixed ratio), and contributes an estimated 2 percent systematic uncertainty to B_{aw}.

The standard deviation of the mean value is used as the measurement of the random uncertainty of the 70 °C value of B_{aw}. As seen in table 2, this amounts to 2 percent. The first of the tabulated 70 °C results appears low relative to the others; if it were dropped from consideration, the standard deviation of the mean would decrease to 0.7 percent. However, there seems to be no valid reason for rejecting the point. (Note that, in table 7, the overall uncertainty would become 7 percent instead of 12 percent.)

The remaining discussion in this section applies to the −10 and −20 °C experiments. The standard deviations for the pressure and temperature measurements are the standard deviations of the means obtained during the experiments, while the standard deviations of the mixing ratios are based on the standard deviations of the weighings of the water absorption tubes and of the air containers.

The systematic uncertainty in the temperature measurements is the sum of estimated systematic uncertainties in the instrumentation, in the ice point resistance of the resistance thermometer, and in the resistance versus temperature curves used to represent the thermometer calibration data, plus an allowance of 0.005 °C for the possible deviation of the measured temperature from the temperature of saturation.

The systematic pressure uncertainty is primarily the sum of estimated systematic uncertainties in the curve used to represent the calibration of the manometer, in the manometer zero reading, plus small contributions from other corrections associated with the manometer.

The assigned systematic errors in the mixing ratio account for the possibility of water passing unabsorbed through the U-tubes [5], plus small contributions from the bouyancy corrections applied to the air containers during weighing and the effects of different starting and finishing pressures in the high-pressure lines.

Table 5 summarizes the experimental error sources and magnitudes, and the errors they induce in B_{aw}, for the experiments at −10 and −20 °C.

b. Contributions from Calculated Quantities

The error contributions from the various calculated quantities were obtained by changing the quantity by the amount of its estimated error, recalculating B_{aw}, and comparing with the originally calculated value.

Sengers et al. [16] estimate the 3σ error in B_{aa} to be 1.2 cm³/mol. Uncertainties in B_{ww}, C_{aaa}, and C_{www}, were estimated by comparing available data, as described in [2], or, in the cases of C_{aaw} and C_{aww}, arbitrarily selected to indicate possible error magnitudes. The intent was to be conservative, but that cannot be guaranteed. The estimated uncertainties associated with the various virial coefficients are summarized in table 6, along with the systematic errors they induce in B_{aw}. Table 6 similarly lists the effects of the uncertainties in the Henry's and gas constants, and in the saturation vapor pressure. Below 0 °C, we indicate separately the error arising from use of eq (8). Above 0 °C, the 60 ppm error associated with the vapor pressure equation [25] was lumped into the experimental vapor pressure error. The final column of table 6 combines all contributions by quadrature, that is, the square root of the sums of the squares. This is

TABLE 5. *Experimental errors at −10 and -20 °C*

Nominal run conditions		Parameter	Estimated systematic errors			3σ-Random errors		
			Parameter uncertainty	Induced B_{aw} error		Parameter uncertainty	Induced B_{aw} error	
t(°C)	P(bar)			cm³/mol	Percent		cm³/mol	Percent
−10	20	t	0.017 °C	0.81	2.00	0.0003 °C	0.01	0.03
		P	.0172 bar	.43	1.06	.00041 bar	.10	.25
		r[a]	.07%	.38	.94	.11%	.59	1.46
				$\sum$ = 1.62	4.00		Quad[b] = 0.60	1.48
−10	30	t	0.017 °C	0.55	1.33	0.0003 °C	0.03	0.07
		P	.0159 bar	.18	.44	.0062 bar	.07	.17
		r	.09%	.30	.72	.10%	.43	1.04
				$\sum$ = 1.03	2.49		Quad = 0.44	1.06
−20	20	t	0.017 °C	0.82	1.89	0.0015 °C	0.07	0.1
		P	.0172 bar	.41	.95	.0041 bar	.10	.23
		r	.14%	.72	1.66	.10%	.51	1.18
				$\sum$ = 1.95	4.50		Quad = 0.52	1.21

[a] r = Mass water/mass air, g/g
[b] Combined by quadratures, i.e., the square root of the sum of the squares.

TABLE 6. *Systematic uncertainties in B_{aw} from calculated parameters*

Temp.	Press.	Source of error								Quadrature
		B_{aa}	B_{ww}	C_{aaa}	C_{www}	C_{aaw}	C_{aww}	Other	e_s	
		Estimated error in source, percent								
		[a]	6	15	46	50	50	[b]	–	
°C	bar	Estimated error in B_{aw}, percent								
70	24.1	3.26	1.54	0.44	0.36	1.27	2.25	0.14	–	4.47
		Estimated error in source, percent								
		[a]	100	20	100	150	150	[b]	0.1	
		Estimated error in B_{aw}, percent								
−10	20.0	1.34	0.31	0.41	0.00	3.11	0.19	0.16	1.34	3.69
−10	29.1	1.42	.43	.29	.00	2.22	.18	.16	0.88	2.84
−20	20.0	1.32	.20	.29	.00	2.22	.09	.16	1.19	2.87

[a] Estimated 3σ error is 1.2 cm³/mol.
[b] Quadrature of errors contributed by Henry's law, gas constant, and ignoring the correction to the law of ideal solutions.

justified on the basis that it is unlikely that all errors will contribute, in the same sign sense, to the uncertainty in B_{aw}.

Table 7 summarizes the systematic and random errors in the experimentally derived values of B_{aw}. The estimated contributions from the experimental and calculated parameter systematic sources are shown separately, then combined into a total systematic uncertainty in column 6. The estimated overall uncertainty at 70 °C is 12 percent. At −10 °C, both a calculated and observed estimate of the experimental random errors are available, leading to two estimates of the total error which are in good agreement. The larger estimate is 7 percent. At −20 °C, the total uncertainty is 6 percent.

4.2. Uncertainties in the Predicted Values of B_{aw}

The maximum error bands placed on the predicted values of table 4 reflect the maximum estimated uncertainties in the experimental quantities. For $-50 \leq t < 0$ °C, error bands of ±10 percent have been assigned. This is larger than the 7 percent estimate given in table 7, but since the errors associated with various other virial coefficients are only crude estimates in this region it is felt that the additional 3 percent on the error band is warranted. For $0 \leq t < 45$ °C, a 6 percent error band is assigned, commensurate with the estimated uncertainties of table 3. Above 45 °C, the error band is again increased to 10 percent. All experimental points lie within the error band of the predicted values, and vice versa. If either or both experimental end points (−20 or 70 °C) are omitted, the resultant LJ (12–6) fit still lies within the assigned bands over the entire range of interest.

5. Enhancement Factors

The enhancement factor is defined by eq (1).

To obtain the enhancement factor at a given (P, T) condition, one replaces the f in eq (A–4) of the appendix by eq (1), solves by iteration for x_a, then converts back to f through eq (1).

Table 8 gives the results of such calculations. The

TABLE 7. *Summary of errors in experimentally derived values of* B_{aw}

Temp.	Error source				
°C	Experimental random, $3\bar{\sigma}$[a]	Experimental systematic	Calc. parameters systematic	Quadrature of systematics	Overall quad. syst. $+3\bar{\sigma}$
	Error in B_{aw}, percent				
70	6.42	2.38	4.47	5.06	11.5
−10[b]	1.26	3.24	3.26	4.59	5.9
−10[c]	2.57	3.24	3.26	4.59	7.2
−20	1.21	4.49	2.87	5.33	6.5

[a] $\bar{\sigma}$ = Standard deviation of mean value.
[b] Based on means of the calculated uncertainties at 20 and 29 bar, tables 5 and 6.
[c] Random from the observed $\bar{\sigma}$ of table 2.

TABLE 8. *Predicted enhancement factors*

Total pressure bars	t °C							
	−80[a]	−70	−60	−50	−40	−30	−20	−10
0.25	1.0020	1.0018	1.0016	1.0014	1.0013	1.0012	1.0012	1.0012
.50	1.0041	1.0036	1.0032	1.0029	1.0026	1.0024	1.0022	1.0022
1.00	1.0082	1.0072	1.0064	1.0058	1.0052	1.0047	1.0044	1.0041
1.50	1.0123	1.0109	1.0097	1.0086	1.0078	1.0071	1.0065	1.0060
2.00	1.0165	1.0145	1.0129	1.0116	1.0104	1.0094	1.0086	1.0080
2.50	1.0207	1.0182	1.0162	1.0145	1.0130	1.0118	1.0108	1.0099
3.00	1.0249	1.0219	1.0195	1.0174	1.0156	1.0141	1.0129	1.0119
3.50	1.0291	1.0256	1.0228	1.0203	1.0183	1.0165	1.0150	1.0138
4.00	1.0334	1.0294	1.0261	1.0233	1.0209	1.0189	1.0172	1.0158
4.50	1.0377	1.0332	1.0294	1.0262	1.0236	1.0213	1.0194	1.0177
5.00	1.0420	1.0369	1.0327	1.0292	1.0262	1.0237	1.0215	1.0197
10.00	1.0865	1.0758	1.0669	1.0595	1.0533	1.0480	1.0435	1.0396
20.00	1.184	1.160	1.140	1.124	1.110	1.099	1.089	1.080
30.00	1.293	1.252	1.220	1.193	1.171	1.153	1.138	1.124
40.00	1.417	1.356	1.307	1.269	1.237	1.211	1.189	1.170
50.00	1.556	1.470	1.403	1.350	1.307	1.272	1.243	1.218
60.00	1.71	1.60	1.51	1.44	1.38	1.337	1.300	1.268
70.00	1.89	1.74	1.62	1.53	1.46	1.41	1.360	1.321
80.00	2.10	1.90	1.75	1.64	1.55	1.48	1.42	1.377
90.00	2.33	2.08	1.89	1.75	1.64	1.56	1.49	1.44
100.00	2.59	2.27	2.05	1.88	1.75	1.64	1.56	1.50

See footnote at end of table.

TABLE 8.
Predicted enhancement factors—Continued

Total pressure bars	0 °C	
	Ice	Water
0.25	1.00132	1.00131
.50	1.00221	1.00217
1.00	1.0040	1.0039
1.50	1.0057	1.0056
2.00	1.0075	1.0074
2.50	1.0093	1.0091
3.00	1.0111	1.0108
3.50	1.0129	1.0126
4.00	1.0146	1.0144
4.50	1.0164	1.0161
5.00	1.0182	1.0179
10.00	1.0364	1.0356
20.00	1.074	1.072
30.00	1.113	1.111
40.00	1.154	1.151
50.00	1.197	1.193
60.00	1.242	1.237
70.00	1.289	1.282
80.00	1.338	1.330
90.00	1.389	1.381
100.00	1.44	1.43

TABLE 8. *Predicted enhancement factors*—Continued

Total pressure, bars	*t* °C								
	10	20	30	40	50	60	70	80	90
0.25	1.00148	1.00173	1.00202	1.00223	1.00211	1.00111			
.50	1.00229	1.00251	1.00284	1.00323	1.00358	1.00362	1.00288	1.00051	
1.00	1.00388	1.00400	1.00426	1.00467	1.00519	1.00571	1.00599	1.00564	1.00394
1.50	1.0055	1.00547	1.00564	1.00599	1.00651	1.00713	1.00772	1.00801	1.00754
2.00	1.0071	1.0069	1.00701	1.00728	1.00775	1.00839	1.00910	1.00968	1.00980
2.50	1.0087	1.0084	1.0084	1.0086	1.0090	1.00959	1.01034	1.01108	1.01154
3.00	1.0103	1.0099	1.0097	1.0098	1.0102	1.0108	1.01151	1.01234	1.01300
3.50	1.0119	1.0114	1.0111	1.0111	1.0114	1.0119	1.0125	1.01351	1.01432
4.00	1.0135	1.0128	1.0125	1.0124	1.0126	1.0130	1.0138	1.0146	1.01553
4.50	1.0151	1.0143	1.0138	1.0136	1.0138	1.0142	1.0149	1.0157	1.0167
5.00	1.0167	1.0158	1.0152	1.0149	1.0150	1.0153	1.0159	1.0168	1.0178
10.00	1.0330	1.0308	1.0290	1.0277	1.0269	1.0265	1.0266	1.0271	1.0280
20.00	1.066	1.0615	1.0573	1.0539	1.0512	1.0493	1.0480	1.0474	1.0474
30.00	1.101	1.093	1.087	1.081	1.076	1.073	1.0698	1.0680	1.0670
40.00	1.138	1.126	1.117	1.109	1.102	1.096	1.092	1.0890	1.0869
50.00	1.175	1.161	1.148	1.137	1.128	1.121	1.115	1.111	1.107
60.00	1.215	1.196	1.180	1.167	1.155	1.146	1.139	1.133	1.128
70.00	1.256	1.233	1.213	1.197	1.183	1.172	1.163	1.155	1.149
80.00	1.298	1.271	1.248	1.228	1.212	1.198	1.187	1.178	1.171
90.00	1.343	1.311	1.284	1.261	1.242	1.226	1.212	1.202	1.193
100.00	1.389	1.352	1.320	1.294	1.272	1.254	1.238	1.226	1.216

[a] Values below −50 °C are based on a questionable extrapolation of B_{aw}. They are given as a matter of interest, but no error bands can be assigned.

lowest tabulated pressures at 70, 80, and 90 °C are exceeded by the saturation vapor pressure, precluding the existence of a saturation equilibrium condition. The enhancement factors calculated under those conditions are meaningless in the context of this paper, and have been omitted.

In the error discussion to follow, no attempt was made to assign uncertainties below −50 °C, for reasons discussed in section 3.

However, as a matter of interest, table 8 has been extrapolated to −80 °C. The necessary B_{aw} extrapolation used the Lennard-Jones (12–6) relationship, not eq (9).

For those interested in interpolation, note that, at low pressures, the enhancement factors increase rapidly as the pressure increases from the value of the saturation vapor pressure. The slope then suddenly decreases, the curve becoming more linear. The location of the slope change along the pressure axis, no greater than about 3 bar for the temperatures considered here, is a function of temperature.

578-011 O - 75 - 2

6. Uncertainties in the Predicted Enhancement Ratios

In section 4, the contributions to the B_{aw} uncertainty from various calculated quantities (virial coefficients, saturation vapor pressure, etc.) were outlined. When the uncertainty in B_{aw} is considered as one computes the uncertainties in the predicted enhancement factors, the contributions from the remaining parameters are directly included, as part of the B_{aw} error. Therefore, the only quantity of concern in calculating the uncertainty in the predicted enhancement factors of table 8 is the interaction coefficient B_{aw}. For table generation, pressure and temperature are considered exact. At −50 °C and above the significant figures are given to the place which is affected by the maximum uncertainty (table 9) by no more than five units, plus one more place.

Table 9 outlines the estimated uncertainty in the predicted enhancement factors as a function of pressure and temperature. Linear interpolation of the errors, between adjacent tabulated pressure along the isotherm, allows error estimates to within 0.05 percent.

It is important to reemphasize that, below −50 °C, the error bands are considered unknown and, at present, unobtainable. Research at temperatures below −20 °C will be needed for further B_{aw} extrapolation and bracketing of the enhancement factors.

TABLE 9. *Estimated maximum percentage uncertainties in calculated* f [a]

P bar	Temperature, °C							
	90	70	50	30	+10	−10	−30	−50
1.00	0.001	0.01	0.01	0.01	0.03	0.04	0.05	0.06
2	.01	.02	.03	.03	.06	.07	.10	.13
3	.02	.03	.05	.04	.09	.11	.14	.19
4	.03	.05	.06	.05	.11	.15	.19	.25
5	.04	.06	.08	.07	.14	.18	.24	.32
10	.09	.13	.17	.13	.29	.37	.48	.64
20	.20	.26	.35	.27	.58	.75	.98	1.30
40	.41	.54	.70	.54	1.2	1.5	2.0	2.7
60	.62	.82	1.1	.82	1.8	2.3	3.1	4.2
80	.83	1.1	1.4	1.1	2.4	3.2	4.2	5.8
100	1.1	1.4	1.8	1.4	3.1	4.1	5.4	7.5

[a] No errors are assigned to values below −50 °C, nor should any attempt be made to do so.

7. Comparison With Other Work

Comparisons with other virial coefficient work may be found in [2].

The work of Goff [27] and Webster [28] are the two extensive experimentally based works with which we will compare our air-water vapor enhancement factors.

Table 10 compares selected high pressure data with Webster, while table 11 compares selected low pressure data with Goff. The disagreement with the former is within a factor of two of the NBS estimated maximum uncertainty except at −20 °C and 50 bar. However, the discrepancies will increase as the temperature decreases. The disagreement between NBS and Goff is within the NBS estimated uncertainty in all cases, ranging from 0.01 percent at 0.25 bar to 0.05 percent at 1 bar.

TABLE 10. *Comparison of* f*-values with Webster*

P bar		Temperature, °C		
		−20	0	+50
50	Webster	1.36	1.24	1.14
	NBS	1.243	1.193	1.128
	Difference, percent	9.4	3.9	1.1
100	Webster	1.75	1.50	1.28
	NBS	1.563	1.433	1.272
	Difference, percent	12.0	4.7	0.6

TABLE 11. *Comparison of* f*-values with Goff*

P bar		Temperature, °C				
		60	20	0	−20	−50
0.25	Goff	—	1.0018	1.0014	1.0013	1.0015
	NBS	1.0011	1.0017	1.0013	1.0012	1.0014
0.50	Goff	—	1.0027	1.0024	1.0024	1.0030
	NBS	1.0036	1.0025	1.0022	1.0022	1.0029
1.00	Goff	1.0060	1.0045	1.0044	1.0048	1.0060
	NBS	1.0057	1.0040	1.0040	1.0044	1.0058

8. Summary

New experimental enhancement factor data at −20, −10, and +70 °C, coupled with previously reported values at 30, 40, and 50 °C, have been used to obtain the air-water vapor interaction virial coefficient, B_{aw}, at those temperatures. The B_{aw} values have in turn been fitted by a Lennard-Jones (12–6) potential, to permit extrapolation and interpolation. An empirical equation for B_{aw} versus temperature is also given. Either equation predicts values considered uncertain by no more than 10 percent, for $-50 \leq t \leq 0$ °C and for $45 \leq t \leq 90$ °C. For $0 \leq t \leq 45$ °C, the uncertainty is 6 percent. Using these B_{aw} values, enhancement factors have been derived for air over ice from −50 to 0 °C, and for air over water from 0 to +90 °C, at 10 °C intervals, and at varying pressure intervals from 0.25 to 100 bar. The associated uncertainties vary according to condition, and are best seen in table 9. Extrapolations of the enhancement factor, to −80 °C for air over ice, are presented, but no uncertainties are assigned.

We thank the members of the Office of Weights and Measures of the NBS, and Harry Johnson in particular, for their patience and assistance during our weighings of the air containers on the Russell balance.

9. Appendix

The derivation of eq (12) of [2], which refers only to the gas phase, begins with

$$\mu_i = \frac{\partial G_i}{\partial n_i}, \qquad \text{(A-1)}$$

where μ and n are the chemical potential and number of moles of water vapor, and G the Gibbs function, associated either with the mixture ($i = m$) or pure water vapor ($i = w$).

Equation (A-2) evaluates the Gibbs function difference between the saturated equilibrium state at pressure P and a reference state at pressure P_o.

$$G_i\ (T, P, n_a, n_i) - G_i\ (T, P_o, n_a, n_i) = \int_{P_o}^{P} V_i dP \qquad \text{(A-2)}$$

where n_a is the number of moles of air and V_i the volume of the gas under consideration at temperature T. The volumes V_i are obtained from the appropriate virial equation of state. (Note, however, that the magnitudes of n_i differ in the expressions for V_m and V_w).

The right side of (A-2) is evaluated for the mixture between P_o and the saturated equilibrium pressure P, and for pure water vapor between P_o and the saturation vapor pressure e_s. Equation (A-1) yields the corresponding chemical potential differences. By subtracting the results of these operations and rearranging, one obtains the chemical potential difference $\Delta\mu$ of the water vapor between the equilibrium conditions at pressure P in the mixture and e_s in the pure phase.

Let P_o be low enough so that both the mixture and pure water vapor can be considered as ideal gases in the reference state. The term $\mu_m\ (T, P_o, n_a, n_m)$ appearing in the expression for $\Delta\mu$ can be written as

$$\mu_m(T, P_0, n_a, n_m) = \mu_m(T, P_0, 0, n_m) + RT \ln x_w \qquad \text{(A-3)}$$

where x_w is the mole fraction of water vapor. Then, since in the ideal gas limit $\mu_m(T, P_0, 0, n_m)$ cancels a similar term, $-\mu_w(T, P_0, 0, n_w)$, and since all nonideal contributions become negligible when the integrals of (A-2) are evaluated at $P = P_0$, one is left with eq (12) of [2], with the left side replaced by $\Delta\mu$. Two wrong signs appearing in eq (12) are corrected in eq (29a) of [2]. Equation (29a), reproduced here as eq (A-4), is used for the general calculation of the enhancement ratio, after substituting for f its definition, eq (1) of this paper. The procedure is one of iteration, to solve for the mole fraction of air, x_a. This same equation may be inverted into a quadratic form in B_{aw}, to permit evaluation of B_{aw} from experimental enhancement factor data, as was done in [2].

$$\begin{aligned} RT \ln f = {} & g(T,P) + RT \ln (1 - kx_aP) + B_{aa}x_a^2P \\ & - B_{ww}(P - e_s - x_a^2P) + C_{aaa}\frac{x_a^3P^2}{RT} \\ & + C_{aaw}\frac{3x_a^2(1-2x_a)P^2}{2RT} - C_{aww}\frac{3x_a^2(1-x_a)P^2}{RT} \\ & - B_{aa}^2\frac{3x_a^4P^2}{2RT} - C_{www}\frac{(1+2x_a)(1-x_a)^2P^2 - e_s^2}{2RT} \\ & - B_{aa}B_{ww}\frac{x_a^2(1-3x_a)(1-x_a)P^2}{RT} \\ & - B_{ww}^2\frac{e_s^2 - (1+3x_a)(1-x_a)^3P^2}{2RT} \\ & + B_{aw}\left[-2x_a^2P - B_{aa}\frac{2x_a^3(2-3x_a)P^2}{RT}\right. \\ & \left. + B_{ww}\frac{6x_a^2(1-x_a)^2P^2}{RT}\right] \\ & - B_{aw}^2\frac{2x_a^2(1-x_a)(1-3x_a)P^2}{RT} \end{aligned} \qquad \text{(A-4)}$$

where B_{aa}, B_{ww} = the second virial coefficients for air and water, cm³/mol

B_{aw} = the second interaction virial coefficient for air-water vapor mixtures, cm³/mol

C_{ijk} = third virial coefficients for air and water ($i=j=k$), or third interaction virial coefficients (cm³/mol)²

R = universal gas constant, 83.1434 bar-cm³/mol-K

T = absolute temperature, K

P = total pressure, bar

e_s = saturation vapor pressure of the pure condensed water phase, bar

x_a = mole fraction of air in the gas mixture

k = Henry's "constant," mol fraction/bar

$g(T, P)$ = the product of the specific volume of pure phase, at the given (T, P) condition, and the difference ($P - e_s$).

one needs, in addition to other equations given in this paper, the following relationships, discussed in [2]:

$$B_{ww} = 33.97 - \frac{55306}{T} \times 10^{\frac{72000}{T^2}}\ \text{cm}^3/\text{mol} \qquad \text{(A-5)}$$

$$C_{www} = 2.85558\,\frac{B_{ww}^3}{T} + B_{ww}^2\ \text{cm}^6/\text{mol}^2 \qquad \text{(A-6)}$$

$$\begin{aligned} C_{aww} \times 10^{-6} = {} & -0.20263 + 0.52695 \cdot 10^{-2}t \\ & - 0.74761 \cdot 10^{-4}t^2 \\ & + 0.57576 \cdot 10^{-6}t^3 \\ & - 0.18065 \cdot 10^{-8}t^4\ \text{cm}^6/\text{mol}^2 \end{aligned} \qquad \text{(A-7)}$$

t = degrees Celsius, $T = t + 273.16$

Equations (A–5) and (A–6) are modifications of Goff's equations [27], which are based on IPTS–48. Use of $T=t+273.15$ causes insignificant changes in the results of this paper (see sec. 2).

10. References

[1] Hyland, R. W., and Wexler, A., The enhancement of water vapor in carbon dioxide-free air at 30, 40, and 50 °C, J. Res. Nat. Bur. Stand. (U.S.), **77A** (Phys. and Chem.), No. 1, 115–131 (Jan.–Feb. 1973).

[2] Hyland, R. W., and Wexler, A., The second interaction (cross) virial coefficient for moist air, J. Res. Nat. Bur. Stand. (U.S.), **77A** (Phys. and Chem.), No. 1, 133–147 (Jan.–Feb. 1973).

[3] Greenspan, L., Low frost-point humidity generator, J. Res. Nat. Bur. Stand. (U.S.), **77A** (Phys. and Chem.), No. 5, 671–677 (Sept.–Oct. 1973).

[4] Russell, H. H., The NBS 1000 lb balance, Report of the 40th Nat'l. Conf. on Wts. and Meas., Nat. Bur. Stand. Misc. Pub. 216 (1955).

[5] Wexler, A., and Hyland, R. W., The NBS standard gravimetric hygrometer (NBS monograph 73, May 1, 1964); also see A. Wexler and W. A. Wildhack, Eds., Humidity and Moisture, Vol. **III** (Reinhold Publishing Corp., New York, 1964), p. 389.

[6] Stimson, H. F., International temperature scale of 1948, J. Res. Nat. Bur. Stand. (U.S.), **42,** 209–217 (March 1949) RP1962.

[7] The International Practical Temperature Scale of 1968, Metrologia **5,** 35 (1969).

[8] Harrison, L. P., Fundamental concepts and definitions, Humidity and Moisture, Vol. **III,** A. Wexler and W. A. Wildhack, Eds. (Reinhold Publishing Corp., New York, 1964), p. 8.

[9] Ginnings, D. C., and Corruccini, R. J., An improved ice calorimeter—the determination of its calibration factor and the density of ice at 0 °C, J. Res. Nat. Bur. Stand. (U.S.), **38,** 583–591 (June 1947) RP1796.

[10] Jakob, M., and Erk, S., Warmeausdehnung des Eises zwischen 0 und −253 °C, Wiss. Abh. Physik-Techn. Reichsanst. **12,** 301 (1928–29).

[11] Powell, R. W., Preliminary measurements of the thermal conductivity and expansion of ice, Proc. Roy. Soc. **A247,** 464 (1958).

[12] Butkovich, T. R., Thermal expansion of ice, J. App. Phys. **30,** 350 (1959).

[13] Dantl, Gerhard, Warmeausdehnung von H_2O- und D_2O-Einkristallen, Z. fur Phys. **166,** 115 (1962).

[14] LaPlaca, S., and Post, B., Thermal expansion of ice, Acta Cryst. **13,** 503 (1960).

[15] Leadbetter, A. J., The thermodynamic and vibrational properties of H_2O ice and D_2O ice, Proc. Roy. Soc. **A287,** 403 (1965).

[16] Sengers, J. M. H. L., Klein, M., and Gallagher, J. S. Pressure-volume-temperature relationships of gases: Virial coefficients, Report No. AEDC TR–71–39, Arnold Engineering Development Center, AFSC, Arnold Air Force Station, Tennessee (1971).

[17] Hilsenrath, J., et al., Tables of Thermal Properties of Gases, Nat. Bur. Stand. (U.S.), Circ. 564 (1955).

[18] Mason, E. A., and Monchick, L., Survey of the equation of state and transport properties of moist gases, Humidity and Moisture, Vol. **III,** A. Wexler and W. A. Wildhack, Eds. (Reinhold Publishing Corp., New York, 1965), p. 257.

[19] Loomis, A. G., Solubilities of gases in water, International Critical Tables, Vol. **3,** E. W. Washburn, Ed. (McGraw-Hill Book Co., New York, 1928), p. 255.

[20] Jones, H. B., Solubilities of various gases in water, Handbook of Chemistry and Physics, 33rd edition, C. D. Hodgman, Ed. (Chemical Rubber Publishing Co., Cleveland, Ohio, 1951), p. 1482.

[21] Dorsey, N. E., Properties of Ordinary Water Substance (Reinhold Publishing Corp., New York, N.Y., 1940).

[22] Wiebe, R., Gaddy, V. L., and Heins, C., Jr., The solubility of nitrogen in water at 50, 75, and 100 °C from 25 to 1000 atmospheres, J. Am. Chem. Soc. **55,** 947 (1933).

[23] Krichevsky, I. R., and Kasarnovsky, J. S., Thermodynamical calculations of solubilities of nitrogen and hydrogen in water at high pressures, J. Am. Chem. Soc. **57,** 2168 (1935).

[24] Goff, J. A., Saturation pressure of water on the new Kelvin scale, Humidity and Moisture, Vol. **III,** A. Wexler and W. A. Wildhack, Eds. (Reinhold Publishing Corp., New York, 1964), p. 289.

[25] Wexler, A., and Greenspan, L., Vapor pressure equation for water in the range 0 to 100 °C, J. Res. Nat. Bur. Stand. (U.S.), **75A** (Phys. and Chem.), No. 3. 213–230 (May–June 1971).

[26] Hanley, H. J. M. and Klein, M., On the selection of the intermolecular potential function: Application of statistical mechanical theory to experiment, Nat. Bur. Stand. Tech. Note 360 (1967).

[27] Goff, J. A., Standardization of thermodynamic properties of moist air, Heating, Piping and Air Cond. **21,** 118 (1949).

[28] Webster, T. J., The effect on water vapor pressure of superimposed air pressure, J. S. C. I. **69,** 343 (1950).

(Paper 79A4–858)

JOURNAL OF RESEARCH of the National Bureau of Standards—A. Physics and Chemistry
Vol. 79A, No. 4. July–August 1975

The Enthalpies of Combustion and Formation of Thianthrene

Walter H. Johnson

Institute for Materials Research, National Bureau of Standards, Washington, D.C. 20234

(May 12, 1975)

The enthalpy of combustion of thianthrene (diphenylene disulfide) has been determined in an oxygen-bomb calorimeter. The enthalpy of formation has been derived using data from the available literature. The results obtained are as follows:

$$C_{12}H_8S_2(c) + 17\ O_2(g) + 228\ H_2O(liq) = 12\ CO_2(g) + 2[H_2SO_4 + 115\ H_2O]\ (liq)$$

$$\Delta H_c^\circ(25\ ^\circ C) = -7253.27 \pm 1.40\ kJ/mol\ (-1733.65 \pm 0.33\ kcal/mol)$$

$$\Delta Hf^\circ(25\ ^\circ C) = 184.23 \pm 1.50\ kJ/mol\ (44.03 \pm 0.36\ kcal/mol)$$

A comparison is given of the results of this investigation with those of previous investigators.

Key words: Combustion; enthalpy; formation; heat; secondary standard; sulfur compound; thianthrene.

1. Introduction

This investigation is part of a program on the selection of secondary thermochemical standards. Because the combustion calorimetry of sulfur-containing compounds requires certain special techniques in order to obtain accurate enthalpy values there is need for a standard reference material which contains this element.

Thianthrene (diphenylene disulfide) has been proposed as a secondary standard for organic sulfur compounds. It is a solid, crystalline material, stable in moist air, has a very low vapor pressure, forms reasonably good pellets, can be ignited and burned completely without the need for an auxiliary substance and is available in high purity. It has been studied extensively and the values obtained by independent investigators are in good agreement.

In order to obtain reliable data for the heat of combustion of sulfur compounds, the bomb cavity must be lined with an inert material to prevent reaction with sulfuric acid, provision must be made for thorough mixing of the bomb solution following combustion of the sample, and the bomb atmosphere must contain some nitrogen to prevent the formation of sulfur dioxide [1].[1]

[1] Figures in brackets indicate the literature references at the end of the paper.

2. Materials

Thianthrene [2]

The sample was obtained from the Aldrich Chemical Company as sample 12,244–0. It was purified by nine passes through a zone-melting apparatus in an argon atmosphere; the impurities were concentrated in 1/3 of the sample which was rejected. The purified sample was a colorless crystalline material which was stable in air and was essentially non-hygroscopic.

An elemental analysis of the sample yielded the following values in wt percent:

	Found	Theoretical
C	66.64 ± 0.06	66.63
S	29.41 ± .20	29.64

Benzoic Acid

The benzoic acid used for the calibration experiments was Standard Reference Material (SRM) 39i.

[2] The source of certain materials are identified in order to adequately specify the experimental procedure. In no case does such identification imply recommendation or endorsement by the National Bureau of Standards, nor does it imply that the materials identified are the best available for the purpose.

Oxygen

The oxygen was obtained from the Matheson Company as Ultra-Pure Oxygen. A certificate of analysis furnished with the cylinder gave the major impurities in ppm as: Kr, 12.0; N_2, 3.0; Xe, 0.7; and N_2O, 0.8.

3. Apparatus and Procedure

The adiabatic rotating-bomb calorimeter, the control system and the method of temperature measurement have been described [2].

A sample of approximately 0.24 g was pressed into a pellet, weighed into a platinum crucible and placed in the crucible support of the bomb which contained 3.000 cm^3 of water. A 2-cm length of platinum wire, 0.075 mm in diameter, connected between the electrodes so that it was in contact with the sample, served as a fuse. The bomb was sealed and filled with 31.62 atm of oxygen without flushing. The temperature of filling was determined, the calorimeter jacket was evacuated and the bomb was heated electrically to 24.98 °C. The adiabatic temperature controls were put into operation and the system left overnight. On the following morning temperatures were observed at intervals of a few minutes during a 30-min initial rating period. The sample was ignited by discharging an 18,000 μF condenser, previously charged to 23 V, through the platinum wire fuse. The bomb was then rotated to mix the bomb solution. Thermal equilibrium was obtained after about 20 min and calorimeter temperatures were observed during a 40-min final rating period. Due to the heating effect of the electric current through the platinum resistance thermometer, a steady increase in temperature of approximately 0.001 K/h was observed during the rating periods.

The calorimeter was opened and the bomb removed. In three of the experiments the gaseous contents were passed through a weighed CO_2-absorption tube. The bomb was then opened and the liquid contents transferred to a weighed polyethylene bottle. Weighed aliquots were taken for titration with standard alkali to determine the total acid. The quantity of nitric acid was taken as the difference between the total acid and the theoretical quantity of sulfuric acid calculated from the mass of sample.

4. Results and Calculations

The results of the benzoic acid calibration experiments are given in table 1. The headings, in the order in which they appear in the tables are described as follows: *EEE-Std* is the effective energy equivalent of the standard empty calorimeter including the bomb and all internal platinum parts except the crucible; *Cv-cont(i)* is the heat capacity of the initial contents of the bomb including the crucible, sample, bomb solution, and oxygen; *Corr to tm* is a correction applied for deviation of the actual mean temperature of the experiment from 26.5 °C; *Corr-parts* is a correction applied for changes in the calorimeter system during the series of experiments; *EEE-actual* is the effective energy equivalent of the actual calorimeter system at the mean temperature of the experiment; *Temp rise* is the observed increase in temperature following ignition of the sample; *Q-total* is the total quantity of energy released, which is obtained as the product of *EEE-actual* and the *Temp rise*; *q-ign* is the electrical energy used to ignite the sample; *q-decomp* HNO_3 is the calculated quantity of energy required to decompose any nitric acid, formed from traces of nitrogen in the bomb atmosphere, into gaseous nitrogen, oxygen, and liquid water; *q-WC* is the Washburn Correction [3] used to correct the actual bomb process to the standard process with all reactants and products in their respective thermodynamic standard states at the actual final temperature; *q-corr to 28 °C* is a correction applied to correct the standard reaction at the actual final temperature to 28 °C, the selected final temperature; *Q-std react* is the energy evolved by the standard reaction at 28 °C, obtained as the sum of *Q-total* and the energy corrections. Division by the mass of sample yields ΔU_c° (28 °C) in J/g.

The calibration experiments (table 1) yield *EEE*-std

TABLE 1. *Results of the benzoic acid calibration experiments*

Expt. No.	495	524	525	526	527	529
EEE-Std....J/K...	2519.47	2519.63	2519.47	2519.70	2519.68	2519.46
Cv-cont(i)....J/K...	4.82	4.81	4.72	4.73	4.70	4.74
Corr to *tm*....J/K...	0.08	0.11	0.15	0.09	0.10	0.14
Corr-parts....J/K...	−.16	.00	.00	.00	.00	.00
EEE-actual....J/K...	2524.20	2524.55	2524.34	2524.52	2524.48	2524.34
Temp rise....K...	3.133364	3.108335	3.159280	3.089474	3.100061	3.173467
Q-total....J...	−7909.24	−7847.16	−7975.09	−7799.44	−7826.05	−8010.91
q-ign....J...	1.22	1.06	1.18	0.79	1.11	1.16
q-decomp HNO_3....J...	0.70	0.21	0.30	.47	0.17	0.84
q-WC....J...	6.26	6.20	6.29	6.16	6.13	6.36
q-corr to 28 °C....J...	−0.04	−0.04	−0.06	−0.03	−0.04	−0.06
Q-std react....J...	−7901.10	−7839.73	−7967.38	−7792.05	−7818.67	−8002.62
m_s....g...	0.299167	0.296843	0.301676	0.295038	0.296046	0.303011
ΔU_c°(28 °C)....J/g...	−26410.36	−26410.36	−26410.36	−26410.36	−26410.36	−26410.36
Mean, *EEE*-std....J/K...	2519.56					
sdm....	0.046					

TABLE 2. *Results of the thianthrene combustion experiments*

Expt. No.	533	534	536	538	539	543
EEE-Std ..... J/K...	2519.56	2519.56	2519.56	2519.56	2519.56	2519.56
Cv-cont(i) ..... J/K...	15.89	20.07	20.08	20.07	20.08	19.84
Corr to *tm* ..... J/K...	0.22	0.21	0.24	0.01	0.06	0.07
Corr-parts ..... J/K...	3.60	.00	.00	.00	.00	.00
EEE-actual ..... J/K...	2539.27	2539.84	2539.88	2539.64	2539.70	2539.47
Temp rise ..... K...	3.230779	3.217870	3.258237	2.991124	3.059317	1.095284
Q-total ..... J...	−8203.83	−8172.87	−8275.52	−7596.37	−7769.75	−2781.44
q-ign ..... J...	0.91	1.29	0.94	1.20	1.31	0.89
q-decomp HNO_3 ..... J...	9.39	8.19	6.62	9.99	7.47	3.61
q-WC ..... J...	4.98	7.00	7.06	6.70	6.82	3.78
q-corr to 28 °C ..... J...	0.01	0.01	0.02	0.00	0.00	−0.05
Q-std react ..... J...	−8188.53	−8156.38	−8260.88	−7578.47	−7754.15	−2773.22
m_s ..... g...	0.244666	0.243654	0.246746	0.226366	0.231675	0.082832
ΔU_c°(28 °C) ..... J/g...	−33468.15	−33475.25	−33479.23	−33478.85	−33469.91	−33479.89
Mean, ΔU_c°(28 °C) ..... J/g...	−33475.21					
sdm	2.08					

from the certificate value for benzoic acid, this value is then used in table 2 to determine ΔU_c°. The precision uncertainty is the standard deviation of the mean which is calculated as $\sqrt{\Sigma\Delta^2/n(n-1)}$ where Δ is the deviation of each value from the average and n is the number of experiments performed.

All calculations were performed by computer[3] and the values in the tables have been taken directly from the print-out. Due to rounding of the individual values from the print-out, the results obtained from the tabulated values may differ slightly from the more exact results obtained by the computer. For the benzoic acid calibration experiments the values of *EEE*-std were obtained by an iterative procedure from the mass of sample. The certified value for benzoic acid, Standard Reference Material (SRM) 39i under certificate conditions was taken as 26434 J/g; this reduces to −26410.36 J/g for ΔU_c° at 28 °C.

The following values were used in the computations

	Density/ g·cm^{-3}	Cp/J·g^{-1}K^{-1}	$\left(\frac{\partial U}{\partial P}\right)_t$/J·g^{-1}·atm^{-1}
Benzoic Acid	1.32	1.21	−0.0125
Thianthrene	1.44	1.50	−0.02

The unit of energy is the joule, for conversion from the conventional thermochemical calorie, one calorie is equivalent to 4.184 joules. The 1971 table of atomic weights has been used throughout this paper [4].

The results of the thianthrene combustion experiments are given in table 2 and correspond to the reaction:

$$C_{12}H_8S_2(c) + 17\,O_2(g) + 198\,H_2O(liq) = 12\,CO_2(g) + 2[H_2SO_4 + 100\,H_2O](liq) \qquad (1)$$

[3] The computer program originally prepared by Howard Shomate of the Naval Ordnance Test Station, China Lake, California, and later modified by G. T. Armstrong and E. J. Prosen of this bureau following the procedure of W. N. Hubbard, D. W. Scott, and G. Waddington [5].

$$\Delta U_c^\circ(28\ °C) = -33475.21 \pm 6.41\ J/g = -7241.20 \pm 1.40\ kJ/mol$$
$$\Delta H_c^\circ(25\ °C) = -7253.27 \pm 1.40\ kJ/mol\ (-1733.57 \pm 0.33\ kcal/mol)$$
$$\Delta Hf°(25\ °C) = 184.23 \pm 1.50\ kJ/mol\ (44.03 \pm 0.36\ kcal/mol)$$

The uncertainties assigned to ΔU_c° have been obtained by combination of 2 sdm for the calibration experiments with 2 sdm for the combustion experiments, 0.01 percent for the uncertainty in the certified value for benzoic acid and 0.01 percent for the effect of possible impurities in the sample.

The uncertainty assigned to $\Delta Hf°$ was obtained by combination of the uncertainty assigned to ΔU_c° with 0.01 percent in the values taken for the heats of formation of CO_2(gas), H_2O(liq), and H_2SO_4(aq) [6].

A comparison of the results of this investigation with other reported values is given in table 3. For this comparison the results have been adjusted to correspond to reaction (2) to conform to the other reported values.

$$C_{12}H_8S_2(c) + 17\,O_2(g) + 228\,H_2O(liq) = 12\,CO_2(g) + 2[H_2SO_4 + 115\,H_2O](liq) \qquad (2)$$

$$\Delta H_c^\circ(25\ °C) = -7253.59 \pm 1.42\ kJ/mol = -1733.65 \pm 0.34\ kcal/mol$$

TABLE 3. *Comparison with existing data*

Investigator	ΔH_c°(25 °C), kcal/mol	
Hubbard, Katz, and Waddington	−1733.15 ± 0.53	[7]
Keith and Mackle	−1732.87 ± .69	[8]
Sunner and Lundin	−1733.29 ± .28	[9, 10]
Hu, Yen, and Geng	−1733.40 ± .52	[11]
This investigation	−1733.65 ± .33	

It is interesting to note that in all cases the results are within the assigned uncertainty intervals. It would appear, therefore, that thianthrene would be a com-

pletely satisfactory substance for use as a secondary standard in the combustion calorimetry of sulfur-containing compounds.

This work was supported by the NBS Office of Standard Reference Materials.

5. References

[1] Sunner, S., Sartryck ur Svensk Kemisk Tidskrift **59,** 71 (1946).
[2] Prosen, E. J., and Johnson, W. H., in preparation. For a partial description of the calorimeter, see G. T. Armstrong and W. H. Johnson NBSIR 73–158 (July 1973).
[3] Washburn, E. W., Bur. Standards J. Res. Nat. Bur. Stand. (U.S.), **10,** 525–558 (1933) RP546.
[4] Commission on International Atomic Weights, Pure and Applied Chemistry (1971).
[5] Hubbard, W. N., Scott, D. W., and Waddington, G., J. Phys. Chem. **58,** 152 (1954).
[6] Wagman, D. D., Evans, W. H., Parker, V. B., Halow, I., Bailey, S. M., and Schumm, R. H., Selected Values of Chemical Thermodynamic Properties, Nat. Bur. Stand. (U.S.), Tech. Note 270–3, 268 pages (Jan. 1968).
[7] Hubbard, W. N., Katz, C., and Waddington, G., J. Phys. Chem. **58,** 142 (1954).
[8] Keith, W. A., and Mackle, H., Trans. Faraday Soc. **54,** 353 (1958).
[9] Sunner, S., and Lundin, B., Acta Chem. Scand. **7,** 1112 (1953).
[10] Sunner, S., Acta Chem. Scand. **17,** 728 (1963).
[11] Hu, J-H., Yen, H-K., and Geng, Y-L., Acta Chimica Sinica **32,** 242 (1966).

(Paper 79A4–859)

JOURNAL OF RESEARCH of the National Bureau of Standards—A. Physics and Chemistry
Vol. 79A, No. 4, July–August 1975

Unbound Water Content From Application of Adsorption Theory

William V. Loebenstein

Institute for Materials Research, National Bureau of Standards, Washington, D.C. 20234

(May 19, 1975)

It is standard procedure to fit an applicable isotherm equation to water vapor adsorption data using the method of least squares in arriving at a value for the surface area accessible to the water molecule. The least squares technique has been extended in the present investigation to determine, in addition and simultaneously, a "best value" for the zero-humidity sample weight of the material. The application is equally valid for desorption insofar as the zero-humidity weight is concerned, although the derived value for "surface area" from desorption data will be over-estimated in the general case because of hysteresis. There is no limitation on the range of humidities since the method is not restricted to the BET equation (i.e., between 0.1 and 0.3 r.h.). In fact, good agreement with the zero-humidity points measured experimentally has been obtained even from drying curves in which the relative humidity has been confined to the region above 50 percent. An iterative method is employed in the calculations for which computer assistance is especially adaptable. Fortran IV programs are included in the appendix whose use requires no extensive computer experience. A fraction of a second in computer processing time is all that is required for each determination.

Key words: Adsorption; computer application; desorption; dry weight determination; moisture content; surface area; water content; water vapor adsorption.

1. Introduction

What constitutes the dry weight of a solid has never been completely resolved. Some materials like hydroxide gels of aluminum, silicon, iron, etc., continue to lose water when evacuated at ambient temperatures and more so on heating, yet a trace of water always seems to remain. Other materials readily give up their water, but suffer irreversible changes in the process. This leads to the adoption of a concept of water of constitution as distinguished from excess water.

A novel approach to this problem of dry weight prediction is portrayed in this paper based on the assumption that adsorbed water is certainly not water of constitution, and, consequently, is excess. To establish the precise point of dryness, therefore, it is only necessary to determine the weight of the solid under conditions where the amount of physically adsorbed water would be zero. This is determined by fitting vapor adsorption theory to the experimental data by an unorthodox application of the least-squares technique.

Since the development in 1938 of the Brunauer, Emmett, and Teller (BET) multimolecular adsorption free-surface equation [1][1], many other adsorption isotherm theories [2, 3, 4, 5 6, 7] have appeared in the literature. Most of the resultant isotherm equations, despite their differences, shared certain important attributes:

(1) They were expressable in some linear form.
(2) Each equation possessed physically significant parameters which could be evaluated either from the slope or intercept of the experimental plot or a combination of both.
(3) These parameters bore a simple functional relationship with the specific surface of the adsorbent.

For these reasons, any such theory would appear to qualify as a candidate for prediction of dry weight in the method to be described.

At the onset of this study, no *a priori* preference was made of any one adsorption theory over the others, although, in practice, the BET equation is probably more widely used than all of the others combined. This reason alone would justify its inclusion among the theories selected. In addition to the BET, the other adsorption theories tested in this work were: the Polarization theory [6], Harkins and Jura (H-J) theory [3], and Polanyi's Potential theory [6].

It will be shown that the same experimental points that are normally employed using least-square methods to determine only the surface area of an adsorbent can, at the same time, be called upon to furnish an additional piece of information; namely, its dry weight.

[1] Figures in brackets indicate the literature references at the end of this paper.

2. Theoretical Development

(1) The BET [1] free-surface equation in its most familiar form may be represented as a linear function of the relative pressure:

$$y = a + bx \tag{1}$$

where x = relative pressure (humidity, where water vapor is the adsorbate) expressed as a dimensionless decimal such that $0 \leq x \leq 1$. The dependent variable y is, in itself, an expression:

$$y = x/[q\ (1-x)] \tag{2}$$

containing both x and q. The latter quantity represents the number of moles of adsorbate per g of adsorbent obtained under steady state conditions at the corresponding value of x.

The y-intercept, a, and slope, b, are the parameters $1/(q_m c)$ and $(c-1)/(q_m c)$, respectively. The quantity q_m, in turn, represents the number of moles of adsorbate required to constitute a monolayer and, as such, is proportional to the surface area. The c-value is related exponentially to an average energy of adsorption. In the conventional application of eq (1), the parameters a and b are evaluated from the experimentally obtained adsorption points (x, q) preferably by use of the method of least squares [8]. These "best" estimates of a and b are then used to obtain q_m and c. Finally, the surface area is obtained conventionally by multiplying q_m by an appropriate constant sometimes referred to as the "packing factor."

Most laboratory workers in surface chemistry are painfully aware of the fact that the good linearity of eq (1) is destroyed when the experimentally determined initial weight of the sample is in error. One should, therefore, expect that *the* best straight line would result only when a zero-point weight very close to the correct value is used in the calculations. This criterion was employed in the present investigation for determining the dry weight of a solid adsorbent when water vapor was the adsorbate. In other words, the humidified sample weights themselves, utilizing a least-squares technique, were permitted to determine that value of the dry weight, p, along with the usual two parameters a and b required to optimize the linearity:

If W_i represents the weight (in grams) of the sample at the ith point corresponding to a relative humidity x_i, the number of moles of water vapor adsorbed per g of dry adsorbent would be

$$q_i = \frac{W_i - p}{18p}. \tag{3}$$

The value of x_i is assumed to be error-free here as it is in the conventional derivation.

The residual, R_i, is the experimental error of the ordinate of the ith point as indicated by the difference $y_i - (a + bx_i)$. Equations (1), (2), and (3) may be combined to yield:

$$R_i = \frac{18x_i p}{(1-x_i)(W_i - p)} - (a + bx_i). \tag{4}$$

It is required to determine the values of the three parameters p, a, and b for which the sum of the squares of the residuals is a minimum.[2]

This amounts to solving three nonlinear simultaneous equations for these parameters given by eqs (5), (6), and (7):

$$\frac{\partial}{\partial p}\left[\sum_{i=1}^{n} R_i^2\right] = 0 \tag{5}$$

$$\frac{\partial}{\partial a}\left[\sum_{i=1}^{n} R_i^2\right] = 0 \tag{6}$$

$$\frac{\partial}{\partial b}\left[\sum_{i=1}^{n} R_i^2\right] = 0. \tag{7}$$

By taking the partial derivative of the summation with respect to p as indicated by eq (5), the result is eq (8):

$$a\sum_{i=1}^{n}\frac{x_i W_i}{(1-x_i)(W_i-p)^2} + b\sum_{i=1}^{n}\frac{x_i^2 W_i}{(1-x_i)(W_i-p)^2} - 18p\sum_{i=1}^{n}\frac{x_i^2 W_i}{(1-x_i)^2(W_i-p)^3} = 0. \tag{8}$$

In the same way, eqs (6) and (7) give rise to eqs (9) and (10), respectively.

$$an + b\sum_{i=1}^{n} x_i = 18p\sum_{i=1}^{n}\frac{x_i}{(1-x_i)(W_i-p)} \tag{9}$$

$$a\sum_{i=1}^{n} x_i + b\sum_{i=1}^{n} x_i^2 = 18p\sum_{i=1}^{n}\frac{x_i^2}{(1-x_i)(W_i-p)} \tag{10}$$

A cursory inspection of eqs (8), (9), and (10) discloses that the nonlinearity is ascribable entirely to the unknown parameter, p. In fact, the terms to the left of the equals signs in eqs (9) and (10), respectively, are identified with those obtained [8] in the "normalized" equations during the derivation of the least-square solution for a linear system. This observation suggests a relatively simple method for the simultaneous solution of eqs (8), and (9), and (10) for the parameters p, a, and b. An initial value p_1 is selected for p which is not quite as large as the lowest value of W_i. This value of p is substituted in eqs (9) and (10)

[2] This is rigorously valid only when the error represented by R_i has a normal (Gaussian) distribution over its entire range. Experience has confirmed that in the present application, this assumption is reasonably well approximated.

making it possible to solve them simultaneously for a and b which are then designated a_1 and b_1, respectively. The values of a_1, b_1, and p_1 are then substituted in the left side of eq (8). The resultant value is called Φ_1.

Since p_1 was initially selected to be somewhat high, it is decreased by a small predetermined amount to obtain its second iterative value, p_2. Corresponding values of a_2 and b_2 are again calculated from eqs (9) and (10), as before, and all three contribute to the determination of Φ_2 from eq (8). If Φ_2 has the same sign as Φ_1, it should be smaller in absolute value and the iterative process is repeated until there is a change in sign of Φ. At that point the incremental change in p is reduced to one-tenth of its previous value and its sign is automatically reversed. Again, the new direction is maintained with the smaller increment until the next change in sign of Φ is encountered. The process is repeated until negligible changes are obtained in successive values of p, a, and b while successive values of Φ approach zero in the limit. Usually this occurs within about 25 iterations and gives an estimate of surface area and goodness of fit as well as the dry weight of the sample.

The entire process has been programmed for computer operation (FORTRAN IV) and is given in the appendix (fig. A1) in a form used with a teletype time-sharing terminal.[3]

The values for the slope and the intercept were combined in the usual way at the end of each iteration by taking the reciprocal of their sum to obtain q_m. The factor $7.529 \times 10^4 m^2/mol$ was used [10] to convert q_m to surface area. Only the final value, however, after convergence was complete could be considered valid.

(2) The Harkins and Jura (H-J) isotherm equation.

A linear relationship based on a two-dimensional equation of state was proposed by Harkins and Jura [3]. It took the form

$$\omega = \frac{A}{q^2} - B \tag{11}$$

where

$$\omega = \ln (1/x) \tag{12}$$

while A and B are constants.

There are no relative humidity restrictions on its range of applicability. (This is in contrast to the more familiar BET equation valid only within the inclusive values from about 0.1 to 0.3.) The surface area applicable to the H-J equation is proportional to the square root of the parameter A. The proportionality constant is, of course, dependent upon the adsorbate and the temperature of the isotherm. The value used in this work corresponding to water vapor at 23 °C was $5.620 \times 10^4 m^2/mol$ [12].

Using the same procedure described for the BET theory, the least square normalized equations resulting from the H-J isotherm equation are:

$$\Phi = Ap \left\{ \sum_{i=1}^{n} \frac{W_i \omega_i}{(W_i - p)^3} - (18)^2 A p^2 \sum_{i=1}^{n} \frac{W_i}{(W_i - p)^5} + B \sum_{i=1}^{n} \frac{W_i}{(W_i - p)^3} \right\} \tag{13}$$

$$(18)^2 p^2 A \sum_{i=1}^{n} \frac{1}{(W_i - p)^2} - Bn = \sum_{i=1}^{n} \omega_i \tag{14}$$

$$(18)^2 p^2 A \sum_{i=1}^{n} \frac{1}{(W_i - p)^4} - B \sum_{i=1}^{n} \frac{1}{(W_i - p)^2} = \sum_{i=1}^{n} \frac{\omega_i}{(W_i - p)^2}. \tag{15}$$

The iterative procedure previously described was again resorted to and a computer program given in appendix (fig. A2) was tailored to accommodate the H-J equation. This resulted in converged estimates of dry weight and surface area while at the same time affording a measure of goodness of fit.

(3) Other Isotherm Equations

The Polarization Equation of deBoer and Zwikker [9]:

$$q = a' + b' \ln \omega \tag{16}$$

and the Polanyi Potential Theory [9]:

$$q = a'' + b'' \omega^{-1/3} \tag{17}$$

were both subjected to the same treatment as described for the other two theories and will be discussed in a later section.

3. Equipment and Procedures

The gravimetric adsorption equipment employed used a circulatory flow system and a means for supplying water vapor at predetermined humidities to the carrier gas as described in a recent publication [10]. A drying tube mounted vertically and filled with P_2O_5 supported on glass wool had a trap sealed to its lower end for holding back the phosphoric acid produced and isolating it from the gas stream during desiccation of a sample. The drying step was carried out at room temperature (23 °C) as were all of the humidity exposures. Drying was performed either initially or at the end of a humidity sequence, depending upon whether it was an adsorption or desorption series. The zero-humidity data were, of course, not used in the calculations and served only as experi-

[3] The Control Data "KRONOS" System (6000 series) high-speed digital computer required only about 1¼ s in a typical computation. The central computer time can be further shortened to about ⅛ s when several independent determinations are performed, since the compiling time (c.a. 1 s) need not be repeated. Similar results were obtained using the Sperry Rand "UNIVAC 1108" System.

Certain commercial materials and equipment are identified in this paper in order to specify adequately the experimental procedure. In no case does such identification imply recommendation or endorsement by the National Bureau of Standards, nor does it imply that the material or equipment identified is necessarily the best available for this purpose.

mental verification of the calculated values. Saturated salt solutions were used for obtaining the desired humidities, details of which were described previously [10]. However, any standard commercial equipment would work equally well in order to apply the technique in any particular case.

The order in which the experimental points are obtained is extremely important. They must be in a continually decreasing (desorption or drying) or in a continually increasing (adsorption) sequence to avoid hysteresis scanning loops [11].

Table 5 shows that even low area adsorbents respond well in dry weight prediction regardless of whether adsorption or desorption data are used.

The dry weights predicted in table 6 are significant because most of the data were collected at relative humidities above 50 percent. The ability to do this is especially valuable in nondestructive testing where complete dehydration might cause irreversible changes in the sample.

4. Results

Tables 1 through 6 summarize the results of several determinations. The grouping of the experiments helps to emphasize the capabilities as well as the limitations inherent in the method.

Most of the examples in table 1 give reasonably good agreement in surface area between BET and H-J. The experimentally measured dry weights, in the majority of cases, are slightly greater than the calculated values. This suggests the possibility that the last traces of physically adsorbed water may not have been completely removed by the experimental procedure used. In one instance this effect is rather striking.[4]

The two experiments involving barium glass[5] (water extracted) represent the initial and final adsorption sequence in an adsorption-desorption-adsorption cycle in which the relative humidity started at zero—went stepwise to saturation—then down to zero—and finally back up again to 0.334.

Good agreement between surface area predicted from desorption data with that from adsorption is not generally to be expected. Table 2 shows exceptions occur where hysteresis is either absent entirely or negligibly small.

Some insight may be deduced from the results of both isotherm equations even when only desorption (drying) data are available. Fair agreement between the "areas" as shown in the latter two examples of table 3 where hysteresis is known to be virtually nonexistent suggests that these values may be reasonably valid estimates of the true surface area.

Table 4 is self explanatory and shows consistency of both surface areas and predicted dry weights between widely different portions of the adsorption isotherm.

[4] See Cellulose Acetate Membrane (table 4).
[5] Corning Glass Company X95–1FD.

TABLE 1. *Adsorption*

Low humidity range (0.082 → 0.334)
Comparison of BET with H-J for the Same Data

Expt. No.		Surface area (m^2/g)	Dry weight (g)
A503094	Synthetic Hydroxyapatite (6 points)		
	Calculated:		
	BET	47.2	0.2708
	H-J	44.4	.2717
	Experimental		.2733
A444168	Activated Bentonite (5 points)		
	Calculated:		
	BET	181.4	.7161
	H-J	182.5	.7193
	Experimental		.7378
A444161	Polycarboxylate Cement (4 points)		
	Calculated:		
	BET	60.4	1.255
	H-J	61.3	1.241
	Experimental		1.249
A444143	Zinc Phosphate Cement (6 points)		
	Calculated:		
	BET	41.8	1.5646
	H-J	32.4	1.5703
	Experimental		1.5779

TABLE 1. *Adsorption*—Continued

Expt. No.		Surface area (m^2/g)	Dry weight (g)
A444155	Barium Glass—as received (6 points)		
	Calculated:		
	BET	3.22	1.2886
	H-J	3.15	1.2889
	Experimental		1.2895
A444156	Barium Glass—Water Extracted (4 points)		
	Calculated:		
	BET	8.7	0.9636
	H-J	4.6	.9648
	Experimental		.9649
A444175	Barium Glass—Water Extracted (6 points)		
	Calculated:		
	BET (no convergence)		—
	H-J	9.5	.9646
	Experimental		.9657
A444164	Zinc Oxide-Eugenol Cement (4 points)		
	Calculated:		
	BET (no convergence)		—
	H-J	5.2	3.1274
	Experimental		3.1297

TABLE 2. *Adsorption versus desorption*

Expt. No.	Hysteresis: Absent or minimal	Surface area (m^2/g)	Dry weight (g)
	Poly(methyl methacrylate) (Low Humidity range 0.082 → 0.334)		
A444065	Adsorption (5 points)		
	Calculated:		
	BET	30.4	3.5029
	H-J	24.9	3.4878
A444064	Desorption (6 points)		
	Calculated:		
	BET	(31.6)	3.5022
	H-J	(29.4)	3.4847
	Experimental		3.5039
	"BIO GEL" (commercial hydroxyapatite)		
A444136	Adsorption (Intermediate Humidity range 0.312 → 0.804)		
	Calculated (4 points):		
	BET (not applicable)	—	—
	H-J	43.3	0.3788
A444138	Desorption (High Humidity range 0.926 → 0.542)		
	Calculated (5 points):		
	H-J	(47.2)	.3792
	Experimental		.3802

TABLE 3. *Desorption*

Low Humidity Range (0.334 → 0.082) Comparison of BET with H-J for the same data

Expt. No.		Surface area (m^2/g)	Dry weight (g)
A444159	Barium Glass – Water Extracted (5 points)		
	Calculated:		
	BET	(9.2)	0.9639
	H-J	(2.3)	.9659
	Experimental		.9657
A503137	NPG-GMA Coated HA (6 points)		
	Calculated:		
	BET	(14.6)	.4808
	H-J	(12.6)	.4799
	Experimental		.4805
A444139	"BIO GEL" (commercial hydroxyapatite) (5 points)		
	Calculated:		
	BET	(40.5)	.3792
	H-J	(59.4)	.3784
	Experimental		.3811

TABLE 4. *Adsorption*

Low humidity versus high humidity

Expt. No.		Surface area (m^2/g)	Dry weight (g)
	Dentin		
A503140	Calculated (6 points 0.082 → 0.334)		
	BET	146	2.0202
	H-J (poor convergence)	–	–
	Experimental		2.0671
A503078	Calculated (5 points 0.082 → 0.312)		
	BET (no convergence)	–	–
	H-J	143	.2847
A503079	Calculated (4 points 0.334 → 1.000)		
	BET (not applicable)	–	–
	H-J	150	.2848
	Experimental		.2898
	Cellulose Acetate Membrane		
A444148	Calculated (6 points 0.082 → 0.334)		
	BET	191	.06424
	H-J	176	.06480
A444149	Calculated (7 points 0.435 → 1.000)		
	BET (not applicable)	–	–
	H-J	197	.06491
	Experimental		.06681

TABLE 5. *Adsorption–desorption*

High humidity range (0.435–0.971)

Expt. No.		Surface area (m^2/g)	Dry weight (g)
	Pulverized Dental Amalgam		
A444124	Adsorption (7 points)		
	Calculated		
	H-J	0.44	5.6135
A444126	Desorption (4 points)		
	Calculated		
	H-J	(0.74)	5.6132
	Experimental		5.6145

TABLE 6. *High humidity drying (desorption) curves for predicting water content* *

Expt. No.		Surface area (m^2/g)	Dry weight (g)
A444145	Cellulose Acetate Membrane (Humidity Range 0.926→ 0.655)		
	Calculated (4 points): H-J	(148.3)	.06645
	Experimental		.06681
A444153	Barium Glass (Humidity Range 0.926→ 0.435)		
	Calculated (6 points): H-J	(2.5)	1.28897
	Experimental		1.28947
A444158	Extracted Barium Glass (Humidity Range 0.971→ 0.435)		
	Calculated (7 points): H-J	(3.4)	.9663
	Experimental		.9657
A444171	Activated Bentonite (Humidity Range 0.926→ 0.542)		
	Calculated (5 points): H-J	(242)	.7113
	Experimental		.7378
A503091	Commercial Synthetic Hydroxyapatite (Humidity Range 1.000→ 0.757)		
	Calculated (5 points): H-J	(117)	.2612
	Experimental		.2733
A503136	NPG–GMA Coated HA (Humidity Range 1.000→ 0.542)		
	Calculated (7 points): H-J	(25)	.4788
	Experimental		.4805

*Other examples included in tables 2 and 5.

5. Discussion

The fact that the least-squares technique can be applied successfully for determining unbound water content along with surface area for the BET and the H-J isotherm equations raises the question of whether it would work equally well for other adsorption theories. Accordingly, computer programs were developed for testing the Potential theory and the Polarization theory, each of which could be expressed in linear form [9]. It soon became clear that this method would not be applicable to either one of these latter isotherm equations. They seemed to be "ill-conditioned" or not sufficiently sensitive to perturbation in sample weight to be of practical use in instances where both BET and H-J converge readily. Further testing was therefore abandoned. The possibility remains that still other isotherm equations [2, 4, 5] (besides the four tested here) might well be adaptable to this technique.

It is instructive to assess the relative advantages of BET and of H-J as applied to the present work:

(1) The H-J would, of course, be used for all values beyond the relative pressure (about 0.3) of the applicable BET range.

(2) For very small surface area samples where the points in the BET range may be too erratic for successful convergence, the points higher up on the isotherm may have sufficiently reduced relative error to give successful convergence using H-J.

(3) In the valid BET region where both isotherm equations could be used, the BET equation appeared to be the more sensitive. When the experimental

error of the points was excessive, neither computer program would converge. At moderate error such that only one equation led to successful convergence it was usually H-J (see tables 1 and 4).

(4) In many instances where no convergence was found when using the BET equation, a minimum in the residual variance (mean-square deviation of the ordinates of the experimental points from the assumed curve) was useful as a rough estimate of the correct dry weight and surface area.

(5) When convergence was attained using both isotherm equations and the predicted surface areas were in reasonably good agreement (see first four experiments in table 1), it served to reinforce one's confidence in the validity of the results. When agreement was somewhat less than desired for a homogeneous adsorbent (see table 1, Expt A444156), the BET value would be preferred. Note that the BET surface area value of 8.7 m^2/g (rather than the H-J value of 4.6) was in better agreement with the results of Experiment A444175 for the same adsorbent (also table 1) for which the H-J value of 9.5 m^2/g was calculated.

(6) For a nonhomogeneous adsorbent where aggregate behavior might lead to an erroneous BET value [12] as a result of large differences in energies of adsorption among the components of the solid, the H-J area would always be preferable.

Throughout tables 2, 3, 5, and 6 surface area values obtained from desorption experiments are shown in parenthesis. They are likely to be erroneous unless the desorption curve is substantially a retracing of the adsorption curve (absence of hysteresis). This is a property of the adsorbent-adsorbate system and must be considered case by case. Virtual absence of hysteresis is portrayed by the materials listed in table 2 and exists to only a slight degree for those listed in table 3. The dry weight values, however, are just as valid with desorption as with adsorption provided the desorption originates at saturation resulting in a descending boundary curve [13]. Other instances which have been found to agree with the experimental results for dry weight include primary descending scanning curves; although the predicted surface area would not be valid. A case in point is illustrated by an experiment not shown in the tables. Water vapor was adsorbed on a desiccated sample of Bio Gel[6] to a relative humidity of 0.804 after which seven additional successive desorption values were obtained. Convergence was successful using H-J resulting in a predicted dry weight of 0.3788 g compared with the experimental value of 0.3811 g obtained after taking the sample again to dryness.

Desorption along scanning curves other than those already mentioned as well as adsorption along scanning curves, will invariably result in erroneous values for dry weight prediction in spite of satisfactory convergence of the computer program. Two experiments performed with the same sample of human dentin will serve to illustrate this. In both cases, the starting point was saturation (relative humidity = 1.00). In the first experiment (A444090), desorption occurred along the descending boundary curve to a value of 0.175 relative humidity. This was followed by adsorption along a primary ascending scanning curve to a relative humidity of 0.757. Desorption was next carried out stepwise along this secondary descending scanning curve. The sample weights measured were: 0.249303 g, 0.247758 g, 0.246568 g, and 0.245402 g at the corresponding relative humidities of 0.757, 0.655, 0.542, and 0.435, respectively. The dry weight predicted from using the H-J equation was 0.2356 g as compared with 0.2288 g measured experimentally. In the other experiment (A444091) the initial turning point between the descending boundary curve and the primary ascending scanning curve took place at 0.122 r.h. (instead of 0.175 r.h.). In this experiment, the sample weights at the same respective humidities along the secondary descending scanning curve were 0.248456 g, 0.247364 g, 0.245881 g, and 0.244989 g. These values gave rise to a predicted dry weight of 0.2369 g. It is significant that in both of these experiments the dry weight was predicted about four percent on the *high* side compared with the actual measurement. A detailed study of the behavior of scanning curves in adsorption-desorption hysteresis is beyond the scope of this paper [13].

It was stated earlier in this discussion (subparagraph 3) that the BET equation was extremely sensitive regarding the effect of experimental error on convergence of the computer program. If a sufficient number of points are available in a system in which the BET equation is known to be valid and yet the computer program does not converge, it is useful to plot the original data especially when it is impractical (or impossible) to repeat the experiment. If one of the points does not fit a smooth curve which passes through the remaining points, those remaining points may very well allow the computer program to converge. Of course, the results should be examined carefully for reasonableness of the predicted quantities before they are accepted. This suggestion is submitted in lieu of a valid test for outliers [14] in a system as complicated as this.

It is appropriate to caution the reader that the method described in this paper is *not* proposed as a substitute for measuring the zero humidity point in routine surface area determinations. It is also entirely feasible that experimental errors might combine in such a way as to permit convergence and yet yield incorrect results. In other words, the need for careful experimental work is probably even more important when the additional demand is placed on the sorption points to estimate the zero humidity value as well as the surface area.

Some applications in which the methods described in this paper would be especially valuable are:

(1) Where routine measurements have yielded good linear BET results yet, now and then, a sample of the same type of material when plotted in accordance with eq (1) produced a curve instead of a straight line.

[6] BIO-RAD Laboratories, Richmond, California.

In such instances, the entire experiment would normally have to be discarded and all because an error in the experimental determination of the dry weight was reflected in all the *other* points on the plot.

(2) Dry weight of materials that evolve gases during decomposition at low pressures.

(3) In agricultural products (such as grain) and other materials where the last traces of water may be extremely slow coming off during drying (desorption), provided again that the isotherm equation employed is known to be appropriate for that system.

(4) In biological applications where viability of the organism (or tissue) would be destroyed by complete drying while, perhaps, equilibration at, say, fifty percent relative humidity might be tolerated, non-destructive determinations of dry weight could be made. This would be especially useful in growth rate studies.

(5) In situations where no other method may be available for estimation of dry weight and/or surface area from previously obtained data which may be incomplete.

6. Summary

(1) It has been demonstrated that adsorption or desorption data are capable of estimating the unbound water content of solid adsorbents. This was accomplished by the convergence of a computer program which employed a least-squares technique applied to an appropriate isotherm equation.

(2) The Brunauer, Emmett, and Teller free surface equation and the Harkins and Jura equation were readily adaptable to this treatment (the Polarization equation and the Potential theory equation did not respond).

(3) A valid estimate of surface area was also obtained when data from adsorption experiments were used or with such desorption experiments for which no hysteresis existed. Where there was hysteresis, the predicted surface area while incorrect was a useful order-of-magnitude estimation, usually as an upper limit.

(4) Applications of the technique for determining the dry weights were compared with experimentally measured values for solids which cover a wide range in surface area. The agreement was within about one percent and the calculated dry weight was usually on the low side.

(5) The capabilities as well as the limitation in the application of these methods were compared and discussed.

7. Appendix. Procedure for Using Isotherm Data With Time Sharing Teletype Terminal

Fortran Computer programs are given in figure A1 for the BET equation in figure A2 for the Harkins and Jura equation. A minimum of four data points is required, although a larger number is preferred. The adsorption (or desorption) data can be pre-punched on paper tape before connecting the terminal with the computer. (The input format has been designed such that the same data tape may be used with either program.) A typical data file, for example, (A444153) transposed from the tape is shown in table A1. The initial line (here designated as 10) contains:

a. The number of data points in the experiment (in this case, 6).
b. The maximum number of iterations.
c. A starting value (tentative) for the dry weight.
d. The initial decrement (or amount by which the preceding numeral is changed in initiating the iterative process).

Subsequent lines of table A1 contain the sample weight along with the corresponding humidity to which the sample was exposed until that steady-state weight had been attained.

The order of the points in table A1 indicates in this illustration that a desorption process originating at a relative humidity of 1.00 was measured initially at 0.926 r.h., and finally at 0.435. While a maximum of 33 iterations was provided for in this example, only about 20 were needed before no further change of any consequence resulted.

TABLE A1. *Input data for Expt. A444153*

```
10 06 33 01.289000 −0.000400
11 01.294267 0.926
12 01.291396 0.804
13 01.290930 0.757
14 01.290616 0.655
15 01.290353 0.542
16 01.290112 0.435
```

The initiating value of 01.289000 g was chosen to be less than any of the data points and yet obviously greater than the expected dry weight. The choice of −0.000400 for the weight change meant that a value of 1.288600 g for a tentative dry weight would be tested by the computer in its next iteration. The Harkins and Jura program (HARJUR) would, of course, be used for the data file A444153, since the humidities are beyond the valid range applicable to the BET theory.

In the course of the computer run the value of Φ must change signs repeatedly as it converges toward zero. This is a necessary criterion for a successful determination. The value predicted for dry weight for this particular set of data was 1.28897 g while the predicted [7] surface area was 2.49 m^2/g. (Other columns present in the computer printout (not shown here) represent intermediate steps in the calculations or estimate the goodness of fit to the linear form of the isotherm equation.)

An interesting application of the computer program is the degenerate case where the iterations are suppressed. This would occur when the dry weight is

[7] The predicted surface area would normally *not* be valid in the case of a desorption experiment (such as this) unless hysteresis was absent. It is useful, however, as an estimate of the order of magnitude of the surface area.

578-011 O - 75 - 3

```
00010 PROGRAM WASSER (INPUT,OUTPUT,TAPE1)
00020*THIS PROGRAM IS DESIGNED TO FIND THE DRY WEIGHT P(JJ) WHERE
00030*X(I) IS THE RELATIVE HUMIDITY, V(I) IS THE WEIGHT OF SAMPLE
00040*AT EQUILIBRUM WITH X(I), AND J IS THE ITERATION OF THE PAR-
00050*AMETER.  MAX I IS II.  MAX J IS JJ.  THE VALUE OF II
00060*MUST BE AT LEAST 4.  THE RANGE OF X(I) SHOULD BE 0.08 TO 0.33.
00070 DIMENSION V(50), X(50), P(99), F3(50), F4(50), F5(50),
00080+ F6(50), F8(50)
00090 READ (1,61) II, JJ, P(1), DELP
00100 61 FORMAT (3X, I2, 1X, I2, 1X, F9.6, 1X, F9.6)
00110 PRINT 62
00120 62 FORMAT (/3X, 2HII, 1X, 2HJJ, 5X, 4HP(1), 7X, 4HDELP//)
00130 PRINT 61, II,JJ, P(1), DELP
00140 READ (1,63) (V(I), X(I), I=1,II)
00150 63 FORMAT (3X, F9.6, 1X, F5.3)
00160 PRINT 64
00170 64 FORMAT (///5X, 4HV(I), 5X, 4HX(I)//)
00180 PRINT 63, (V(I), X(I), I=1,II)
00190 PRINT 65
00200 65 FORMAT (////1X, 1HJ, 6X, 4HP(J), 8X, 3HPHI, 9X, 1HA, 9X,
00210+ 1HE, 8X, 4HAREA, 7X, 10HMN SQR DEV//)
00220 AII = II
00230 PREPHI = 0.0
00240 DO 104 J=1,JJ
00250 GX2 = 0.0
00260 DO 92 I=1,II
00270 92 GX2 = GX2 + X(I)**2
00280 GX = 0.0
00290 DO 94 I=1,II
00300 94 GX = GX + X(I)
00310 DEN = AII*GX2 - GX**2
00320 DO 111 I=1,II
00330 111 F3(I) = X(I)/(1.0-X(I))/(V(I)-P(J))
00340 GF3 = 0.0
00350 DO 112 I=1,II
00360 112 GF3 = GF3 + F3(I)
00370 DO 113 I=1,II
00380 113 F4(I) = X(I)*F3(I)
00390 GF4 = 0.0
00400 DO 114 I=1,II
00410 114 GF4 = GF4 + F4(I)
00420 DO 115 I=1,II
00430 115 F5(I) = F3(I)*V(I)/(V(I)-P(J))
00440 GF5 = 0.0
00450 DO 116 I=1,II
00460 116 GF5 = GF5 + F5(I)
00470 DO 117 I=1,II
00480 117 F6(I) = X(I)*F5(I)
00490 GF6 = 0.0
00500 DO 118 I=1,II
00510 118GF6 = GF6 + F6(I)
00520 DO 119 I=1,II
00530 119 F8(I) = F3(I)*F5(I)
00540 GF8 = 0.0
00550 DO 120 I=1,II
00560 120 GF8 = GF8 + F8(I)
00570 A = 18.0*P(J)*(GX2*GF3 - GX*GF4)/DEN
00580 B = 18.0*P(J)*(AII*GF4 - GX*GF3)/DEN
00590 AREA = 7.529E+04/(A+B)
00600 PHI = A*GF5 + B*GF6 - 18.0*P(J)*GF8
00610 SSQRS = 0.0
00620 DO 4 I=1,II
00630 4 SSQRS = SSQRS + (V(I) - P(J)*(1.0 + 18.0*X(I)/
00640+ (1.0 - X(I))/(A + B*X(I))))**2
00650* SSQRS OF DEVS OF V(I) FROM CURVELINEAR REGRESSION
00660 VAR = SSQRS/(AII - 3.0)
00670 PRINT 99, J, P(J), PHI, A, B, AREA, VAR
00680 99 FORMAT (I2, 2E13.5, 2E10.2, 2E12.4)
00690 IF (PHI*PREPHI) 95,96,96
00700 95 DELP = -0.1*DELP
00710 96 PREPHI = PHI
00720 P(J+1) = P(J) + DELP
00730 104 CONTINUE
00740 STOP
00750 END
```

FIGURE A1. *Computer Program, WASSER, (FORTRAN IV) for determination of unbound water content (dry weight) and Surface Area from water vapor sorption data according to the BET adsorption theory.*

```
00010 PROGRAM HARJUR(INPUT,OUTPUT,TAPE1)
00020*THIS PROGRAM IS DESIGNED TO FIND THE DRY WEIGHT P(JJ)
00030*WHERE X(I) IS THE RELATIVE HUMIDITY, W(I) IS THE
00040*WEIGHT OF SAMPLE AT EQUILIBRUM WITH X(I), AND J IS THE
00050*ITERATION OF THE PARAMETER.  MAX I IS II.  MAX J IS JJ.
00060*THE VALUE OF II MUST BE AT LEAST 4.
00070 DIMENSION W(50), X(50), P(99), H1(50), H2(50)
00080 READ(1,61) II, JJ, P(1), DELP
00090 61 FORMAT (3X, I2, 1X, I2, 1X, F9.6, 1X, F9.6)
00100 PRINT 62
00110 62 FORMAT (/3X,2HII,1X,2HJJ,5X,4HP(1),7X,4HDELP//)
00120 PRINT 61, II,JJ, P(1), DELP
00130 READ(1,63) (W(I),X(I), I=1,II)
00140 63 FORMAT (3X,F9.6,1X,F5.3)
00150 PRINT 64
00160 64 FORMAT (///5X, 4HW(I), 5X, 4HX(I)//)
00170 PRINT 63, (W(I), X(I), I=1,II)
00180 PRINT 65
00190 65 FORMAT (////1X, 1HJ, 6X, 4HP(J), 8X, 3HPHI, 9X,
00200+ 1HA, 9X, 1HB, 8X, 4HAREA, 7X, 10HMN SQR DEV///)
00210 AII = II
00220 PREPHI = 0.0
00230 DO 104 J = 1,JJ
00240 DO 90 I = 1,II
00250 90 H1(I) = ALOG(1.0/X(I))
00260 GH1 = H1(1)
00270 DO 91 I = 2,II
00280 91 GH1 = GH1 + H1(I)
00290 DO 92 I = 1,II
00300 92 H2(I) = 1.0/(W(I) - P(J))
00310 GH2 = H2(1)**2
00320 DO 93 I = 2,II
00330 93 GH2 = GH2 + H2(I)**2
00340 GH12 = H1(1)*H2(1)**2
00350 DO 94 I = 2,II
00360 94 GH12 = GH12 + H1(I)*H2(I)**2
00370 GH4 = H2(1)**4
00380 DO 95 I = 2,II
00390 95 GH4 = GH4 + H2(I)**4
00400 GHV3 = W(1)*H2(1)**3
00410 DO 96 I = 2,II
00420 96 GHV3 = GHV3 + W(I)*H2(I)**3
00430 GH1V3 = W(1)*H1(1)*H2(1)**3
00440 DO 97 I = 2,II
00450 97 GH1V3 = GH1V3 + W(I)*H1(I)*H2(I)**3
00460 GHV5 = W(1)*H2(1)**5
00470 DO 98 I = 2,II
00480 98 GHV5 = GHV5 + W(I)*H2(I)**5
00490 DEN = (18.0*P(J))**2*(AII*GH4 - GH2**2)
00500 ANUM = AII*GH12 - GH1*GH2
00510 A = ANUM/DEN
00520 ENUM = (18.0*P(J))**2*(GH2*GH12 - GH1*GH4)
00530 B = ENUM/DEN
00540 PHI = A*P(J)*(GH1V3 - A*(18.0*P(J))**2*GHV5 + B*GHV3)
00550 SSQRS = 0.0
00560 DO 4 I = 1,II
00570 DISC = A/(H1(I) + B)
00580 IF (DISC) 70,69,69
00590 69 DSCR = DISC
00600 SSQRS = SSQRS + (W(I)-P(J)*(1.0+18.0*SQRT(DSCR)))**2
00610 GO TO 4
00620 70 SSQRS = 1.0E+08
00630 4 CONTINUE
00640* SSQRS OF DEVS OF W(I) FROMM CURVILINEAR REGRESSION
00650 VAR = SSQRS/(AII-3.0)
00660 IF (A.LT.0.0) GO TO 111
00670 AREA = 5.62E+04*SQRT(A)
00680 GO TO 112
00690 111 AREA = 0.0
00700 112 PRINT 99, J, P(J), PHI, A, B, AREA, VAR
00710 99 FORMAT (I2, 2E13.5, 2E10.2, 2E12.4)
00720 IF (J.EQ.1) GO TO 101
00730 IF (PHI*PREPHI) 100,100,101
00740 100 DELP = -0.1*DELP
00750 101 PREPHI = PHI
00760 P(J+1) = P(J) + DELP
00770 104 CONTINUE
00780 STOP
00790 END
```

FIGURE A2. *Computer Program, HARJUR, (FORTRAN IV) for determination of unbound water content (dry weight) and Surface Area from water vapor sorption data according to the H-J adsorption theory.*

578-011 O - 75 - 4

available experimentally along with the rest of the data points and the experimenter is primarily interested in the least-squares value of the surface area. In the first line of the input data file (table A1) he would set the number of iterations equal to 01 and would insert the known dry weight for the initial value of p which is the next entry on that same first line. The final entry (corresponding to the initial decrement) while it will be ignored by the computer should, never-the-less, be present even if all its digits are zeroes.

The computer programs used in this work are reproduced in figures A1 and A2.

8. References

[1] Brunauer, S., Emmett, P. H., and Teller, E., Adsorption of gases in multimolecular layers, J. Am. Chem. Soc. **60,** 309–319 (1938).

[2] Dubinin, M. M., Zaverina, E. D., and Radushkevich, L. V., Sorption and structure of activated carbon, I. Investigation of adsorption of organic vapors, Zhur Fizich Khim **21,** 1351–1362 (1947).

[3] Harkins, W. D., and Jura, G., Surfaces of solids XIII. A vapor adsorption method for the determination of the area of a solid without the assumption of a molecular area, and the areas occupied by nitrogen and other molecules on the surface of a solid, J. Am. Chem. Soc. **66,** 1366–1373 (1944).

[4] Halsey, G. D., Jr., A new multilayer isotherm equation with reference to surface area, J. Am. Chem. Soc. **73,** 2693–2696 (1951).

[5] Pierce, C., The Frenkel-Halsey-Hill Adsorption Isotherm and Capillary Condensation, Proc. of the 34th National Colloid Symposium (American Chemical Society), Lehigh Univ., Bethlehem, Pa. **64,** 86–89 (1960).

[6] Adamson, A. W., Physical Chemistry of Surfaces, (Interscience Publishers, Inc., New York, N.Y., 1960), p. 501.

[7] Venkateswaran, A., Sorption of aqueous and non-aqueous media by wood and cellulose, Chem. Reviews **70,** 619–637 (1970).

[8] Scarborough, J. B., Numerical Mathematical Analysis, 2d Ed. (The Johns Hopkins Press, Baltimore, 1950), pp. 451–469.

[9] Adamson, A. W., Physical Chemistry of Surfaces, (Interscience Publishers, Inc., New York, 1960), pp. 499–500.

[10] Loebenstein, W. V., Adsorption of water on tooth components and related materials, J. Dent. Res. **52,** 271–280 (1973).

[11] Rao, K. S., Hysteresis in sorption, II, III, IV, V, J. Phys. Chem. **45,** 506–531 (1941).

[12] Loebenstein, W. V., The surface area of aggregates applied to dental materials, J. Biomedical Materials Res. **9,** 35–53 (1975).

[13] Everett, D. H., Adsorption Hysteresis, The Solid Gas Interface, Chapter 36, Flood, E. A. Ed. (Marcel Dekker, Inc., N.Y., 1967).

[14] Tietjen, G. L., Moore, R. H., and Beckman, R. J., Testing for a Single Outlier in Simple Linear Regression, Technometrics **15,** 717–721 (1973).

(Paper 79A4–860)

JOURNAL OF RESEARCH of the National Bureau of Standards — A. Physics and Chemistry
Vol. 79A, No. 4, July-August 1975

Publications of the National Bureau of Standards*

Citations with Selected Abstracts

J. Res. Nat. Bur. Stand. (U.S.), **79A** *(Phys. and Chem.)*, No. 3 (May-June 1975), SD Catalog No. C13.22/sec.A:79/3.

The enthalpies of combustion and formation of ortho- and parafluorobenzoic acid, W. H. Johnson and E. J. Prosen.

The enthalpies of combustion and formation of acetanilide and urea, W. H. Johnson.

The enthalpies of combustion and formation of cholesterol [cholest-5-en-3-ol (3β)], W. H. Johnson.

The third spectrum of copper (Cu III), A. G. Shenstone.

Monogr. 12, Section 12. **Standard x-ray diffraction powder patterns. Section 12-data for 57 substances,** H. F. McMurdie, M. C. Morris, E. H. Evans, B. Paretzkin, J. H. de Groot, C. R. Hubbard, and S. J. Carmel, Nat. Bur. Stand. (U.S.), Monogr. 25-Sec. 12, 90 pages (Feb. 1975) SD Catalog No. C13.44:25/Sec. 12, $1.50.

Key words: crystal structure; integrated intensities; lattice constants; peak intensities; powder patterns; reference intensities; standard; x-ray diffraction.

Standard x-ray diffraction patterns are presented for 57 substances. Twenty-five of these patterns represent experimental data and 32 are calculated. The experimental x-ray powder diffraction patterns were obtained with an x-ray diffractometer. All d-values were assigned Miller indices determined by comparison with computed interplanar spacings consistent with space group extinctions. The densities and lattice constants were calculated, and the refractive indices were measured whenever possible. The calculated x-ray powder diffraction patterns were computed from published crystal structure data. Both peak height and integrated intensities are reported for the calculated patterns.

Monogr. 125, Suppl. 1. **Thermocouple reference tables based on the IPTS-68: Reference tables in degrees Fahrenheit for thermoelements versus platinum (Pt-67),** R. L. Powell and G. W. Burns, Nat. Bur. Stand. (U.S.), Monogr. 125, Suppl. 1, 46 pages (Jan. 1975) SD Catalog No. C13.44:125/Suppl. 1, $1.05.

Key words: base metals alloys; noble metal alloys; temperature scale; temperature standards; thermoelements; thermometry.

Reference tables for several thermoelements versus platinum (Pt-67) are given with values of the thermoelectric voltage as a function of temperature in degrees Fahrenheit. Only tables for standard letter-designated thermoelements are included: Types BP, BN, JP, JN, KP (same as EP), KN, TP, and TN (same as EN). These tables supplement those given in NBS Monograph 125 and were calculated from the power series expansions presented in that Monograph. They are based upon the absolute electrical units and the International Practical Temperature Scale of 1968 (IPTS-68).

H114. **General safety standard for installations using nonmedical x-ray and sealed gamma-ray sources, energies up to 10 MeV.** *(ANS N43-5)*, E. H. Eisenhower, Chairman of American National Standards Subcommittee N43-5, Nat. Bur. Stand. (U.S.), Handb. 114, 69 pages (Feb. 1975) SD Catalog No. C13.11:114, 90 cents.

Key words: gamma-ray equipment; radiation installations; radiation safety; x-ray equipment.

This standard establishes requirements for the design and operation of common types of installations which use gamma and x radiation for non-medical purposes. Its objective is to protect persons who work with or are near such installations, as well as the general public, against excessive exposure to radiation. Maximum permissible dose limits established by the National Council on Radiation Protection and Measurements are cited. Methods for achieving adequate radiation protection are described, including structural details, surveys and inspections, and operating procedures. Appendixes contain technical information useful for design of radiation shielding barriers. (Revision of ANS Z54.1-1963, published as NBS Handbook 93).

SP260-46. **Standard reference materials: Thermal conductivity and electrical resistivity. Standard reference materials: Austenitic stainless steel, SRM's 735 and 798, from 4 to 1200 K,** J. G. Hust and P. J. Giarratano, Nat. Bur. Stand. (U.S.), Spec. Publ. 260-46, 42 pages (Mar. 1975) SD Catalog No. C13.10:260-46, $1.00.

Key words: austenitic stainless steel; electrical resistivity; high temperature; low temperature; standard reference materials; thermal conductivity.

A historical review of the development of selected thermophysical standard reference materials, SRM's, is given and selection criteria for those SRM's are listed. Thermal conductivity and electrical resistivity data for austenitic stainless steel, SRM's 735 and 798, are critically evaluated. Recommended values are presented for the temperature range 4 to 1200 K. Material variability studies, including the effects of heat treatment, have been performed at low temperatures. No irreversible transformations are observed up to temperatures of 1200 K. Based on the results of several types of characterization measurements, effects of material variability are believed to be less than 1 percent in electrical resistivity and not significantly more in thermal conductivity. The uncertainty of the recommended electrical resistivity data is estimated at 1 percent at low temperatures and 2 percent at higher temperatures. The corresponding uncertainty for thermal conductivity is 2 percent below 100 K, increasing to 3 percent at 300 K, and 5 percent at higher temperatures.

SP400-13. **Semiconductor measurement technology: Improved infrared response technique for detecting defects and impurities in germanium and silicon *p-i-n* diodes,** A. H.

**Publications with prices and SD Catalog numbers may be purchased directly from the Superintendent of Documents, U.S. Government Printing Office, Washington, D.C. 20402 (foreign: one-fourth additional). Microfiche copies of the above, plus paper copy and microfiche versions of NBS Interagency Reports (NBSIR's), may be purchased from the National Technical Information Service (NTIS), Springfield, Va. 22161. Prices are subject to change. Reprints from the NBS Journal of Research and non-NBS publications may often be obtained directly from the authors.*

Sher, Nat. Bur. Stand. (U.S.), Spec. Publ. 400-13, 26 pages (Feb. 1975) SD Catalog No. C13.10:400-13, 75 cents.

Key words: carrier trapping; gamma-ray detector; germanium; Ge(Li) detector; infrared response silicon.

An infrared response (IRR) technique was evaluated for its utility in qualifying germanium for radiation detector use. Because of several improvements in the sensitivity and interpretation of the technique made during the evaluation, it was possible to observe a number of discrete energy levels lying within the forbidden energy gap of germanium which had passed unobserved in previous studies. These levels correlate with the type of defects and vacancies introduced by radiation damage into germanium as measured using such techniques as photoconductivity and Hall effect measurements after irradiation. Furthermore, the improved infrared response measurement method was used to identify impurities, such as copper, gold, and iron, and dislocations resulting from heat treatments in germanium. A major advance was made when it was determined that the IRR spectra could be grouped into five distinct types on the basis of spectral features observed in the energy range from 0.6 to 0.7 eV. One of the spectrum types represented crystals from which good quality detectors could be fabricated; the other four represented crystals that yielded poorer quality detectors due to carrier trapping, or crystals that presented problems such as low lithium drift mobility in detector fabrication. Three of the four spectrum types representative of poor crystal quality could be duplicated by suitably degrading specimens of a good quality crystal. The material and detector characteristics of crystals within each spectrum type were found to be similar.

SP410. **NBS metric kit,** Nat. Bur. Stand. (U.S.), Spec. Publ. 410, envelope containing 7 items (1975) SD Catalog No. C13.10:410, $2.00.

Key words: bibliography of metric information; customary units; history of measurement systems; metric chart; metric information.

This kit is a compilation of seven metric information items and is intended primarily for the teacher, student, and others seeking authentic information on the metric system.

A handy, wallet-sized card that converts customary units of measure into metric units and vice versa; a 15 centimeter (6 inch) ruler; "What About Metric," which explains in simple terms all anyone needs to know about using metric units in daily living; a brief history of measurement systems, and a colorful chart explaining base units of the metric system; a bibliography of metric information that also includes sources of metric teaching aides for educators, and an article by Dr. Richard W. Roberts, Director of the National Bureau of Standards.

SP413. **Special technical facilities at the National Bureau of Standards,** H. L. Mason and I. M. Lloyd, Nat. Bur. Stand. (U.S.), Spec. Publ. 413, 56 pages (Jan. 1975) SD Catalog No. C13.10:413, $1.10.

Key words: acoustic facilities; accelerators; calorimeters; electrical measurements facilities; high pressure facilities; high temperature facilities; spectroscopy facilities.

Among the major technical facilities of the NBS laboratories in Gaithersburg, Md. and Boulder, Colo., are some which are unique and many which feature equipment that is relatively uncommon. These important resources deserve to be more widely known and used by the scientific and engineering community, including the Bureau's own staff, other Government agencies, industrial research associates, academic researchers, and postdoctoral fellows. Those facilities which are available for shared use, either occasional or extended, are briefly described in the pages of this publication.

SP416. **Attacking the fire problem: A plan for action,** K. Giles and P. Powell, Eds., Nat. Bur. Stand. (U.S.), Spec. Publ. 416, 37 pages (May 1975) SD Catalog No. C13.10:416, $1.00.

Key words: building design; consumer protection; fire control, fire detection; fire research; fire spread; flammability.

The mission of the Center for Fire Research is to insure the development of the technical base for the standards and specifications needed in support of the National goal to reduce fire losses by 50 percent over the next generation. A systems approach to accomplish this mission is described. The Center consists of three basic programs in the area of Fire Science and five applied research programs in the area of Fire Safety Engineering. Each applied program addresses an aspect of the Fire Problem, using fundamental information supplied by the basic research function. Active participation by staff members in voluntary standards organizations is the principal means of making this technology available for codes and standards needed to reduce the Nation's fire loss.

SP418. **National Bureau of Standards, Annual Report,** F. P. McGehan, M. King, and R. S. Franzen, Eds., Nat. Bur. Stand. (U.S.), SP418, 32 pages (Apr. 1975) SD Catalog No. C13.10:418, $1.00.

Key words: annual report; computer; energy; environment; health; product safety; research; science and technology; standards.

This document describes how resources were utilized during fiscal year 1974 and highlights major achievements as a result of work performed at the National Bureau of Standards. Using the theme, "Standards for daily living," the book presents brief discussions of accomplishments within major program areas. The report serves as 1) an annual account of NBS activities and 2) promotional information about NBS. The Table of Contents includes: From the Director; Standards for Daily Living: Historical Pioneer, Catalyst for Change, Information Programs; The Year in Review: Expanding Measurement Capabilities, Toward Solving the Energy Problem, Improving Man's Environment, Striving for Safer Products, Aiding Health Care, Advancing Computer Technology; Interaction is the Key: Public Interest, Government Projects, Industry Cooperation, Information Services; Funds and Facilities; Organization; People.

BSS61. **Natural hazards evaluation of existing buildings,** C. G. Culver, H. S. Lew, G. C. Hart, and C. W. Pinkham, Nat. Bur. Stand. (U.S.), Bldg. Sci. Ser. 61, 958 pages (Jan. 1975) SD Catalog No. C13.29:2/61, $11.10.

Key words: buildings; damage; disaster; dynamic analysis; earthquakes; hurricanes; natural hazards; structural engineering; tornadoes; wind.

A methodology is presented for survey and evaluation of existing buildings to determine the risk to life safety under natural hazard conditions and estimate the amount of expected damage. Damage to both structural and nonstructural building components resulting from the extreme natural environments encountered in earthquakes, hurricanes, and tornadoes is considered. The methodology has the capability of treating a large class of structural types including braced and unbraced steel frames, concrete frames with and without shear walls, bearing wall structures, and long-span roof structures. Three independent but related sets of procedures for estimating damage for each of the natural hazards are included in the methodology. The first set of procedures provides a means for qualitatively determining the damage level on the basis of data collected in field surveys of the building. The second set utilizes a structural analysis of the building to determine the damage level as a function of the behavior of critical elements. The third set is based on a computer analysis of the entire structure. All three sets of procedures are based on the current state of the art. The procedures are presented in a format which allows updating and refining. Numerical examples illustrating application of the procedures are included.

FIPS PUB 34. **Guide for the use of International System of Units (SI),** R. R. Roundtree, Standards Coordinator, Nat. Bur.

Stand. (U.S.), Fed. Info. Process. Stand. Publ. (FIPS PUB) 34, 4 pages (1975) SD Catalog No. C13.52:34, 25 cents.

Key words: ADP standards; computers; data processing, Federal Information Processing Standards; metric conversion; SI units; standards.

The use of SI (International System of Units) within the United States is increasing. The Secretary of Commerce has established the policy that publications of the Department will provide dual-dimensions to the extent practicable.

The Federal Information Processing Standards (FIPS) Program in response to Public Law 89-306 (the Brooks Act) strives to improve the utilization of ADP equipment, goods and services within the Federal Government through the establishment of uniform Federal automatic data processing standards. These standards and guidelines which are published by the National Bureau of Standards as FIPS contain specifications which should be expressed as dual-dimensions. Accordingly, this guideline will be used in the preparation of all new FIPS PUBS and existing FIPS PUBS when revised.

PS1-74. **Construction and industrial plywood.** *(ANS A199.1-1974),* K. G. Newell, Technical Standards Coordinator, Nat. Bur. Stand. (U.S.), Prod. Stand. 1-74, 34 pages (Mar. 1975) SD Catalog No. C13.20/2:1-74, 85 cents.

Key words: construction and industrial plywood; industrial plywood; plywood, construction, and industrial.

This Voluntary Product Standard covers requirements and methods of test for the wood species, veneer grading, glue bonds, panel construction and workmanship, dimensional tolerances, marking, moisture content, and packing of plywood intended for construction and industrial uses.

Also included are a glossary of trade terms and a quality certification program. Information regarding generally available sizes, methods of orderings, and reinspecting practices, is provided in the appendix.

PS62-74. **Grading of diamond powder in sub-sieve sizes.** *(ANS Z300.1-1974),* C. W. Devereux, Technical Standards Coordinator, Nat. Bur. Stand. (U.S.), Prod. Stand. 62-74, 5 pages (Jan. 1975) SD Catalog No. C13.20/2:62-74, 55 cents.

Key words: diamond powder, grading; grading of diamond powder; powder, diamond; sizes, sub-sieve of diamond powder.

This Voluntary Product Standard covers the quality requirements of sub-sieve sizes of diamond powder and establishes the standard particle size ranges for micron sizes. It establishes size designations of the size ranges and the grading limits that are acceptable in each size range. It also gives a method of inspection to determine compliance with this standard and directions for the labeling of powder to indicate such compliance.

TN658. **Development of electric and magnetic near-field probes,** F. M. Greene, Nat. Bur. Stand. (U.S.), Tech. Note 658, 53 pages (Jan. 1975) SD Catalog No. C13.46:658, $1.10.

Key words: electric near-field probe; electromagnetic-field hazard; field-strength measurements; magnetic near-field probe; near-field measurements; r-f hazard measurements; semiconducting transmission line.

This publication describes the development and design of small electric and magnetic near-field probes for measuring hazard-level fields up to 20,000 V/m and 100 A/m, respectively. They were originally designed to be used over the frequency range from 10 to 30 MHz, and consist of short dipole antennas and small, single-turn balanced, loop antennas to measure the electric- and magnetic-field components, respectively. The probes are intended for use by various researchers in their electromagnetic, radiation-exposure programs for determining the effects of hazard-level, nonionizing, EM fields on living tissue, electroexplosive devices, and volatile fuels.

In order to later extend the use of the probes to frequencies above 30 MHz, a detailed analysis was made of several types of measurement errors likely to be encountered. The principal errors result from a variation with frequency in: the effective length and impedance of the dipoles; and the electric-dipole response and partial resonance of the loops. Corresponding corrections are given for each type of error as a function of the operating frequency from 10 to 1000 MHz, and as a function of the physical and electrical sizes of the probes.

As a result of the analysis, the dipoles can now be used for measurements at frequencies up to 750 MHz and the loops to 75 MHz with an estimated uncertainty of 0.5 dB. Applying recommended corrections will provide a substantial further increase in the usable frequency range.

TN660. **Molecular beam tube frequency biases due to distributed cavity phase variations,** S. Jarvis, Jr., Nat. Bur. Stand. (U.S.), Tech. Note 660, 43 pages (Jan. 1975) SD Catalog No. C13.46:660, $1.00.

Key words: accuracy evaluation; atomic beam frequency standards; cavity phase shift.

For atomic beam frequency standards, an analysis is described for estimating the frequency bias due to distributed cavity phase difference over finite beam widths, and for estimating the resulting inaccuracy in power shift and beam reversal experiments. Calculated atomic trajectories and simplified rf-field distributions are used, as well as certain assumptions about beam tube alignment. The results are applied to one of the present NBS primary time and frequency standards and a shorter tube geometry.

One conclusion is that beam reversal experiments are not necessarily much more accurate than power shift experiments and that the use of both methods (plus the use of pulse techniques) is desirable.

TN662. **A review of precision oscillators,** H. Hellwig, Nat. Bur. Stand. (U.S.), Tech. Note 662, 24 pages (Feb. 1975) SD Catalog No. C13.46:662, 70 cents.

Key words: accuracy; atomic clocks; clocks; crystal oscillator; frequency standards; stability; survey of clocks.

Precision oscillators used in PTTI applications include quartz crystal, rubidium gas cell, cesium beam, and hydrogen maser oscillators. A general characterization and comparison of these devices is given including accuracy, stability, environmental sensitivity, size, weight, power consumption, availability and cost. Areas of special concern in practical applications are identified and a projection of future performance specifications is given. An attempt is made to predict physical and performance characteristics of new designs potentially available in the near future.

TN663. **Characterization of a high frequency probe assembly for integrated circuit measurements,** R. L. Jesch and C. A. Hoer, Nat. Bur. Stand. (U.S.), Tech. Note 663, 55 pages (Apr. 1975) SD Catalog No. C13.46:663, $1.10.

Key words: high frequency probe assembly; integrated circuit transistors; parasitic element; S-parameters.

A detailed, applications-oriented description of a measurement technique that characterizes a high-frequency probe assembly for integrated circuit measurements is given along with the procedure that extracts the parasitic effects of the probe assembly from measurements made at the input connectors of the probe assembly. The scattering parameters of an integrated-circuit device or transistor can now be extracted and accurately determined up to 2 GHz at the wafer stage of assembly. This represents a significant advance over conventional techniques that enable only dc parameters to be measured. Measurement results using this technique are given along with the

precision of values obtained as well as the nature of the measurement bias introduced by the probe assembly.

TN664. **Hydrogen-future fuel—A bibliography (with emphasis on cryogenic technology),** N. A. Olien and S. A. Schiffmacher, Nat. Bur. Stand. (U.S.), Tech. Note 664, 131 pages (Feb. 1975) SD Catalog No. C13.46:664, $1.95.

Key words: cryogenic technology; data; energy fuel; hydrogen; hydrogen properties; LNG/SNG; production; safety; storage.

This NBS Technical Note is a compilation of references dealing directly and indirectly with the possible future use of hydrogen as a fuel. The references were selected using an automated information system operated by the Cryogenic Data Center. This bibliography of references emphasizes the use of cryogenic technology in the hydrogen field. Articles are indexed under 40 subject headings and an author index is included. Over 1600 references are included in this bibliography.

TN665. **A pyroelectric power meter for the measurement of low level laser radiation,** C. A. Hamilton and G. W. Day, Nat. Bur. Stand. (U.S.), Tech. Note 665, 41 pages (Feb. 1975) SD Catalog No. C13.46:665, $1.00.

Key words: laser; power; pyroelectric.

A 1 cm^2 plastic (PVF_2) pyroelectric detector, developed in this laboratory, has been applied to measure low level laser power. The result is a compact instrument which has a low noise equivalent power (10^{-8} $W/Hz^{1/2}$), and fast response (1 s averaging time), and which is precise ($\sigma \sim \pm 1\%$), uniform ($\sim \pm 1\%$), and inherently free from short term drift. This note describes the fabrication of the detector, the design of the instrument, and the results of an extensive evaluation of three such instruments.

TN666. **Efflux of gaseous hydrogen or methane fuels from the interior of an automobile,** J. M. Arvidson, J. Hord, and D. B. Mann, Nat. Bur. Stand. (U.S.), Tech. Note 666, 56 pages (Mar. 1975) SD Catalog No. C13.46:666, $1.10.

Key words: automobile; detection; dispersion; explosion; fire; hydrogen; leakage; methane; safety; vents.

Gasoline-powered automobiles are being converted to operate on gaseous fuels such as H_2 or CH_4. These fuels are commonly stored in containers located in the trunk of the car. Potential leakage of these gaseous fuels into the passenger compartment of the vehicle constitutes a safety threat. Definitive experiments were performed to identify the explosion hazards, establish venting criteria and obviate general safeguards for H_2 or CH_4 fueled passenger vehicles. Appropriately designed ventilation systems significantly reduce the safety hazards associated with accumulated combustible gases. Vents are recommended for all autos *converted* to burn H_2 or CH_4 and may possibly be eliminated in new cars that are *designed* for gaseous fuel operation. Combustible gas warning systems are recommended, at least in the interim, for all (converted and new-design) gaseous fueled vehicles. H_2 and CH_4 gases appear equally safe as vehicular fuels if used in properly designed vehicles.

TN854. **A system of Fortran IV computer programs for crystal structure computations,** L. W. Finger, Nat. Bur. Stand. (U.S.), Tech. Note 854, 133 pages (Feb. 1975) SD Catalog No. C13.46:854, $2.00.

Key words: computer programs; contour plotting; constrained refinement; crystallographic calculations; Fourier section; Fourier synthesis; least squares.

This report gives detailed descriptions and instructions for use of a system of programs for crystallographic calculations, including least-squares refinement with generalized systems of constraints, calculation of bond distances and angles with errors, Fourier synthesis, plotting of contours in Fourier maps, and preparation of structure factor tables for publication.

TN860. **NBS reactor: Summary of activities July 1973 to June 1974,** R. S. Carter, Nat. Bur. Stand. (U.S.), Tech. Note 860, 143 pages (Apr. 1975) SD Catalog No. C13.46:860, $2.05.

Key words: activation analysis; crystal structure; diffraction; isotopes; molecular dynamics; neutron; nuclear reactor; radiation; radiography.

This report summarizes all those programs which depend on the NBS reactor. It covers the period from July 1973 through June 1974. The programs range from the use of neutron beams to study the structure and dynamics of materials through nuclear physics, and neutron standards and neutron radiography to sample irradiations for activation analysis, isotope production and radiation effects studies.

TN861. **A survey for the collection of professional opinion on selected fire protection engineering topics,** G. A. Harrison and J. L. Houser, Nat. Bur. Stand. (U.S.), Tech. Note 861, 30 pages (Mar. 1975) SD Catalog No. C13.46:861, 80 cents.

Key words: building construction; detectors; flame spread; furnishings; interior finishes; noncombustible; smoke development; sprinklers; survey.

A questionnaire survey on selected fire protection engineering topics was sent to 422 persons from every state and major city in the United States and, also, parts of Canada. The surveyed included architects, engineers, insurance and government representatives, academics, and fire services personnel. One hundred and eighty-six questionnaires were returned, a 46.2 percent return rate. This return rate is more than double the National average on survey returns. The questionnaire covered topics such as the adequacy of the term "noncombustible" as contained in the National Fire Protection Association's National Fire Code, hazards of fire loading concepts, code regulation and enforcement, furnishings, sprinkler systems and smoke detectors. In addition to the questionnaire data, many of the surveyed took the time to write in various unsolicited comments.

Although this survey does not represent a statistical study approach, it is the best effort to date to gather and document the current professional thinking on fire protection matters. When the data permitted, obvious and significant group thought ideas and patterns are documented. The objective of this survey is to collect and document professional opinions on selected fire protection engineering topics for the purpose of determining current professional thinking, and indications of future trends of thought.

NBSIR 73-177. **Comparison of the fire performance of neoprene and flame retardant polyurethane mattresses,** W. J. Parker, 46 pages (Apr. 1973). Order from NTIS as COM 75-10336, $3.75.

Key words: fire retardant; fire test; heat release ignition; mattress; smoke; toxic gases.

Full scale fire tests of a neoprene and two different types of flame-retardant polyurethane mattresses were performed in a room-sized compartment at the National Bureau of Standards. The mattresses were tested in two orientations, horizontal and vertical and with two types of coverings, a fire retardant treated cotton and a high temperature nylon ticking, in addition to the bare mattress insert. In addition to the visual observations, the burning rates, ceiling temperatures, optical density of the smoke, and the toxic gas concentrations were measured. This series of tests were repeated on small mattress sections to examine the relevance of small scale tests as a means of predicting full scale behavior. The flame spread index was measured with the radiant panel (ASTM E162); and the smoke and toxic gas concentrations were measured in the NBS smoke density chamber. Measurements were also performed in the heat release rate calorimeter and the ease of ignition test apparatus.

NBSIR 73-262. **Some cutting experiments on human skin and synthetic materials,** J. R. Sorrells and R. E. Berger, 70 pages (Oct. 1973). Order from NTIS as COM 75-10370, $4.25.

Key words: cut; edges, hazardous; experimental studies; human tolerances; injury; injury thresholds; inspection of edges; laceration; safety; simulation; skin; skin, cutting; synthetic materials, cutting; toys.

Human skin specimens were cut in vitro with edges of varying geometry over a normal force range of 0 to 89 newtons. Generally, at a given force, the smaller the included angle and tip radius of an edge, the deeper the resulting cut. For a given edge and skin specimen, empirical curves fitted to the data indicate that the depth of cut increases with force, and that this rate of increase diminishes exponentially. Based on the experimental data, a convention was proposed for labelling the edges as safe or hazardous.

Synthetic materials were sought which, when applied in a specific manner to the test edges, would be completely penetrated by only those edges labelled hazardous. Then such materials could be used in an inspection procedure for unknown edges. Tests were conducted on many synthetics, but only a few showed possibilities in this regard.

NBSIR 73-343. **Calibration of impulse noise generators,** G. R. Reeve, 77 pages (Oct. 1973). Order from NTIS as COM 75-10282, $4.75.

Key words: impulse; impulse generator calibration; impulse noise; impulse noise generator.

This report covers work performed by the Electromagnetics Division, Institute for Basic Standards, National Bureau of Standards, on a Signal Corps contract to develop a calibration system for impulse noise generators. Various technical approaches are discussed with their respective problems. A prototype system which was constructed is presented along with some measurements of its capability. Finally another approach is suggested utilizing newer techniques and instrumentation which should come closer to achieving the desired level of performance.

NBSIR 74-372. **Cryogenic refrigerators for shipboard forward looking infrared applications,** R. O. Voth, 75 pages (June 1974). Order from NTIS as AD/A006037, $4.75.

Key words: cryogenics; infrared detector; 77 K refrigerator; low capacity; reliability; shipboard.

The Naval Ordnance Laboratory (NOL) has asked the Cryogenics Division of the National Bureau of Standards to investigate and evaluate 1) commercially available refrigerators, 2) refrigerators under development, and 3) new or novel ideas applicable to a refrigerator to cool infrared detectors in a shipboard Forward Looking Infrared (FLIR) system. Although a refrigerator has been selected for two prototype FLIR units, the study was initiated to select the most appropriate refrigerator for additional purchases of FLIR units. The FLIR requires a refrigerator capacity of approximately 2 watts at 77 K and a physical configuration allowing for an interface to the FLIR unit. Information was collected by interviewing FLIR manufacturers, surveying refrigerator manufacturers and by contacting users of similar systems. Correlation of this information with the NOL requirements is presented herein. The primary difference between airborne/spaceborne refrigerators and a shipborne refrigerator is the accessibility for minor repairs on-board ship although major repairs may be deferred for extended periods of time. It is anticipated that the shipboard units will operate away from major maintenance facilities, for periods as long as 6 months, with the refrigerator operating at least half of this time. Thus, reliability and ease of maintenance are emphasized when evaluating the various systems.

NBSIR 74-391. **Electromagnetic noise in Lucky Friday Mine,** W. W. Scott, J. W. Adams, W. D. Bensema, and H. Dobroski, 139 pages (Oct. 1974). Order from NTIS as COM 74-10258, $5.75.

Key words: amplitude probability distribution; digital data; electromagnetic interference; electromagnetic noise; emergency communications; Fast Fourier transform; Gaussian distribution; impulsive noise; magnetic field strength; measurement instrumentation; mine noise; spectral density; time-dependent spectral density.

Measurements of the absolute value of electromagnetic noise and attenuation along a hoist rope were made in an operating hard-rock mine, Lucky Friday Mine, located near Wallace, Idaho. Spectra of electromagnetic noise generated by various pieces of equipment, spectra of specific noise signals at various depths, and noise and attenuation on the 4250 foot (1295 meter) hoist, were measured. Three techniques were used to make the measurements. First, noise was measured over the entire electromagnetic spectrum of interest for brief time periods. Data were recorded using broadband analog magnetic tape for later transformation to spectral plots. Second, noise amplitudes were recorded at several discrete frequencies for a sufficient amount of time to provide data for amplitude probability distributions. A third technique gave attenuation data through the direct measurement of field strength at various depths.

The specific measured results are given in a number of spectral plots, amplitude probability distribution plots and amplitude curves as a function of depth.

NBSIR 74-394. **A rack-mounted precision waveguide-below-cutoff attenuator with an absolute electronic readout,** C. C. Cook, 45 pages (Nov. 1974). Order from NTIS as COM 75-10126, $3.75.

Key words: absolute (unambiguous) readout; piston; precision attenuator; sensor; waveguide-below-cutoff.

A coaxial precision waveguide-below-cutoff attenuator is described which utilizes an absolute (unambiguous) electronic digital readout of displacement in inches in addition to the usual gear-driven mechanical counter/dial readout in decibels. The attenuator is rack-mountable and has the input and output rf connectors in a fixed position. The attenuation rate for 55, 50, and 30 MHz operation is given along with a discussion of sources of errors. In addition, information is included to aid the user in making adjustments on the attenuator should it be damaged or disassembled for any reason.

NBSIR 74-395. **Bibliography of the Electromagnetics Division, June 30, 1973 to June 30, 1974,** M. L. Woolley, 26 pages (Nov. 1974). Order from NTIS as COM 75-10161, $3.75.

Key words: antenna parameters; attenuation; automated measurements; EM Metrology; field strength; impedance; noise; phase; power; pulsed quantities; squids; transmission lines; waveform analysis; waveguides.

This bibliography lists the publications of the NBS Electromagnetics Division between June 30, 1973 and June 30, 1974.

NBSIR 74-398. **Provisional values for the thermodynamic functions of ethane,** R. D. Goodwin, 342 pages (June 1, 1974). Order from NTIS as COM 75-10130, $9.50.

Key words: densities; enthalpies, entropies; equation of state; internal energies; isobars; isochores; isotherms; Joule-Thomson inversion; latent heats of vaporization; melting line; orthobaric densities; specific heats; speeds of sound; vapor pressures.

Thermophysical properties are tabulated at uniform temperatures over the entire range of fluid states from 90 to 600 K along isobars to 700 bar. A new, rational equation of state is employed for the first time. Thermodynamic functions in the compressed liquid at $T < T_c$ are obtained by use of specific heats $C_\mu(T)$ along a high pressure isobar.

NBSIR 74-465. **Shear and tension-bending fatigue test methods for threaded airframe fasteners,** D. J. Chwirut, D. E. Marlowe, and J. S. Steel, 56 pages (Sept. 1974). Order from NTIS as COM 75-10417, $4.25.

Key words: airframe fastener; double shear; fatigue; single shear; tension-bending; test methods.

Fatigue test methods for threaded airframe fasteners loaded in other than direct tension are described. The types of loading considered are single shear, double shear, and tension-bending. The test fixtures used in these tests are described. Results of tests on lots of fasteners from different manufacturers indicate that fasteners considered identical on the basis of direct tension procurement tests exhibit different fatigue life characteristics when loaded in shear and/or tension-bending. Thus the test methods described herein may be of future value as procurement tests for airframe fasteners.

NBSIR 74-482. **An automated system for precision calibration of accelerometers,** B. F. Payne, 196 pages (Apr. 1974). Order from NTIS as COM 75-10147, $7.25.

Key words: acceleration; automation; calibration; measurements; minicomputer; shakers; standards; transducers; vibration; vibration exciters; vibration pickups.

The report describes an automated system for accelerometer calibration under realtime control by a small, dedicated digital computer. The hardware components of the system and the software programs are given. The software automatically regulates the rate and amount of data collected based on analysis of input data. Printout of the frequency response of test accelerometers is on a teletypewriter and also can be stored on a magnetic tape. Manual operation of the system is also described.

NBSIR 74-488. **Measurements of railroad noise-line operations, yard boundaries, and retarders,** J. M. Fath, D. S. Blomquist, J. M. Heinen, and M. Tarica, 108 pages (Dec. 1974). Order from NTIS as COM 75-10088, $5.25.

Key words: acoustics; noise measurement; noise (sound); railroad yard; trains.

A field investigation of noise emission from railroad operations was conducted. The objectives of the study were the establishment of a data base on the noise levels associated with railroad operations, both line (trains in transit) and yard, and the development of measurement procedures that could be utilized in regulations applicable to the noise from rail carrier equipment and facilities. For trains in transit, measurements were made as a function of horizontal distance from the tracks [five locations at 25, 50, 100, 200 and 400 feet] and as a function of microphone height [three different heights at the 25 and 50 foot microphone locations]. Train passby data are presented as the maximum A-weighted sound level observed during the passby and as Single Event Noise Exposure Levels (both A-weighted and one-third octave band levels). A-weighted sound level measurements were made at the boundary of the railyard, at 0.1 second intervals, for periods of time ranging from 1 to 23 hours over several days. These data are presented as the energy equivalent sound level and the level exceeded ten percent of the time. The directionality of retarder noise was also investigated. Measurements were made of the noise emitted in various directions during retarder operation.

NBSIR 74-501. **Development of specifications for archival record materials,** W. K. Wilson, 17 pages (May 23, 1974). Order from NTIS as COM 75-10131, $3.25.

Key words: aging of paper; archival materials; natural aging; old paper; paper, aging of; paper, stability of; paper testing; stability of paper.

Effort on a long range program on the Development of Specifications for Archival Record Materials has included: (1) Reappraisal of research needs; (2) a study of 18 papers made in 1937, tested before and after dry accelerated aging in 1937, and tested again in 1973; (3) evaluation of 19 commercial papers, evaluated before and after moist accelerated aging in 1963, and tested again in 1973; and (4) development of specifications for copies from office copying machines.

A review of the literature on stability of paper and data obtained in this laboratory over the past several years indicate that a fresh approach is needed to a study of the stability of paper. The following tasks are suggested: (1) Continue to use handsheets of known composition; (2) study old papers to determine changes that probably have occurred during natural aging; (3) confine testing to methods that give some clues concerning what happens during aging such as zero span tensile, wet strength, peroxide formation, functional group content, and molecular chain length distribution; and (4) study the effect of cycling of relative humidity on the properties of paper.

NBSIR 74-514. **1973 international activities, Center for Building Technology,** C. C. Raley, 54 pages (July 1974). Order from NTIS as COM 75-10102, $4.25.

Key words: cooperative programs; foreign visitors; information exchange; international building technology; international organization memberships; professional interaction.

This report summarizes the Center for Building Technology's 1973 international activities including formal cooperative programs, exchange programs, special projects, international organization memberships, foreign guests at CBT, and CBT foreign travel.

NBSIR 74-521. **HATCH—A model for fish hatchery analysis,** F. C. Johnson, 73 pages (July 8, 1974). Order from NTIS as COM 75-10187, $4.25.

Key words: benefit/cost; fish hatchery analysis; fish hatchery management; fish hatchery operation; mathematical model.

The HATCH model is an automated system for analyzing the physical, biological and economic factors of fish hatchery operation and for computing optimal hatchery management policies.

NBSIR 74-522. **First interim report on salmon fishery modelling,** F. C. Johnson, 21 pages (July 8, 1974). Order from NTIS as COM 75-10080, $3.25.

Key words: analysis of biological processes; economic performance; fisheries management; fisheries regulation; mathematical models; salmon fisheries model.

The salmon fishery modelling project is a joint State-Federal program for the development of improved techniques for analyzing the economic and biological effects of changes in the Pacific Coast salmon fishery regulatory parameters. This interim report covers the initial program design phase of the project.

NBSIR 74-526. **Analysis of non-reinforced masonry building response to abnormal loading and resistance to progressive collapse,** W. McGuire and E. V. Leyendecker, 67 pages (Nov. 1974). Order from NTIS as COM 75-10087, $4.25.

Key words: abnormal loading; building; gas explosion; load-bearing masonry; load-bearing walls; masonry; masonry research; progressive collapse.

Five case studies of susceptibility to progressive collapse were made of non-reinforced masonry bearing wall buildings. All were assumed to comply with governing building codes. Based on the assumed failure mechanisms, analysis indicated that two of the structures had excellent resistance to progressive collapse, one was marginal, and two had little resistance to progressive collapse. Analytical approaches used are illustrated and areas of needed research are identified.

NBSIR 74-542. **Economics of protection against progressive collapse,** R. E. Chapman and P. F. Colwell, 34 pages (Sept. 1974). Order from NTIS as COM 75-10081, $3.75.

Key words: benefit-cost analysis; building safety; economics; progressive collapse; standards.

Public and government concern about the progressive collapse of buildings caused by abnormal loading has resulted in the development of draft standards to provide protection against progressive collapse. From society's viewpoint, standards for protection against progressive collapse should result in a level of protection which is

more efficient (i.e., the net social benefits from protection should be increased). An economic model utilizing the principles of benefit-cost analysis is developed which establishes a methodology for determining the efficiency of various levels of protection against progressive collapse. An application of the model to a partial evaluation of a specific standard demonstrates some of the capabilities of the model. Recommendations are made for a complete evaluation of this standard and for the further refinement of the model.

NBSIR 74-581. **Development of a solid sorption tube for sampling hydrogen fluoride in the work atmosphere,** J. Wing and J. K. Taylor, 45 pages (Oct. 1974). Order from NTIS as COM 75-10127, $3.75.

Key words: air analysis; air sampling; gas analysis; hydrogen fluoride; industrial hygiene; sodium acetate; sorber; solid; work atmosphere.

The efficiencies of several solid substances in a sorption tube for collecting trace quantities of hydrogen fluoride gas in work atmosphere have been evaluated. Reagent-grade sodium acetate crystals proved to be a very efficient sorbent for hydrogen fluoride. Its solubility in water and pH buffer properties are highly advantageous for subsequent fluoride determination by the ion selective electrode. Experimental results are presented for collection efficiencies of hydrogen fluoride gas at several concentration levels, flow rates, and collection times, the effects of elevated temperatures and humidity, and also breakthrough, bleed-out, storage and shipment studies. Specifications for construction of the sorption tubes are also given.

NBSIR 74-591. **Some problems noted in the use of Taguchi semiconductor gas sensors as residential fire/smoke detectors,** R. W. Bukowski and R. G. Bright, 12 pages (Dec. 1974). Order from NTIS as COM 75-10101, $3.25.

Key words: false alarm; fire detector; fire test; residential smoke detector; semiconductor gas sensor; sensor contamination.

This paper examines some aspects of Taguchi semiconductor gas sensors and their use as residential fire/smoke detectors based on theoretical and experimental considerations. It was found that these sensors have difficulty detecting fires involving complete combustion along with a greater than normal propensity to false alarm to other than fire conditions. Both of these problems raise serious questions as to the suitability of these sensors as residential fire/smoke detectors, at least at their present state of development.

NBSIR 74-596. **Radiative heat transfer from products of combustion in building corridor fires,** K. Bromberg and J. G. Quintiere, 28 pages (Feb. 1975). Order from NTIS as COM 75-10209, $3.75.

Key words: combustion products; full-scale fire; radiative heat transfer.

The contribution of radiative heat transfer from hot combustion products to corridor floors is examined. Data from full-scale corridor fire experiments is used to calculate emissivity and absorptivity of the combustion products. An empirical model based on attenuation by absorption is used to specify the absorption coefficient due to particulates in the products. In these experiments it is shown that radiation from the combustion products is just as significant as radiation from convectively heated walls and ceiling of the corridor. Calculations show that the ratio of radiant heat transfer to the floor due to ceiling emission to that by combustion product emission ranges from about 0.2 to 0.7. Also, molecular gas radiation and particulate radiation can both be significant for the combustion products. Calculations show that the emissivity of the gaseous combustion products alone would be about 0.3, but the inclusion of soot particles yields an emissivity for the total combustion product mixture of as high as 0.73, based on the experimental data considered.

NBSIR 74-605. **Crush characteristics of automobile structural components,** D. C. Robinson, 65 pages (Jan. 1975). Order from NTIS as COM 75-10464, $3.75.

Key words: automobile side impact; crush characteristics; displacement measurements; door structure; drop tests; dynamic crush tests; impact collisions; plastic deformation; static crush tests; strain measurements; structural components; test procedures.

Static and dynamic test procedures were developed for evaluating the crush characteristics of automotive structural components which perform a major structural function in side impacts. Laboratory tests were conducted on several 1969 to 1971 4-door intermediate size automobiles to evaluate the crush characteristics of some of their structural components. Static crush tests were conducted in the 12-million-lbf capacity universal testing machine at the National Bureau of Standards, employing its large working space. The dynamic tests were conducted using the monorails attached to the sensitive crosshead and the tie-down floor system which is incorporated in the foundation of this machine. The crush loads were applied perpendicular to the vehicle side for each of the tests. The response of the structural components was established based on the evaluation of displacement and/or strain measurements and detailed examination of the permanently deformed components following each test. Empirical factors were obtained which are useful for comparison of static and dynamic crush characteristics of a vehicle side door structure over a limited loading range. Further development of the test procedures is required in order to extend the range over which such results would be meaningful.

NBSIR 74-606. **Consumer product noise: A basis for regulation,** P. G. Weissler, G. A. Zerdy, and S. G. Revoile, 80 pages (Nov. 1974). Order from NTIS as COM 75-10340, $4.75.

Key words: consumer products; criteria for safety standards; federal regulations; hearing impairment; hearing survey; noise emission; speech communication interference.

The Consumer Product Safety Commission is charged with the responsibility for promulgating safety standards to protect the public against unreasonable risks of injury associated with consumer products. There is a risk of injury from noisy products, directly by damage to hearing and indirectly by degradation of essential speech communication. This report develops criteria relevant to the specification of Safety Standards for noisy consumer products. Consumer product noise is discussed in relation to the existing body of knowledge regarding noise induced hearing loss and speech communication. Levels of product noise are identified that should protect against hearing impairment and against speech communication degradation. Methods of measurement for consumer product noise are described and a bibliography of standards relevant to the regulation of noisy consumer products is provided. A list of products that are potentially hazardous to the hearing of the operator is included with typical levels and usage patterns. The list is based upon reported data and some measurements made at NBS. Possible discrepancies among noise regulations established by different governmental agencies are discussed with suggestions for obtaining uniformity.

NBSIR 74-608. **Procedure for measuring noise emission from power lawn mowers,** J. I. Adler, 19 pages (Nov. 1974). Order from NTIS as COM 75-10056, $3.25.

Key words: emergency messages; hearing loss; lawn mowers; noise emission; noise pollution; product safety.

A procedure is described for measuring the noise emission from power lawn mowers. The procedure covers both walk-behind and riding mowers, including suggestions of maximum noise levels for protection from hearing loss and for reception of emergency messages. The procedure employs a microphone located near the ear of the operator and mounted on a back-pack worn by the operator.

NBSIR 74-610. **Investigation of procedures for determination of thermal performance characteristics of plastic piping used in housing,** M. Tryon, 36 pages (Nov. 1974). Order from NTIS as COM 75-10072, $3.75.

Key words: chlorinated polyvinyl chloride; hardness; internal stress; polyvinyl chloride; thermal mechanical analysis (TMA); thermal properties; thermogravimetric analysis (TGA); thermoplastic pipe.

The rapid growth of the use of thermoplastic pipe for plumbing in housing has prompted a study to determine the critical factors affecting the performance of the pipe materials. The emphasis in this preliminary study is on thermal properties such as the softening point, relaxation of thermal stress, glass transition temperature, hardness-temperature relationship, and decomposition temperature. The techniques used were thermal mechanical analysis (TMA), thermogravimetric analysis (TGA), and hardness. Preliminary results obtained on several pipe samples of PVC and CPVC commercial samples are reported.

NBSIR 74-612. **Building and evaluation of a second polluted air delivery system,** G. P. Baumgarten, 11 pages (Nov. 1974). Order from NTIS as COM 75-10414, $3.25.

Key words: air pollution; critical flow; laminar flow; nozzle; porous plug; sulfur dioxide concentration; carbon dioxide concentration.

The building and evaluation of a second configuration of a prototype SO_2 and CO polluted air delivery system (PADS) is discussed. The delivery system was built to deliver sulfur dioxide (SO_2) and carbon monoxide (CO) at a rate of 5 liters per minute. The design concentrations by volume were 1.0, 0.5, 0.1, and 0.04 parts per million (ppm) of SO_2 in air and 50, 20, and 2 parts per million of CO in nitrogen. It consists of a diluent air delivery system utilizing a critical flow sonic nozzle and three separate pollutant flow systems utilizing laminar flow porous plugs, one plug for each desired output concentration. The system is contained in a dispatch case and the gases are delivered to it from pressurized containers through detachable supply lines.

By maintaining specific upstream pressures on the critical flow nozzle and the laminar flow porous plugs, PADS 2 produced average output concentrations of: 0.95, 0.50, 0.117, and 0.057 ppm of SO_2; and 52.9 and 18.1 ppm of CO. These concentrations were determined by measurements with NBS calibrated analyzers. The expected output concentrations were 0.03, 0.52, 0.103, and 0.05 ppm of SO_2 and 51.2, 18.0, and 1.49 ppm of CO based on flow calibrations of the individual components. The uncertainty of the output concentration is estimated to be about 7 percent.

NBSIR 74-613. **Preliminary study of the slipperiness of flooring,** A. P. Cramp and L. W. Masters, 42 pages (July 1974). Order from NTIS as COM 75-10059, $3.75.

Key words: floor slipperiness; resilient flooring; slipperiness standards; frictional tests; slip tests; coefficient of friction; human perambulation.

The National Commission on Product Safety reported in 1970, that falls in the home each year kill about 12,000 and injure 6,000,000 in the U.S.A. Slippery floors are listed as a large contributor to these very high casualty figures. Although there are some standardized test methods that are or might be suitable for such standards, there are no slipperiness standards for flooring. Thus, there is an immediate need for studies aimed at the development and establishment of such standards. Consequently, a preliminary study of floor slipperiness was sponsored by the Building Safety Section of the Center for Building Technology. The study included a state-of-the-art investigation on flooring slipperiness research and a laboratory evaluation of three existing test methods for measuring floor slipperiness. Samples of the three most commonly used resilient flooring materials, namely: vinyl asbestos, vinyl and linoleum were used in the study. The sliding material components for the frictional tests were leather and a commonly used styrene butadiene sole and heel rubber. The tests were performed both dry and wet. The results from this study were used in planning a large comprehensive study, which would lead to the development of accepted floor slipperiness standards. This report contains the results of the preliminary study.

NBSIR 74-619. **Measurement methodology for determining the sound output of toy guns,** M. A. Cadoff and D. S. Blomquist, 17 pages (Aug. 1974). Order from NTIS as COM 75-10047, $3.25.

Key words: children; consumer safety; guns; hearing damage; noise; standard apparatus; toys.

In recent years, a great concern has been expressed for consumer protection and safety, especially for children. As an outgrowth of this concern, acoustical testing of potentially-hazardous noise-producing toys has been carried out at the National Bureau of Standards for the Consumer Product Safety Commission under the authority of the Toy Safety Act of 1969. This report outlines a methodology which was developed to measure the noise levels of toy guns. In addition, the rationale and technical back-up for the methodology are discussed, and the regulations setting allowable noise levels for toy guns are given.

NBSIR 74-621. **Stability and strength of home playground equipment,** B. M. Mahajan, 39 pages (Dec. 1974). Order from NTIS as COM 75-10422, $3.75.

Key words: home playground equipment; stability; strength; test; testing; tipping.

Stability tests were performed on some items of home playground equipment to measure the magnitude of the force, applied to generate tipping moment, required to start the tipping of the equipment.

Strength tests were conducted by loading certain components of home playground equipment with estimated loads to determine if the tested equipment had adequate strength.

NBSIR 74-623. **Stability and abuse tests of riding toys,** W. C. Brown and H. A. Baker, 87 pages (Jan. 1975). Order from NTIS as COM 75-10210, $4.75.

Key words: abuse testing; dynamic stability; hazards; obstruction; riding toys; stairway; static stability; test weight; tilt angle; toy testing.

Stability and abuse tests were conducted on 88 riding toys in order to provide information which can be utilized to set realistic abuse performance levels for riding toys, as well as characterize the types of stability hazards associated with this class of toys. The results of these tests are summarized in tabular form and a description of the discrepancies encountered as well as photographs of these discrepancies are presented.

The appendices of this report contain photographs of each test specimen as well as the tabulated raw data for each test conducted.

NBSIR 74-624. **The Shirley Highway Express-Bus-on-Freeway Demonstration Project. A study of reverse commute service,** R. Waksman, 44 pages (Dec. 1974). Order from NTIS as COM 75-10412, $3.75.

Key words: bus-on-freeway operations; choice and captive riders; cost allocation formula; incremental costs and revenues; reverse commute bus service; Shirley Highway; transportation planning.

Bus-on-freeway operations generally provide peak period commuter transit service to persons traveling from suburban residences through congested corridors to jobs in the major employment centers of metropolitan areas. In a few cases, peak period reverse commute operations may provide service to persons traveling from residences

near the downtown employment centers to jobs in the suburbs. In early 1973, two major Shirley Highway Express-Bus-on-Freeway Demonstration Project reverse commute routes began service to office buildings in Northern Virginia.

An analysis of this reverse commute service revealed that it was a successful operation because it provided considerable benefits to its patrons and was slightly profitable to the bus operator on an incremental cost basis.

Four conditions which were important for the success of the service were found to be important for the success of reverse commute operations, in general. The conditions are as follows: (1) A given route should serve a concentrated, high employment area. (2) The route should be accessible to people currently working within the employment area and to captive riders who can fill jobs there. (3) It should be possible to fit most of the reverse commute trips into existing bus schedules. (4) It should be possible to pair with peak direction trips any trips that cannot be fit into existing bus schedules.

Using a procedure which incorporates these conditions, one employment area within the Shirley Highway Corridor was identified as having potential as a market for a reverse commute service.

NBSIR 74-626. **Semiconductor nuclear radiation detector studies—A final report,** A. H. Sher, 10 pages (Sept. 1974). Order from NTIS as COM 75-10411, $3.25.

Key words: carrier trapping; gamma-ray detector; germanium; Ge(Li) detector; infrared response; silicon.

In response to a problem that arose with regard to the availability of germanium for lithium-drifted germanium detectors [Ge(Li) detectors], a comprehensive program was undertaken aimed toward the development of a method for the rapid specification of germanium quality for nuclear radiation detector use, and the determination of factors affecting germanium quality. Measurements on a large number of germanium crystals, most of which had been rejected for detector use, and intercomparison of these measurements and the methods employed, led to significant developments in the measurement of lithium mobility and driftability, carrier trapping, and semiconductor defect and impurity determination via an improved infrared response (IRR) technique. The present improvement of the infrared response technique resulted in the observation of a number of discrete energy levels lying within the forbidden gap of germanium unobserved in previous studies. It was possible to assign the proper position of energy levels detected by IRR in the upper or lower half of the energy gap. It was thus possible, in some instances, to determine the nature of the defects responsible for the observed energy level from results reported in the literature. The goal of developing a method for the rapid specification of germanium quality was achieved.

NBSIR 74-627. **The influence of ink on the quality of fingerprint impressions,** R. T. Moore, 16 pages (Dec. 12, 1974). Order from NTIS as COM 75-10134, $3.25.

Key words: film thickness; film uniformity; fingerprint impressions; fingerprint readers; image quality; ink films; lubricity.

Tests were conducted on several types of ink to determine their influence on the quality of fingerprint impressions which they could produce. The thickness and uniformity of the film used to ink the fingers were found to be the most significant factor in providing high quality impressions. A method is described for metering out printer's ink and estimating whether or not a uniform film of near optimum thickness has been rolled out on a glass inking plate.

NBSIR 74-628. **Mass transport and physical properties of large crystals of calcium apatites: Studies of $Ca(OH)_2$ crystals for use in electrolytic conversion of calcium fluorapatite crystals to calcium hydroxyapatite,** A. D. Franklin and K. F. Young, 22 pages (Sept. 1, 1973-Aug. 31, 1974). Order from NTIS as COM 75-10514, $3.25.

Key words: Ac impedance; calcium apatites; calcium hydroxide; crystal growth; electrolysis; interfacial polarization; ionic conduction; mass transport.

In order to convert single crystals of calcium fluorapatite to calcium hydroxyapatite, an electrolytic cell technique will be explored. To utilize such a technique, the cathode compartment must consist of a source of hydroxyl ions and a barrier to the flow of all others. $Ca(OH)_2$ has been selected for the cathode material, backed by a Pt electrode in an atmosphere containing H_2O and O_2. $Ca(OH)_2$ crystals have been grown and Ag as well as Pt electrodes applied to them. Their ac admittance as a function of temperature has been measured and analyzed. A Warburg contribution to the admittance was observed to depend upon the presence of O_2. Equivalent circuits have been generated from the data allowing us to tentatively characterize the electrical properties of the electroded crystal system.

NBSIR 74-631. **Analysis of proposed air drying process,** L. Greenspan, 11 pages (Dec. 1974). Order from NTIS as COM 75-10208, $3.25.

Key words: absorption; drying; phosphorous pentoxide; water vapor.

NASA proposal No. 7401-6-01A by the GCA Corporation describes a proposed air drying process which has been analyzed. The drying process, intended to reduce the water vapor content of a stratospheric sample to below one part per million by weight, is based upon the removal of the water as it passes through a phosphorous pentoxide absorber. The analysis indicates that the method is feasible. Dependence on ram pressure to maintain flow through the absorber appears questionable and consideration should be given to other means.

NBSIR 74-635. **Method of testing for rating solar collectors based on thermal performance,** J. E. Hill, T. Kusuda, 63 pages (Dec. 1974). Order from NTIS as COM 75-10276, $4.25.

Key words: solar collector; solar energy; solar radiation; standard; standard test; thermal performance.

The National Bureau of Standards has made a study of the different techniques that could be used for testing solar collectors and rating them on the basis of thermal performance. This document outlines a standard test procedure based on that study. It is written in the format of a standard of the American Society of Heating, Refrigerating, and Air Conditioning Engineers and specifies the recommended apparatus, instrumentation, and test procedure.

NBSIR 75-639. **Optical materials characterization,** A. Feldman, D. Horowitz, R. M. Waxler, I. Malitson, M. J. Dodge, 17 pages (Jan. 1975). Order from NTIS as COM 75-10135, $3.25.

Key words: coefficient of thermal expansion; elastic constants; infrared laser window materials; photoelasticity; polycrystalline ZnSe; refractive index; stress-optical constants; thermal coefficient of refractive index.

We have measured the following parameters of chemical vapor deposited polycrystalline ZnSe (CVD ZnSe): Refractive index and change of index of refraction with temperature (dn/dT) over the wavelength range 0.5 μm to 18 μm using the method of minimum deviation; the coefficient of linear thermal expansion and dn/dT at 10.6 μm using Fizeau interferometry; and the elastic moduli and photoelastic moduli using Fizeau and Twyman-Green interferometry. A sensitive technique has been developed for measuring stress-optical constants of materials that exhibit a small stress-optical effect.

NBSIR 75-647. **Mechanical tests of FAA-E2491 airport in-pavement approach and threshold lights,** D. C. Robinson, 26 pages (Jan. 1975). Order from NTIS as COM 75-10418, $3.75.

Key words: airport approach and threshold lights; glass prism; impact tests; light bases; optical cover assembly; photometric measurements; static tests.

Static and impact load tests were performed on two style FAA-E-2491 airport in-pavement approach and threshold lights which were mounted in light bases encased in concrete. Static tests were conducted using either a 6-inch diameter steel plate or a rubber pad through which loads were applied to the center of the light optical cover assembly. Drop tests were conducted using a 5-lb steel ball which was directed to impact at various locations on the optical cover assembly. The old style lights were found to comply with load requirements for the current specification. The maximum load sustained by both style lights when loaded through a rubber pad was about two-thirds of the maximum load sustained when loading directly through the steel plate. A discussion is given of the photometric measurements of the light beam displacement measured during the load tests, the deflections and strains of two new style lights measured under two loading conditions and the test procedures for determining the performance of approach and threshold lights.

NBSIR 75-654. **NBS interagency transducer project—A project report,** P. S. Lederer and J. S. Hilten, 15 pages (Feb. 20, 1975). Order from NTIS as COM 75-10367, $3.25.

Key words: calibration; dynamic; photo flashbulb; pressure; pressure measurement; pressure transducer; thermal transient; transducer.

A method is being developed to apply short-duration thermal transients to pressure transducers and to observe the effects of these transients on transducer performance. The method consists of monitoring pressure transducer output as the transducer is exposed to radiation resulting from the ignition of a photographic flashbulb or from the discharge of an electronic flash. During this reporting period, the work has been exploratory in nature to determine values for method parameters. Thermal energy pulses as high as 0.4 J lasting 4 ms have been generated using an electronic flash; pulses as high as 1 J lasting 18 ms have been generated using No. 22 flashbulbs.

Work being performed for other agencies is also described briefly.

NBSIR 75-658. **Electron microscopic observations of microcracking about indentations in aluminium oxide in silicon carbide,** B. J. Hockey and B. R. Lawn, 39 pages (Jan. 1975). Order from NTIS as AD/A007445, $3.75.

Key words: brittle solids; dislocation networks; electron microscopy; healing; indentations; microcracking; moiré patterns.

Transmission electron microscopy is used to examine the nature of microcracking about small-scale indentations in two highly brittle solids, sapphire and carborundum. The observed crack geometry is discussed in terms of an earlier model of indentation fracture beneath a point force, in which both loading and unloading half-cycles contribute to the crack growth. The residual interfaces are characterised mainly by moiré patterns, sometimes by dislocation networks. These observations are discussed in relation to spontaneous closure and healing mechanisms, and the "lattice mismatch" necessary for their production estimated at about one part in a thousand. It is shown that cleavage steps comprise the main source of obstruction to lattice restoration across the interfaces. Mechanical and thermal treatments of the indented surfaces are found to influence the extent of the residual cracking. Some practical implications of the observations are discussed.

NBSIR 75-659. **A new mode of chipping fracture in brittle solids, and its application in a model for wear under fixed abrasive conditions. I. Mode of chipping fracture. II. Wear model,** B. R. Lawn, 49 pages (Feb. 1975). Order from NTIS as COM 75-10515, $3.75.

Key words: abrasion; brittle solids; brittle surfaces; chipping; fracture; hardness; indentation; residual stress; stress analysis; wear rate.

A description is given of the mode of chipping fracture observed in highly brittle solids. It is pointed out that residual stresses about indentation deformation centers play a vital role. The implications of this mode in a number of mechanical phenomena are discussed.

An explicit model for the wear of brittle surfaces under fixed abrasive conditions is presented in terms of indentation fracture concepts. The predicted wear rate for glass agrees with that observed experimentally to within an order of magnitude. Some implications concerning the parameters which influence the abrasion process, particularly the hardness, are discussed.

NBSIR 75-662. **Sulphur dioxide reference materials,** J. K. Taylor and E. R. Deardorff, 16 pages (Feb. 1975). Order from NTIS as COM 75-10420, $3.25.

Key words: air pollution; chemical analysis; pararosaniline method; quality control; reference materials; sulfur dioxide.

The development of reference materials to serve for quality control and performance evaluation of measurements of sulfur dioxide by the pararosaniline method is described. Powder samples consisting of sodium sulfite dispersed in mannitol can be prepared to evaluate measurements for the concentration levels of ambient interest. The samples are sufficiently stable in routine use, with a service life of at least three months. By the use of a series of five samples of graded sulfite content, measurement errors greater than five percent are significantly detected. A detailed procedure for preparation of the samples is included. Preliminary studies of an alternate method for preparation of quality control samples, by a freeze-drying process are also described.

NBSIR 75-664. **Strength degradation of brittle surfaces: Blunt indenters,** B. R. Lawn, S. M. Wiederhorn, and H. H. Johnson, 40 pages (Feb. 1975). Order from NTIS as AD/A007447, $3.75.

Key words: brittle solids; ceramic surfaces; cracks; degradation; fracture; Hertzian; indentation; strength.

Indentation fracture mechanics is used to develop a theoretical basis for predetermining the strength properties of brittle surfaces in prospective contact situations. Indenters are classified as "blunt" or "sharp," of which only the first is considered in the present work. The classical Hertzian cone crack conveniently models the fracture damage incurred by the surface in this class of indentation event. Significant degradation is predicted to occur at a critical contact load; however, with increasing load beyond this critical level the degradation rate becomes relatively slight. Bend tests on abraded glass slabs confirm the essential features of the theoretical predictions. The role of controlling variables in the degradation process, notably starting flaw size and indenter radius, is systematically investigated. An indication is also given as to optimisation of material parameters. The analysis leads to some novel suggestions concerning surface preparation procedures that might be followed in order to minimize strength losses.

NBSIR 75-665. **Point-to-Point Trip Management Program (preliminary analysis),** W. G. Kienstra and D. J. Minnick, 26 pages (Feb. 7, 1975). Order from NTIS as COM 75-10421, $3.75.

Key words: computers; information systems; mass transportation; telephone systems.

This preliminary analysis of Point-to-Point Trip Management (PTPTM) was prepared for the Urban Mass Transit Administration in Washington, D.C. PTPTM is concerned with providing prospective riders of mass transit with the necessary detailed information for particular trips. This report contains the results of a literature search on automation in the telephone information center, and analyzes the data collected from 29 existing centers. Additionally, on-site visits were made to three operational centers, and tapes of actual telephone inquiries and responses were obtained and analyzed. The use of microfiche and computers are examined as an aid to the operators in

these centers. Total automation of these centers is also discussed. Conclusions and recommendations for further study in this area, and an annotated bibliography, are also part of this report.

NBSIR 75-672. **A preliminary approach to performance requirements and criteria for electrical connections in residential branch circuit wiring,** W. J. Meese, R. L. Cilimberg, and A. A. Camacho, 37 pages (Mar. 1975). Order from NTIS as COM 75-10338, $3.75.

Key words: branch circuits; contact resistance; electrical codes; electrical connections; fire safety; housewiring; performance testing.

During the Operation BREAKTHROUGH Research and Demonstration program the U.S. Department of Housing and Urban Development became concerned with the inability to properly evaluate innovative electrical connections. Innovation in electrical connections has been very slow because of the long-life requirements, stringent fire safety requirements, long established conventional practices and evaluation procedures and lack of a performance base for describing requirements. This preliminary report presents the framework for a proposed method to evaluate electrical connections on a performance basis and supplements information contained in a previous report on current technology of electrical connections used in residential branch circuit wiring. Innovations involving electrical connections may lead to significant advancements in housing construction if it can be demonstrated that functional and safety requirements over the expected life of electrical connections were adequately satisfied. Research is needed to enable prediction of long-term performance of electrical connections based on the results of accelerated performance tests.

NBSIR 75-677. **Hazard assessment of aluminum electrical wiring in residential use,** E. D. Bunten, J. L. Donaldson, and E. C. McDowell, 58 pages (Dec. 1974). Order from NTIS as COM 75-10516, $4.25.

Key words: aluminum wire; consumer product safety; electrical failures; electrical fires; electrical wiring; fire hazards.

In the mid-1960s, aluminum wire began to be used in significant quantities for residential branch-circuit wiring. Reports of problems from various localities in the U.S. raised serious concern and controversy as to the safety of this application. An official determination on this matter is within the jurisdiction of the Consumer Product Safety Commission. This report reviews the history of the use of aluminum in residential wiring and describes the characteristics essential to data to be used to evaluate the performance of aluminum wiring in the field. The examination of existing field data shows that no available data have the characteristics necessary to develop a reliable estimate of the level of risk to consumers associated with aluminum wiring. Neither can the available data be used to establish the relative risk of aluminum compared to copper wiring. There is only a gross estimate of the extent to which aluminum wiring is now in use in U.S. residences. Statistically sound estimates of risk would be possible only after data collection on a large scale.

NBSIR 75-679. **Measurements of the behavior of incidental fires in a compartment,** J. B. Fang, 29 pages (Mar. 1975). Order from NTIS as COM 75-10419, $3.75.

Key words: buildings; combustibility; fire intensity; flames; furnishings; heat release; ignition; smoke; thermal radiation; upholstery; waste receptacle.

A variety of upholstered chairs and wood cribs were burned within a ventilated compartment. The experimental measurements of weight loss, smoke concentration, temperature and heat flux levels are summarized. A reproducible fire obtained from burning a standardized wood crib array was found to be capable of representing the essential features of incidental fires of moderate intensity.

NBSIR 75-680. **Mobile home construction standards adopted by state regulatory programs—an analysis,** P. W. Cooke, L. P. Zelenka, and H. K. Tejuja, 107 pages (Mar. 1975). Order from NTIS as COM 75-10423, $5.25.

Key words: enforcement; legislation; mobile homes; regulation; standards; state-of-the-art study.

This study examines the extent to which the nationally recognized standard for the construction of mobile homes (i.e., ANSI Standard A119.1/NFPA 501B) has been adopted and amended by the individual States that have implemented enforcement programs for the regulation of mobile homes. Summary data is presented on the existing status of the various versions of the standard adopted in each State. State-adopted amendments to the technical requirements in the national standard are compiled by State and construction discipline for comparative analysis.

NBSIR 75-806. **Phase equilibrium and flow-induced desorption data for He-CO, He-N_2O, and He-N_2 systems,** W. G. Steward, R. O. Voth, J. Hord, W. R. Parrish, C. F. Sindt, and J. M. Arvidson, 62 pages (Mar. 1975). Order from NTIS as COM 75-10368, $4.25.

Key words: binary mixture; cavitating venturi; enhancement factors; experimental vapor-liquid equilibria; flow induced desorption; helium-carbon monoxide system; helium-nitrous oxide system; Henry's law constants; two phase choking; two phase flow.

Liquid-vapor equilibrium data were obtained for the helium-carbon monoxide and helium-nitrous oxide systems at pressures to 138 bars. Liquid and vapor phase compositions were measured at nominal temperatures of 80, 85, 90, 100, and 120 K (144, 153, 162, 180, and 216 °R) for the helium-carbon monoxide system, and at 235, 245, 265, and 285 K (423, 441, 477, and 513 °R) for the helium-nitrous oxide system. Internal consistency of the data was checked by using pseudo-Henry's law constants and enhancement factors.

The effects on flow of helium absorption and subsequent flow-induced desorption were investigated by means of reduced scale model experiments. Friction losses attributable to helium desorption in the long channels proved to be negligible both in experimental measurements and in calculations based on assumed equilibrium of liquid and gas. Contrarily, the assumption of phase equilibrium leads to gross miscalculations of flow rates in cavitating or near cavitating nozzles or venturis. Actual venturi mass flow rates reached in the experiments were fifty times the theoretical choking flow rates; however, definite mass flow rate reductions due to helium desorption were measured, ranging from four percent for nitrogen to twelve percent for nitrous oxide. Pertinent experiences in handling these fluids and operating the test equipment are also discussed.

This column lists all outside publications by the NBS staff, as soon after issuance as practical. For completeness, earlier references not previously reported may be included from time to time.

Achenbach, P. R., **Simplified laboratory procedures for simulating the effect of air leakage into refrigerated enclosures,** (Proc. Joint Conf. Office for Research and Experiments of the International Union of Railways and International Institute of Refrigeration, Vienna, Austria, May 6-8, 1969), Chapter in *Refrigerated Vehicles and Containers, Annex 1969-3,* pp. 89-94 (International Union of Railways, Paris, France, 1969).

Key words: air leakage; cooling load measurement; refrigerated enclosures; testing of vehicles; wind effects on structures.

A laboratory test method is needed that can be used universally for rating or acceptance of refrigerated vehicles and containers employed in international transport. Various investigators have shown that air and moisture leakage into an insulated body under the influence of impact air pressure or wind can represent a significant

fraction of the total cooling load. Since road testing and laboratory testing of vehicles and containers under realistic air flow conditions are both complex and expensive, simplified test procedures are urgently needed for simulating the effect of air leakage during cooling load tests. By making certain logical assumptions regarding the distribution of openings in an insulated body and the nature of the fluid flow through these openings, it is shown that a negative pressure of 1 mm W.G. (0.04 in W.G.) inside the cargo space will produce an air leakage into the body as large as a 100 km/hr (62.5 mph) wind on one end or a 50 km/hr (31.3 mph) wind on one long side of most vehicles and containers. A second simplified method involves determining the total cooling load by the addition of the measured heat transmission with interior heating and a calculated air leakage effect based on a measured air flow rate and an assumed change in sensible and latent heat content of the leakage air. Both of these methods need laboratory study.

Adair, R. T., Simmonds, M. B., Kamper, R. A., Hoer, C. A., **RF attenuation measurements using quantum interference in superconductors,** *IEEE Trans. Instrum. Meas.* **IM-23,** No. 4, 375-381 (Dec. 1974).

Key words: Josephson junction; quantum interference; rf attenuation; superconductivity.

A unique portable system has been developed for measuring RF attenuation over a dynamic range of 62 dB at 30 MHz. A superconducting quantum interference device (SQUID) is the basis of the system. A SQUID is a loop of superconducting metal closed by a weak point contact called a Josephson junction, operating in liquid helium. It converts variations in magnetic flux to periodic variations in impedance which are sensed at microwave frequencies. This provides a convenient natural means of measuring electrical quantities such as voltage, current, power, and attenuation.

Ambler, E., Mangum, B. W., Pfeiffer, E. R., Utton, D. B., **Magnetic ordering of crystalline and vitreous $Gd(PO_3)_3$,** *Phys. Lett.* **50A,** No. 4, 249-250 (Dec. 16, 1974).

Key words: antiferromagnetism; comparison of magnetic properties of glasses and crystals; $Gd(PO_3)_3$; glass; magnetic order; polycrystal; vitreous $Gd(PO_3)_3$.

We have measured the magnetic susceptibilities of vitreous and polycrystalline $Gd(PO_3)_3$. The Weiss constants for these materials were found to be -0.3 K. Vitreous $Gd(PO_3)_3$ exhibited short-range antiferromagnetic order below 0.175 K and polycrystalline $Gd(PO_3)_3$ short-range order between 0.242 K and 0.052 K and long-range order below 0.052 K.

Ambrose, J. R., Kruger, J., **Tribo-ellipsometric studies of the relationship between repassivation kinetics and stress corrosion of low carbon steel,** (Proc. 5th Int. Congress on Metallic Corrosion, Tokyo, Japan, May 21-27, 1972), Paper in *5th International Congress on Metallic Corrosion,* pp. 406-409 (National Association of Corrosion Engineers, Houston, Texas, 1974).

Key words: chloride; ellipsometry; low carbon steel; nitrate; nitrite; repassivation; stress corrosion.

Since the susceptibility of a material to stress corrosion cracking (SCC) may be related to the rupture of a protective film and the repassivation rate of the material thus exposed, a technique, tribo-ellipsometry, has been developed which simulates film rupture by abrading off the surface oxide. During the subsequent repassivation of this exposed surface, tribo-ellipsometry allows simultaneous determination of film growth kinetics by ellipsometry and current transient following removal of a protective film. From these measurements a repassivation ratio R_p (total change/film thickness) can be determined. Using R_p, the following results were found: 1) SCC susceptible system (1N $NaNO_3$ at 90 °C)—partial passivation, high rate of metal dissolution; 2) SCC nonsusceptible system—(1N $NaNO_2$ at 25 °C)—rapid and effective passivation low metal dissolution rate; and 3) SCC nonsusceptible but highly corrosive system (1N NaCl)—no passivation, high metal dissolution rate.

Andrews, J. R., **Precision picosecond-pulse measurements using a high-quality superconducting delay line,** *IEEE Trans. Instrum. Meas.* **IM-23,** No. 4, 468-472 (Dec. 1974).

Key words: delay line; picosecond; pulse measurement; superconductivity.

A high-quality superconducting delay line now makes it possible to perform direct oscillographic measurements of the picosecond transition times of very fast electrical signals that do not furnish pretriggers. A 15-m superconducting delay line package has been assembled. The package consists of connectors, connector adapters, normally conducting input/output air lines, and a 15 m length of a miniature 1.6-mm superconducting coaxial transmission line. The package exhibits an attenuation of 0.8 dB at 10 GHz and a system 10-90 percent transition time of 18 ps. Some applications of this delay line are shown. They include the measurement of the pulse output from a mercury switch and the transient response of a traveling-wave oscilloscope.

Ausloos, P., Eyler, J. R., Lias, S. G., **Thermal energy charge transfer reactions involving CH_4 and SiH_4. Lack of evidence for nonspiralling collisions,** *Chem. Phys. Lett.* **30,** No. 1, 21-25 (Jan. 1, 1975).

Key words: charge transfer; Franck-Condon factors; ion-molecule reactions; methane; rare gas ions; rate constants; silane.

Rate constants for reaction of a number of thermal ions with methane and silane have been determined. It is demonstrated that within experimental error none of the reactant pairs undergoes a charge transfer reaction with a rate constant higher than the estimated collision rate constant. It is concluded that there is no evidence for the occurrence of charge transfer reactions of thermal ions by an "electron jump" mechanism involving nonspiralling ion-molecule collisions in which no momentum is transferred.

Ayres, T. R., Linsky, J. L., Shine, R. A., **A possible width-luminosity correlation of the Ca II K_1 and Mg II k_1 features,** *Astrophys. J.* **195,** No. 3, L121-L124 (Feb. 1, 1975).

Key words: Ca II; spectral line; stellar chromospheres.

Existing high resolution stellar profiles of the Ca II and Mg II resonance lines suggest a possible width-luminosity correlation of the K_1 minimum features. We show that such a correlation can be simply understood if the continuum optical depth of the stellar temperature minimum, τ_c^*, is relatively independent of surface gravity as suggested by three stars studied in detail.

Barnes, I. L., Shields, W. R., Murphy, T. J., Brill, R. H., **Isotopic analysis of Laurion lead ores,** Chapter 1 in *Archaeological Chemistry, Advances in Chemistry Series,* No. 138, 1-10 (1975).

Key words: archaeology; isotopic ratios; Laurion; lead; mass spectrometry; ores.

The lead isotopic ratios of a carefully selected suite of ore samples from the Laurion region have been determined by a precise mass spectrometric procedure. The ores were taken from various levels in mines, some known to have been worked in ancient times. All are nearly indistinguishable isotopically within the precision of the method (±0.05%), and they closely match leads from archaeological objects found in Greece. A comparison with isotopic data for ores from other mining regions in the ancient world has been made. The uniformity of the Laurion ores facilitates the interpretation of lead isotope data for archaeological objects from Greece.

Bordé, Ch., Hall, J. L., **Ultrahigh resolution saturated absorption spectroscopy,** (Proc. Conf. on Laser Spectroscopy, Vail,

Colo., June, 1973), Paper in *Laser Spectroscopy*, pp. 125-142 (Plenum Press, New York, N.Y., 1975).

Key words: laser spectroscopy; methane spectra; recoil; saturated absorption.

Conventional wisdom holds that natural lifetime sets the basic resolution limit in Saturated Absorption Spectroscopy. Since suitable molecular transitions are known which have lifetime-limited line Q above 10^{12}, it is interesting to try to achieve such resolution experimentally. By minimizing the usual broadening effects and by using large apertures (5 cm) to minimize the transit broadening, we have studied the hyperfine structure of a certain methane transition at 3.39 μm. Our highest resolution (2.4×10^{10}) leads to good evidence for recoil *splitting* (not *shift*) of the observed absorption line. Another factor of 2 resolution increase is expected from the new absorption cell (38 cm diam by 13 m length).

Brauer, G. M., **Adhesion and adhesives,** Chapter 2 in *Scientific Aspects of Dental Materials*, J. A. von Fraunhofer, Ed., pp. 49-96 (Butterworths, London, England, 1975).

Key words: adhesion; adhesive restoratives; bonding to teeth; dental cements; dental sealants; reactivity of tooth surfaces.

The development of a truly adhesive restorative material is a primary goal of researchers in the field of dental materials. This review discusses the many fundamental investigations dealing with the reactivity of the tooth-adherent surface, followed by discussions of methods to modify hard tissue surfaces with the aim of enhancing adhesion. Potential adhesive systems are described that exhibit clinically significant adhesion to the hard tissues, especially enamel, in an environment approximating that encountered in the oral cavity. Evaluation of future adhesives will necessitate the development of well-designed standardized in vitro testing procedures that correlate with clinical experience. About 190 references are included in this extensive survey of studies conducted both at the National Bureau of Standards and by many other investigators.

Brauer, G. M., Termini, D. J., **Grafting of polymeric side chains to soft tissues,** *J. Biomed. Mater. Res.* **8,** 451-470 (1974).

Key words: ceric ion initiated grafting; chemical attachment to ratskin; grafting to tissues; persulfate initiated grafting; surface grafting; tissue modification.

Soft tissues such as calfskin or ratskin can be modified by acrylic, methacrylic or vinyl monomers containing a variety of functional groups using ceric ions, persulfate-bisulfite or comonomers forming donor-acceptor complexes as initiators. Reactions take place within 20 minutes to 3 hours under experimental conditions which, with suitable changes, might be tolerated clinically. The resulting products are insoluble in solvents for the respective homopolymers. It is likely that the polymeric side chain is attached chemically to the collagenous backbone. With ratskin, the grafting takes place mainly at the surface, resulting in a change in wettability and water sorption of the substrate. Modified hydrophilic, hydrophobic or even oil repellent surfaces can be prepared by judicious choice of monomer used. Thus, hydrophobic, oleophobic subdermal ratskin surfaces are obtained on reaction with fluorinated monomers. Treated ratskins appear more resistant to micro-organisms than the original substrate. It is conceivable that the polymeric side chains could act as adhesive liners since the modified surface may improve the ability of the substrate to adhere to restorative materials.

Breckenridge, F. R., Tschiegg, C. E., Greenspan, M., **Acoustic emission: Some applications of Lamb's problem,** *J. Acoust. Soc. Amer.* **57,** No. 3, 626-631 (Mar. 1975).

Key words: acoustic emission; calibration of transducers; electrostatic transducers; Lamb's problem; seismic pulses; ultrasonic transducers.

A method for obtaining the signatures (waveforms) of certain acoustic-emission events has been developed. The waveform is that at the source, free of contamination by ringing of the specimen, apparatus, and transducer. The technique is based on the comparison of two signals at the transducer, one from the event in question and one from an artificial event of known waveform. The apparatus is also adapted to the calibration of transducers in a certain sense. The configurations of source (real or simulated acoustic-emission event) and receiving transducer correspond to those of some special cases of Lamb's problem. As a byproduct, the results may be of some interest to seismologists.

Brill, R. H., Barnes, I. L., Adams, B., **Lead isotopes in some ancient Egyptian objects,** Paper in *Recent Advances in Science and Technology of Materials*, A. Bishay, Ed., **3,** 9-27 (Plenum Publishing Corp., New York, N.Y., 1974).

Key words: archaeological materials; Egyptian glasses; galena ores; kohl; lead isotopes; Ptolemaic and Roman Periods.

The determination of isotope ratios in lead extracted from a variety of archaeological materials is very useful for classifying the objects according to their geographical origins. On the basis of data for lead from about 450 ancient objects and galena ores, geographical patterns have been established. Our previous studies have included metallic leads, bronze alloys, silver and gold coins, pigments, glazes and glasses from many areas of the Ancient World. In this study we have investigated specimens of ancient Egyptian glasses and glazes containing the colorant-opacifier $Pb_2Sb_2O_7$, samples of kohl (which consist of powdered galena) and a few ores from Egypt. The leads used for making the pigment and kohl are similar to one another, but very different from leads from other parts of the Ancient World, and are almost certainly made of locally-occurring galena ores. Relatively small differences among the ancient Egyptian kohls separate those dating from different dynasties. Glasses and bronzes of the Ptolemaic and Roman Periods excavated in Egypt do not contain the same type of lead found in the earlier glasses and kohls. The later leads are of the Laurion, "Levantine" and Italian types. The authenticity of one very important glass object of the XVIIIth Dynasty has been verified by this technique.

Bussey, H. E., Morris, D., Zal'tsman, E. B., **International comparison of complex permittivity measurement at 9 GHz,** *IEEE Trans. Instrum. Meas.* **IM-23,** No. 3, 235-239 (Sept. 1974).

Key words: cavity resonators; dielectric constant; loss measurements.

Dielectric constant and loss measurements made by three government laboratories (of the USSR, Canada, and the U.S.A.) are compared. The two materials measured were glasses. The measurements utilized cavity resonators in the H_{01n} mode. The errors in dielectric constant reported by the laboratories were usually ± 0.3 percent; actual differences between laboratories of the average corrected results were only ± 0.05 percent. The loss tangent results disagreed when multimoding occurred; however, the errors may be as low as $\pm$ 0.00002 or ± 3 percent, whichever is the larger, if multimoding is avoided.

Byerly, R., **New developments in the measurement of gaseous pollutants in air,** *IEEE Trans. Nucl. Sci.* **NS-22,** No. 2, 856-869 (Apr. 1975).

Key words: air pollution; instrument; measurement; oxides of nitrogen; sulfur dioxide.

The pollution measurement needs driving the development of new techniques are reviewed as an introduction. These include needs for more sensitivity and more simplicity in actual use. Selected examples are described as illustrations: The phenomenon of chemiluminescence is used to measure ozone, sulfur, and oxides of nitrogen. Chemiluminescence refers to the emission of light from excited product molecules formed when the substance to be measured undergoes a chemical reaction. Fluorescence is used to measure SO_2

and NO. The molecule of interest is radiated with one wavelength light and emits (fluoresces) another wavelength which is detected. Absorption of infrared radiation by a pollutant molecule can be used to measure low concentrations. The use of tuneable diode lasers to measure sulfur dioxide and ethylene is described. Also described is the technique of tuning the pollutant absorption into coincidence with a fixed laser line by application of magnetic or electric fields. This technique, perturbation spectroscopy, has been used for vinyl chloride and nitric oxide measurement. Finally, a brief mention is made of the importance of long path techniques and possible approaches.

Cezairliyan, A., Beckett, C. W., **Electrical discharge techniques for measurements of thermodynamic properties of fluids at high temperatures,** Chapter 24 in *Experimental Thermodynamics, Vol. II. Experimental Thermodynamics of Non-Reacting Fluids*, B. Le Neindre and B. Vodar, Eds., pp. 1161-1192 (Butterworth and Co., London, England, 1975).

Key words: capacitor discharges; high-speed measurements; high temperatures; thermodynamics; thermophysics.

Electrical discharge techniques (millisecond and submillisecond resolution) which may be used for the measurement of thermodynamic properties of electrically conducting fluids (liquids and gases) at high temperatures (above 2000 K) are described. Design considerations, including electrical circuit characteristics and discussion of various phenomena, are presented. Measurement of experimental quantities, such as current, voltage, temperature, are discussed and various other high-speed techniques, such as high-speed photography, high-speed recording, are reviewed. Pertinent examples of utilization of discharge techniques for the measurement of thermodynamic properties are given.

Chow, L. C., Brown, W. E., **Formation of $CaHPO_4 \cdot 2H_2O$ in tooth enamel as an intermediate product in topical fluoride treatments,** *J. Dent. Res.* **54,** No. 1, 65-76 (Jan.-Feb. 1975).

Key words: dicalcium phosphate dihydrate; fluorapatite; fluoride; hydroxyapatite; tooth enamel.

Significant amounts of $CaHPO_4 \cdot 2H_2O$ (DCPD) were deposited in tooth enamel by pretreatment with a solution saturated with respect to DCPD. When these enamel samples were treated with a given fluoride solution, the fluoride uptake increased with increasing amounts of DCPD produced by the pretreatment. The interactions between enamel and acidic solutions to yield DCPD can be understood as dissolution-precipitation reactions and analyzed through the use of solubility phase diagrams.

Clough, R. B., **A new method for determination of proportional limit and machine stiffness,** *J. Test. Eval.* **3,** No. 2, 143-146 (Mar. 1975).

Key words: proportional limit; stiffness of testing machines.

A new method for determining the proportional limit of engineering materials, characterized by maximum stress rate, is presented. Simultaneous measurement of stress rate and strain rate also permits a new means of measuring machine stiffness which has certain advantages over present techniques.

Collin, G. J., **Réactions des ions iso-$C_4H_8^+$ et t-$C_4H_9^+$ avec l'isobutène en phases liquide et gazeuse,** *Can. J. Chem.* **52,** No. 12, 2341-2347 (1974).

Key words: free radical reactions; G-values; ion-molecule reactions; neopentane; proton transfer; radiolysis.

The radiolysis of neopentane has been studied in gas and liquid phases. It was shown that, in the liquid phase, the iso-$C_4H_8^+$ ion reacts at least as quickly with isobutene as with methylcyclopentane. The t-$C_4H_9^+$ ion reacts at least 10 times more rapidly with isobutene and the main reaction is one of resonant transfer of a proton with isobutene; fewer than 5 percent of the t-$C_4H_9^+$ ions add to isobutene. In the gas phase, the condensation reaction is more important than that of resonant proton transfer since proton transfer represents only 30 percent of the total reaction: k(addition)/k(transfer) $\simeq 2.35 \pm 0.15$. Finally, the resonant transfer of a deuteron occurs about 2.9 more slowly than proton transfer.

Cook, R. K., **Colloquium on infrasound in Paris,** *J. Acoust. Soc. Amer.* **56,** No. 2, 721-722 (Aug. 1974).

Key words: atmospheric acoustics; infrasound; physiological effects of infrasound.

The Colloque International sur les Infra-sons, held 24-27 September 1973 in Paris, France, was organized by the Centre National de la Recherche Scientifique and by the Groupement des Acousticiens de Langue Francaise. Professor L. Piminow planned the program of the Colloquium to "contain all aspects of atmospheric infrasounds, namely production, diffusion, detection and measurements; infrasounds of natural sources (oceanic origin, high atmosphere, meteorites, etc....); infrasounds of technical origins, technical applications of infrasounds, the inconveniences of infrasounds in physiology and industry, particularly in the chambers of combustion, detection of explosions, etc...." Infrasound was regarded as being oscillations at frequencies below 20 Hz.

Crawford, M. L., **Evaluation of reflectivity level of anechoic chambers using isotropic, 3-dimensional probing,** (Proc. 1974 Int. IEEE/AP-S Symp., Atlanta, Ga., June 10-12, 1974), Paper in *1974 International IEEE/AP-S Symposium Digest*, pp. 28-34 (IEEE Inc., New York, N.Y., June 1974).

Key words: anechoic chamber evaluation; omni-directional probe; reflectivity; three-dimensional scanning.

This paper describes an experimental technique for evaluating anechoic chamber reflectivity utilizing a new NBS isotropic probe mounted on a polyfoam track and support structure designed for probing the chamber's quiet zone in all three orthogonal planes. The probe is omni-directional within ± 1 dB and has sufficient sensitivity to permit evaluation of reflectivity levels as low as 59 dB. It can be used from 150 MHz to 10.0 GHz. Complete scattering information is obtained without applying a receiving antenna pattern correction with only 3 orthogonal scans per frequency required. The paper presents a brief treatment of the theory involved, a description of the system and measurement technique employed, and a discussion of typical measurement results.

Cutkosky, R. D., Field, B. F., **Standard cell enclosure with 20-μK stability,** *IEEE Trans. Instrum. Meas.* **IM-23,** No. 4, 295-298 (Dec. 1974).

Key words: Ac transformer-ratio bridge; platinum resistance thermometer; standard cell enclosure; standard cells.

Groups of standard cells are needed to maintain the National Bureau of Standards (NBS) volt between periodic reassignments via $2e/h$. An enclosure to hold six standard cells has been designed and three enclosures have been assembled. The enclosures consist of four concentric aluminum cylinders separated by foamed polystyrene insulation. Two of the four cylinders are controlled, an outer one by a platinum resistance thermometer and dc amplifier and the inner one at 30 °C by a second platinum resistance thermometer and an ac transfomer-ratio bridge followed by a phase-sensitive detector, a dc amplifier, and a heater. The innermost of the four cylinders is a thermally lagged cell compartment. The temperature excursions over periods of at least several days were found to be less than 20 μK, thus having a negligible effect on the standard cell EMF's.

Cutkosky, R. D., **New NBS measurements of the absolute farad and ohm,** *IEEE Trans. Instrum. Meas.* **IM-23,** No. 4, 305-309 (Dec. 1974).

Key words: absolute farad; absolute ohm; calculable capacitor; cross capacitor; electrical units; farad; ohm; units.

A recently completed calculable cross capacitor in conjunction with a previously described collection of ac and dc bridges has made possible a highly accurate measurement of the farad and the ohm. The cross capacitor and its auxiliary equipment, as well as those components of the measurement system which have not been covered in prior publications, are described in detail. The measurements indicate that the National Bureau of Standards (NBS) unit of capacitance is given by $F_{NBS} = 1\ F + 1.787\ \mu F$, and that the NBS unit of resistance is given by $\Omega_{NBS} = 1\Omega - 0.819\ \mu\Omega$.

Dalke, J. L., **Why metric and when?,** *Tappi* **57,** No. 12, 72-75 (Dec. 1974).

Key words: conversion; international standards; legislation; measurement language; metrication; metric system.

Whatever the relative merits of the metric system, it has won overwhelming international approval in the last 20 years. The Chinese, Japanese, Indians, and all English-speaking nations of the British Commonwealth are abondoning their traditional measurement language and going metric. The metric system has been legal in the United States since 1866. In the past our major trading partners used the British Imperial system of measurements which also forms the basis for our customary system of units. Major industrial companies and some state educational systems in the United States are now switching. Legislation is before Congress that would coordinate and facilitate an orderly change from predominately customary to predominately metric usage on a voluntary and reasonable basis. This paper explores the problems that would accompany such a change in technology, economics, international relations, and other areas.

DePrima, C. R., Johnson, C. R., **The range of $A^{-1}A^*$ in $GL(n, C)$,** *Linear Algebra and Its Applications* **9,** 209-222 (1974).

Key words: adjoint; Hilbert's Theorem 90; involution; normal; similar; spectrum; unitary.

Let A be an invertible linear operator on a finite dimensional complex Hilbert space. We carry out a detailed study of the map $A \rightarrow A^{-1}A^* \equiv \Phi(A)$. It is shown that the range of Φ is exactly the set of all invertible operators T for which T^{-1} is similar to T^*. In particular, unitaries and similarities of unitaries are in the range of Φ and we prove, among other things, the equivalence of the assertions: (i) T is similar to a unitary, (ii) every $A \in \Phi^{-1}(T)$ is congruent to a normal operator, (iii) there exists $B \in \Phi^{-1}(T)$ whose field of values omits the origin of the complex plane. For general T in the range of Φ, we determine *all* $A \in \Phi^{-1}(T)$ in terms of the self-adjoint invertible operators fixed by the map $X \rightarrow T^* XT$. Many of the results contained in this paper have known analogues for operators which are similar to their adjoints.

Durst, R. A., **Ion-selective electrode response in biologic fluids,** (Proc. Conf. on Workshop on Ion-Selective Microelectrodes, Boston, Mass., June 5, 1973), Chapter 2 in *Ion-Selective Microelectrodes,* H. J. Berman and N. C. Hebert, Eds., pp. 13-21 (Plenum Publ. Corp., New York, N.Y., 1974).

Key words: electrode response in biological fluids; electrodes; ion-selective electrodes; microelectrodes.

The response of ion-selective electrodes in biological fluids may be affected by a wide variety of physical and chemical factors. These may influence the indicator electrode directly or may affect the liquid junction of the reference electrode. A brief discussion is presented of the various sources of error and uncertainty in electrode measurements in biologic media especially with microelectrodes. A serious need exists for the development of practical standards for the calibration of ion-selective electrodes in physiologic media in order to ensure the consistency of interlaboratory measurements.

Ederer, D. L., Dhez, P., **Some applications of GM counters in the vacuum ultraviolet spectral region,** *Rev. Sci. Instrum.* **46,** No. 2, 144-146 (Feb. 1975).

Key words: absolute radiation detector; absorption measurements; filters; GM counter; sensitive detector; vacuum ultraviolet.

The applicability of GM and proportional counters naturally extends into the vacuum ultraviolet (vuv) spectral region. A simple modification to this detector enables GM counters to be used to measure very small cross section variations or to be used as high efficiency detectors over a narrow spectral range with excellent second order discrimination.

Ederer, D. L., Lucatorto, T. B., Saloman, E. B., Madden, R. P., Sugar, J., **Photoabsorption of the 4d electrons in barium,** *J. Phys. B: Atom. Molec. Phys., Letter to Editor* **8,** No. 3, L21-L25 (1975).

Key words: barium vapor; configuration interaction; $N_{IV,V}$ ionization thresholds; photoabsorption; 4d absorption; 4f orbital contraction.

The absorption spectrum of gaseous barium was obtained between 120 Å, the region of the $N_{IV,V}$ thresholds. The similarity to lanthanum of some of the features observed in barium suggests that the 4f orbital contracts and overlaps the 4d orbit. This contraction produces two terms, ^3P and ^3D, of the $4d^9\ 4f$ configuration below the 4d ionization limits, while the large electrostatic exchange interaction drives the ^1P term of this configuration some 10 eV above the limit. Furthermore, extensive mixing of the $4d^9\ (6s^2)6p$ configuration with $4d^9(5d^2)6p$ and $4d^9(5d6s)6p$ produces many weak resonances in addition to the resonances associated with the $4d^9\ 4f$ configuration. A suggested classification of these features is given with the aid of known features of the La I spectrum. Finally, from the known x-ray splitting of the $N_{IV,V}$ threshold and the energy interval between the $6s^2\ 6p\ ^2P$ and $6s^2\ ^1S$ levels in La I and La II, the ionization thresholds of the 4d electron were determined to be 814 800 (1000) cm^{-1} and 792 500 (1000) cm^{-1}.

Eicke, W. G., Jr., Auxier, L. M., **Regional maintenance of the volt using NBS volt transfer techniques,** *IEEE Trans. Instrum. Meas.* **IM-23,** No. 4, 490-494 (Dec. 1974).

Key words: regional maintenance of the volt; standard cells; surveillance of local units of voltage; voltage standards; voltage transport standards; unit of voltage.

In cooperation with five industrial standards laboratories, the National Bureau of Standards (NBS) studied the feasibility of establishing a regional volt maintenance and surveillance program in the greater Los Angeles, Calif., area. The objectives were to improve surveillance, to reduce dependence on NBS, and to have each laboratory maintain its unit of voltage to within 1 ppm of the U.S. legal volt. A two-phase program was established, the first to characterize the five laboratories and the second to carry out the surveillance. After 3 years all laboratories were found to be maintaining their unit to within better than 1 ppm of the U.S. legal volt.

Eisenhauer, C. M., Simmons, G. L., **Point isotropic gamma-ray buildup factors in concrete,** *Nucl. Sci. Eng.* **56,** 263-270 (1975).

Key words: adjoint; annihilation; buildup factor; concrete; gamma radiation; moments.

Gamma-ray buildup factors in ordinary concrete have been calculated by the moments method. Results for concrete kerma and air kerma are tabulated for source energies from 15 MeV to 15 keV. Parameters are given that allow calculation of the buildup factor by means of a simple analytic expression. Comparisons are made with earlier calculations, and the effects of annihilation radiation are discussed.

Eliason, L. K., Hamlin, G. L., Grover, C. G., **Selection and application guide to fixed surveillance cameras,** *NILECJ-GUIDE-*

0301.00, 24 pages (U.S. Department of Justice, Law Enforcement Assistance Administration, National Institute of Law Enforcement and Criminal Justice, Washington, D.C., Dec. 1974).

Key words: cameras; demand cameras; employee theft; fixed surveillance; motion picture surveillance; robbery; sequence cameras; shoplifting; surveillance; surveillance cameras.

The guide discusses the methods and types of fixed surveillance photography and their application in combating criminals. Its purpose is to provide the potential user with the necessary general background information to analyze his security needs, decide if photographic surveillance seems to answer those needs, plan generally what type of system best fits his requirements, and discuss his needs intelligently with the manufacturers and installers of the equipment. Fixed surveillance photography involves the use of permanently installed cameras and equipment to monitor areas where criminal activity is likely. The three types of equipment addressed are still cameras, motion-picture cameras, and television systems.

Engen, G. F., **An alternative calibration technique for automated network analyzers with application to adapter evaluation,** (Proc. 1974 IEEE S-MTT Int. Microwave Symp., Atlanta, Ga., June 12-14, 1974), Paper in *Microwave Symposium Digest*, pp. 261-262 (IEEE Inc., New York, N.Y., June 1974).

Key words: adapter; automation; calibration; microwave.

Although conceptually straightforward, the application of existing automated network analyzers to the problem of adapter evaluation is inhibited by the limited accuracy of the detection process, the requirement for several impedance standards at each frequency, and software problems. This paper describes a simple hardware modification, which for adapter evaluation yields an order of magnitude improvement in accuracy. An alternative calibration procedure is outlined which exploits this improved accuracy potential, and which requires only one impedance standard.

Engen, G. F., **Calibration technique for automated network analyzers with application to adapter evaluation,** *IEEE Trans. Microwave Theory Tech., Part II, 1974 Symposium Issue*, **MTT-22,** No. 12, 1255-1260 (Dec. 1974).

Key words: adapter; automation; efficiency; microwave; microwave measurement; network analyzer.

Although conceptually straightforward, the application of existing automated network analyzers to the problem of adapter evaluation is inhibited by the limited accuracy of the detection process, the requirement for several impedance standards at each frequency, and software problems. A hardware modification, which yields improved accuracy for adapter evaluation, is described. An alternative calibration procedure is outlined which exploits this improved accuracy potential, and which requires only one impedance standard.

Feeney, J. J., Meijer, P. H. E., **Magnetic properties of paramagnetically doped crystals Fe^{3+}, Nd^{3+} and Ho^{3+} in various compounds,** *J. Phys. Chem. Solids* **36,** 175-185 (1975).

Key words: convergence criterion; crystal field parameters; energy levels; holium 3+ ions; neodymium 3+ ions; susceptibility.

In this work we calculate the energy levels, wave functions and transition probabilities for a number of compounds whose crystal field parameters have been determined. We introduce a convergence criterion in the diagonalization of the Hamiltonian matrices dependent upon a self consistency test on the eigenvectors. This assures us of numerically accurate wave functions.

First we calculated energy level and susceptibility differences in $(Nd^{3+})PbMoO_4$ dependent on the multiplicative constants θ_ν, used with the published A_l^m to determine the crystal field parameters B_l^m, $(B_l^m = \theta_\nu A_l^m)$. Calculated energy levels as a function of external magnetic field strength and orientation are compared with experimental results for three different sets of published crystal field parameters, B_l^m, for $(Fe^{3+})TiO_2$. The ground state energy levels, and wave functions, have been calculated for the non-Kramers Ho^{3+} ion in the crystals $PbMoO_4$, $LaCl_3$ and $HoCl_3$. Easily distinguishable variations in the temperature dependence of the χ_{zz} component of the susceptibility are found as a function of the host crystal. It is pointed out that susceptibility calculations, based upon measured crystal field parameters, in conjunction with subsequent susceptibility measurements, provide a good check on the validity of the crystal field parameters.

Filliben, J. J., **The probability plot correlation coefficient test for normality,** *Technometrics* **17,** No. 1, 111-117 (Feb. 1975).

Key words: correlation coefficient; medians; normal distribution; order statistics; probability plot; statistical methods; statistics; tests of distributional hypotheses.

This paper introduces the normal probability plot correlation coefficient as a test statistic in complete samples for the composite hypothesis of normality. The proposed test statistic is conceptually simple, is computationally convenient, and is readily extendible to testing non-normal distributional hypotheses. An empirical power study shows that the normal probability plot correlation coefficient compares favorably with 7 other normal test statistics. Percent points are tabulated for $n = 3(1)50(5)100$.

Finnegan, T. F., Wilson, J., Toots, J., **Coupling between Josephson junctions and microstriplines,** *IEEE Trans. Magn.* **MAG-11,** No. 2, 821-824 (Mar. 1975).

Key words: arrays; Josephson junctions; microstriplines; microwave filters; voltage standard.

A promising method for microwave coupling to thin-film Josephson devices via microstripline techniques has been developed which has significant advantages over more traditional waveguide techniques. In particular, direct determination of intrinsic junction cavity parameters such as the geometrical resonance frequencies and Q values are made practical and compact cryogenic multi-octave microwave holders readily realized. The results of coupling experiments with Pb-Pb oxide-Pb and Nb-Nb oxide-Pb tunnel junctions are discussed and applications of these results to the design and construction of shielded single junction 2e/h devices and small multijunction arrays are described.

Finnegan, T. F., Wilson, J., Toots, J., **Interactions in small systems of coupled Josephson junctions on microwave frequencies,** *Rev. Phys. Appl.* **9,** No. 1, 199-205 (Jan. 1974).

Key words: coherent radiation; Josephson junction; microstrip; quality factor; transmission coefficient.

A major factor in the practical utilization of any Josephson device for microwave and higher frequency applications (such as the generation and detection of electromagnetic radiation) is the success with which the junction device can be coupled to an external transmission line. As part of an experimental investigation of the electrodynamics of small arrays of Josephson tunnel junctions, the properties of the coherent radiation emitted both by individual junctions and by coupled junction systems have been studied at frequencies between 2 and 12 GHz. Near 9 GHz, more than 10^{-9} W of coherent radiation has been detected from a single Pb-Pb oxide-Pb junction coupled via waveguide. The development of thin film devices in which the tunnel junctions form part of a microstrip line have made it feasible to observe directly (in a single device) the radiation emitted both at the fundamental geometrical frequency and at the low order harmonics. The observed temperature dependence of the junction cavity Q indicate the low temperature losses are primarily due to cavity loading of the external transmission line.

Flynn, D. R., **Accuracy and precision,** *Noise Control Eng.—Editorial Section* **3,** No. 3, p. 2 (Nov.-Dec. 1974).

Key words: accuracy; acoustics; noise; precision; repeatability; reproducibility.

This is an invited editorial pointing out the need for uncertainty estimates in papers published in the noise field.

Flynn, J. H., **Theory of differential scanning calorimetry—coupling of electronic and thermal steps,** Paper in *Analytical Calorimetry*, R. S. Porter and J. F. Johnson, Eds., **3,** 17-44 (Plenum Publ. Corp., New York, N.Y., 1974).

Key words: differential scanning calorimetry (DSC); electronic and thermal coupling; instrumental limitations; supercooling; theoretical model; thermal analysis; thermodynamic properties.

A model system for differential scanning calorimetry (DSC) is developed in which the electronic response of the instrument is coupled with the heat flow across an interface. Equations are derived which relate the time constants for this two-step process with the thermal properties of the sample and the amplitudes, areas, slopes and dwell times of DSC traces. The cases discussed include first and second order transitions, partial and total "supercooling" and effects of a temperature dependence of the heat capacity and the rate of temperature change. The magnitude of the lag terms of these cases is determined from typical experimental data. The equations permit an independent determination of the interfacial time constant and an assessment of the limits for the validity of the theoretical model.

Flynn, T. M., Powell, R. L., Chelton, D. B., Birmingham, B. W., **Superconducting electrical generators for central power station use,** (Proc. 1973 Cryogenic Engineering Conf., Atlanta, Ga., Aug. 8-10, 1973), Paper B-1 in *Advances in Cryogenic Engineering* **19,** 35-43 (Plenum Press, New York, N.Y., 1974).

Key words: cryogenics; electricity; energy; helium; power; superconductivity.

The electrical industry is faced with a need for dramatically larger generators to optimize the utilization of large new power sources, such as gigawatt-sized fast breeder reactors. Earlier increases in generator capacity have been achieved by improving the cooling of the heat-producing components of the generator. For the first time in the evolution of power generators, a unique technology, superconductivity, is available to the electric machine designer. Superconductivity may offer a way of achieving higher capacities while maintaining present costs, weights, and overall dimensions.

In the Fall of 1971, the Cryogenics Division of the NBS began a program in cooperation with industry to accelerate the application of superconductivity to large scale generators. The program stopped short of actual experimental construction since sufficient funds did not become available, but did endure sufficiently to demonstrate outstanding industry-government cooperation in this area of national need. This paper presents the results of several government-industry studies conducted in the course of this program in order to show such potential benefits from the use of cryogenics as improved generator rating, efficiency, reliability, transportation and site erection, cost and power system stability.

Frederikse, H. P. R., **Electrons in oxides: A summary,** *J. Solid State Chem.* **12,** 411-415 (1975).

Key words: applications (optical, magnetic); electronic properties; oxides.

A short overview of the optical, magnetic, electrical and surface properties of oxides is presented. Some of the major applications (electronic, electro-optical, magnetic devices, high temperature components, catalysts, etc.) are listed and the relevant physical parameters are being discussed.

Gadzuk, J. W., **Angular distributions of electrons photoemitted from chemisorbed atoms,** *Solid State Commun.* **15,** No. 6, 1011-1016 (1974).

Key words: angular distributions; chemisorption; photoemission; photoionization.

A theory which describes the angular distributions of electrons photoemitted from chemisorbed atoms is presented. Due to hole delocalization and preferential orientation, interference effects due to emission from various centers in a molecule do not average out, as they do in gas phase photoionization and much more structural information pertaining to chemisorption bonds is contained in such measurements.

Garn, P. D., Diamondstone, B. I., Menis, O., **Variations in the cooling transitions of potassium nitrate,** *J. Therm. Anal.* **6,** 623-630 (1974).

Key words: potassium nitrate; procedure of ICTA Standards Committee and NBS; standard in thermal analysis; transition from I → III.

Because of questions concerning the suitability of potassium nitrate as a dynamic temperature standard for DTA, the relation between the experimental procedure and the resulting curves was ascertained for the Standard Reference Material KNO_3. The material behaves differently *on cooling* in open pans than in cylindrical holders because confinement in the latter case initiates reversion to the room temperature form. Under the conditions of use as a dynamic temperature reference material, the curves are accurately reproducible.

Gebbie, K. B., Steinitz, R., **A mechanism for the production of light and dark contrasts in radiatively controlled lines,** *Solar Phys.* **29,** No. 1, 3-15 (Mar. 1973).

Key words: contrasts in emergent intensity; radiatively controlled lines.

It is argued that visible contrasts can arise even in a line that is controlled wholly by an external radiation field. Lateral differences in the local shapes of the line absorption profile are shown to account for such contrasts. Two cases are treated explicitly: (a) a profile locally broadened by mass flow, and (b) a profile locally narrower due to the suppression of turbulent velocities, as might result from the presence of magnetic fields.

Geist, J., Steiner, B., **Report of the workshop on accurate radiometry for solar conversion,** Paper in *Report and Recommendations of the Solar Energy Data Workshop*, pp. 204-208 (Sept. 1974).

Key words: atmospheric physics; radiometric physics; radiometry; solar conversion.

This report presents recommendations of a workshop on accuracy radiometry for solar conversion that was jointly sponsored by NOAA and NSF.

Giarratano, P. J., Hess, R. C., Jones, M. C., **Forced convection heat transfer to subcritical helium I,** (Proc. 1973 Cryogenic Engineering Conf., Atlanta, Ga., Aug. 8-10, 1973), Paper K-1 in *Advances in Cryogenic Engineering* **19,** 404-416 (Plenum Press, New York, N.Y., 1974).

Key words: critical heat flux; film boiling; forced convection; heat transfer; helium; nucleate boiling; subcritical; supercritical.

Results of an experimental investigation of heat transfer to liquid helium under forced downward flow conditions are reported for a 0.213 cm i.d. × 10 cm long vertical test section subject to the following range of operating conditions: System pressures—1-2 atm (0.1-0.2 MN/m^2); Mass velocities—4-65 $g/s\text{-}cm^2$; Heat fluxes—0.01-1 W/cm^2; Inlet subcooling—0-0.3 K.

Data are presented for the nucleate and film boiling regions and a correlation has been developed for predicting the critical heat flux (transition from nucleate to film boiling). A comparison of forced con-

578-011 O - 75 - 5

vection boiling of helium with other modes of helium heat transfer (pool boiling and supercritical) is also included.

Goebel, D. G., Poole, E. W., Hartsock, R. G., **Instrument for measuring phototube spectral response,** *Appl. Opt.* **8,** No. 8, 1749-1750 (Aug. 1969).

Key words: photodetector; photodetector spectral response; photomultiplier tubes; phototubes.

An instrument has been designed to plot automatically the relative spectral response of a phototube over the range of 0.35 μm to 0.84 μm. The response as a function of wavelength is recorded directly by using a digital printer or an x-y plotter.

Gray, J. E., Allan, D. W., **A method for estimating the frequency stability of an individual oscillator,** *Proc. 28th Annual Symp. on Frequency Control, Fort Monmouth, N.J., May 29-31, 1974,* pp. 243-246 (Electronic Industries Association, Washington, D.C., 1974).

Key words: Flicker noise; frequency stability; noise measurement; oscillator stability.

A method is given for estimating the intensity of random noise frequency modulation of an individual oscillator, using data obtained by comparing it with two or more other oscillators. This method is appropriate even if the oscillators available for comparison are less stable than the oscillator being evaluated, but their frequency fluctuations must be independent. The statistical uncertainty of the results is discussed briefly.

Greer, S. C., Block, T. E., Knobler, C. M., **Concentration gradients in nitroethane + 3-methylpentane near the liquid-liquid critical solution point,** *Phys. Rev. Lett.* **34,** No. 5, 250-253 (Feb. 3, 1975).

Key words: critical point; critical solution point; densimeter, magnetic; diffusion, pressure; gradient, concentration; gradient, density; gravity, effects of; 3-methylpentane; mixture; liquid; nitroethane; sedimentation.

Precise measurements of density profiles in the system nitroethane + 3-methylpentane near the critical solution point demonstrate that concentration gradients form rapidly, but true equilibrium is not achieved even after long times. The data are in qualitative agreement with computer calculations of the behavior of a critical mixture in gravitational field which show that the initial gradients form by sedimentation. Thus, effects due to gravity may affect careful experiments in critical mixtures.

Griffin, R. J., Jr., **The thermesthesiometer—an innovation in heat measurement,** *Lab. Data Winter,* pp. 13-14 (1975).

Key words: computer science; laboratory accreditation; measurement; national measurement system; technology transfer; voluntary standards.

As technology becomes more complex, and as world trade increases, there is a growing need for measurement capabilities and consensus standards. In this interview the Director of the National Bureau of Standards discusses the role of NBS in these vital areas.

Guildner, L. A., Terrien, J., **Mercury absolute manometers,** Chapter 4 in *Experimental Thermodynamics, Vol. II, Experimental Thermodynamics of Non-Reacting Fluids,* B. Le Neindre and B. Vodar, Eds., Part 1, pp. 115-131 (Butterworth and Co., London, England, 1975).

Key words: pressure; manometry; mercury manometer.

The most accurate pressure measurements attainable in the range of 5×10^2 Pa to 1.3×10^5 Pa can be made by using mercury manometers. In the design of a mercury manometer the principal concerns are those of locating the crown of the meniscus, and of determining the height of the mercury column. Different techniques are cited by describing some accurate instruments in use at BIPM, NRLM, NBS and VNIIM.

Hanson, D. W., Hamilton, W. F., **Satellite broadcasting of WWV signals,** *IEEE Trans. Aerosp. Electron. Syst.* **AES-10,** No. 5, 562-573 (Sept. 1974).

Key words: broadcasting; dissemination; frequency; satellite; synchronization; time.

An experiment concerning the broadcasting of time and frequency information from geostationary satellites is discussed. Included are discussions on satellite motion, time delay, Doppler shift, and delay calculations. Ground station requirements, time recovery techniques, and timing resolution and accuracy are also included. Delay computation aids for the user were designed to provide free space delays between the master clock and the user. Measurements made in North and South America demonstrated a timing resolution of about 10 μs and an accuracy of 25 μs.

Harris, F. K., **A cooperative experiment in measurement education,** (Proc. Conf. on Measurement Education, University of Warwick, Coventry, England, July 8-10, 1969), *IEE Conf. Publ. No.* **56,** pp. 140-141 (Institute Electrical Engineers, London, England, 1969).

Key words: measurement education; metrology curriculum.

A discussion of the cooperative NBS-GWU metrology program.

Harris, K. R., Mills, R., Hanley, H. J. M., Woolf, L. A., **The self-diffusion of simple fluids: Tabulated values for argon and methane,** *Aust. Nat. Univ. Rev.* **DRU-RR 2,** pp. 1-32 (The Australian National University Press, Canberra, A.C.T. Australia, 1974).

Key words: argon; critical review; krypton; measurement technique; methane; self-diffusion coefficient.

Data for the self-diffusion coefficient (D) of several simple fluids—He, Ne, Ar, Kr, Xe, CH_4, H_2, N_2, CF_4, CO_2, and SF_6—in the dense gas and liquid states are reviewed. The general behaviour of the self-diffusion coefficient with respect to temperature and density is examined making use of the excess function approach. Tabulated values of D for methane and argon are presented as a function of temperature, pressure and density. The pressure range covered is 2-50 MPa and the temperature range is 170-320 K for methane and 100-250 K for argon. The estimated error of the tabulated coefficients is ± 10 percent.

Hellwig, H., **Atomic frequency standards: A survey,** *Proc. 28th Annual Symp. on Frequency Control, Fort Monmouth, N.J., May 29-31, 1974,* pp. 315-339 (Electronic Industries Association, Washington, D.C., 1974).

Key words: application of standards; basic standards; cesium standards; frequency accuracy; frequency stability; frequency standards; hydrogen standards; ion storage; laser stabilization; rubidium standards; saturated absorption; time standards.

The last comprehensive survey on atomic frequency standards was given by A. O. McCoubrey in 1966 (Proc. IEEE 54, p. 116). This survey reviews the more recent historical background of atomic frequency standards leading to the present developments. A discussion of the underlying physical and engineering principles is given. Modern atomic frequency standards, including their performance, are compared quantitatively, and projections are attempted at likely future developments and performance characteristics.

As in 1966, the standards principally used in technical and scientific applications are rubidium gas cell devices, cesium beam tubes, and hydrogen maser oscillators. However, substantial advances in physical and performance characteristics can be reported.

New developments include passive hydrogen devices, saturated absorption stabilized lasers, ion storage devices, and atomic beams

in the far infrared and infrared region, as well as new techniques to evaluate frequency biases such as those encountered in cesium and hydrogen standards.

The survey includes a discussion of the effects of past and current developments in atomic frequency standards on the technical and scientific user community.

Hellwig, H., Bell, H. E., Bergquist, J. C., Glaze, D. J., Howe, D. A., Jarvis, S., Jr., Wainwright, A. E., Walls, F. L., **Results in operation, research, and development of atomic clocks at the National Bureau of Standards,** (Proc. IX Int. Congress of Chronometry, Stuttgart, Germany, Sept. 16-20, 1974), Paper in *Proc. IX International Congress of Chronometry,* G. Glaser, Ed., A, A5-1 – A5-13 (Herausgegeben von der Deutschen Gesellschaft fur Chronometrie E. V., Stuttgart, Germany, 1974).

Key words: accuracy; atomic clocks; cesium standards; hydrogen standards; hydrogen storage device; methane stabilized helium-neon lasers; noise studies; quartz crystal oscillators; quartz crystal resonators.

Since the last CIC, significant progress has been made in various laboratories leading to new capabilities and new future uses of atomic clocks. This paper summarizes the contributions of the National Bureau of Standards to these developments and tries to forecast future developments.

Two primary cesium standards, NBS-4 and NBS-5, are now in operational use with an accuracy of near 1×10^{-13}, and with a stability of better than 1×10^{-14} (sample time of 3 hours). The concept and feasibility of a passive hydrogen storage device has been demonstrated leading to the projection of long term stabilities (hours to weeks) of at least 1×10^{-14} for these devices. Studies of different electronic systems as well as wall and magnetic field effects promise significant improvements in the accuracy of hydrogen standards. Methane stabilized helium-neon lasers were operated and demonstrated excellent frequency stabilities, and research on a methane beam system is in progress. Novel noise studies of quartz crystal resonators confirmed that quartz crystal oscillators with short-term stabilities of parts in 10^{12} (1 millisecond) are possible, an important fact in its own right and of significance to the development of atomic clocks of extreme short-term stability.

Herron, J. T., Huie, R. E., **Application of beam sampling mass spectrometry to the kinetics of ozone reactions,** *Int. J. Mass Spectrom. Ion Phys.* **16,** No. 1/2, 125-136 (1975).

Key words: kinetics; mass spectrometry; nitrogen dioxide; oelfin; ozone; rate constant.

A beam sampling mass spectrometer designed for the study of chemical reactions in the gas phase is described. It is a three stage, differentially pumped instrument using a molecular beam chopper and phase sensitive detection. The reactions of ozone with NO_2 and some olefins were studied using a temperature controlled stopped-flow reactor in conjunction with the beam sampling mass spectrometer.

Heydemann, P. L. M., Welch, B. E., **Piston gages,** Chapter 4 in *Experimental Thermodynamics, Vol. II. Experimental Thermodynamics of Non-Reacting Fluids,* B. Le Neindre and B. Vodar, Eds., Part 3, pp. 147-202 (Butterworth and Co., London, England, 1975).

Key words: calibration; piston gages; pressure measurement.

Piston gages are instruments which measure pressure as force per unit area. There are a number of sources of error among which elastic distortion is the largest. Several types of piston gages have been developed to reduce the elastic distortion errors and to allow operation at a variety of pressures. A minimum of elastic distortion error is found with the controlled clearance piston gage. Other sources of error include temperature effects, air buoyancy, and head corrections. To reach the highest precision operating procedures must be followed which insure adequate control of all important parameters.

Holt, H. K., **Laser intracavity absorption,** *Phys. Rev. A* **11,** No. 2, 625-629 (Feb. 1975).

Key words: high sensitivity; intracavity absorption; laser; quantitative analysis.

The characteristics of a laser with an intracavity absorption cell have been calculated for the case in which the gain atoms are homogeneously broadened and the absorber atoms are inhomogeneously broadened. The sensitivity of the laser intensity to the density of absorbers is determined.

Hord, H., **Cryogenic H_2 and national energy needs,** (Proc. 1973 Cryogenic Engineering Conf., Atlanta, Ga., Aug. 8-10, 1973), Paper A-1 in *Advances in Cryogenic Engineering* **19,** 1-11 (Plenum Press, New York, N.Y., 1974).

Key words: cryogenic; energy; fuel; hydrogen.

Our impending fossil fuel shortage is a clear challenge to the cryogenics industry and government to provide efficient and economical means of satisfying specific national fuel requirements. Large scale production of liquid hydrogen was stimulated by the U.S. space exploration program. Now, civilian demands for synthetic fuels beckon cryogenic hydrogen.

National and world energy shortages are briefly summarized to demonstrate the relevance of synthetic fuels in satisfying future energy markets. A perspective of national energy needs, as they relate to cryogenic hydrogen fuel, is given. Hydrogen and alternate synthetic fuels are briefly reviewed and potential applications for cryogenic hydrogen are described. Technical research and development efforts, required to satisfy specific current and future national needs, are identified. The mechanism for implementation of synthetic fuels and the indistinct timetable for transition to these fuels are discussed.

Hord, J., **Discussion of "experimental studies on thermodynamic effects of developed cavitation" by Robert S. Ruggeri,** Article in *Fluid Mechanics, Acoustics and Design of Turbomachinery, Part 1,* pp. 394-395 (1974).

Key words: cavitation; cavity pressure; steam; steam vapor pressure; thermodynamic effects; vapor pressure.

A method for predicting thermodynamic effects of cavitation (changes in cavity pressure relative to steam vapor pressure) is presented. The prediction method accounts for changes in liquid, liquid temperature, flow velocity, and body scale. Both theoretical and experimental studies used in formulating the method are discussed. The prediction method provided good agreement between predicted and experimental results for geometrically scaled venturis handling four different liquids of widely diverse physical properties. Use of the method requires geometric similarity of the body and cavitated region and a known reference cavity-pressure depression at one operating condition.

Hord, J., **Research opportunities in cryogenic hydrogen-energy systems,** (Proc. Symp. on Hydrogen Energy Fundamentals, Miami Beach, Fla., March 3-5, 1975), Paper in *Hydrogen Energy Fundamentals,* T. N. Viziroglu, Ed., pp. S3-11 – S3-24 (University of Miami, Coral Gables, Fla., 1975).

Key words: cryogenic; energy; hydrogen; research and development.

As liquid hydrogen pervades the commercial fuel market, new and improved products and technologies will be needed. To meet these demands appropriate research and development (R&D) must be performed on hydrogen fuel systems. Candidate markets for cryogenic hydrogen-energy systems are reviewed and discussed, and associated

R&D needs are outlined herein. A wide variety of cryogenic R&D opportunities exist.

Hougen, J. T., **The assignment of molecular infrared spectra from a laser magnetic resonance spectrometer,** *J. Mol. Spectrosc.* **54,** No. 3, 447-471 (Mar. 15, 1975).

Key words: asymmetric rotors; doublet states; HO_2; laser magnetic resonance; least squares fit; rotational analysis; Zeeman spectrum.

Mathematical techniques are presented which have proved useful in assigning the laser magnetic resonance pure-rotation spectrum of HO_2, i.e., useful in assigning an absorption spectrum obtained when molecular energy levels are Zeeman shifted by an external magnetic field until transition frequencies coincide with a fixed-frequency radiation source. The techniques described should have general applicability to the laser magnetic resonance vibration-rotation spectrum of any molecule in an orbitally nondegenerate electronic state and a doublet electronic spin state ($S=1/2$). Equations involving both Zeeman line positions and Zeeman line intensities are presented. These allow the assignment of M_J quantum numbers, the determination of the spin-rotation interaction constant γ and rotational quantum number N for both the upper and the lower state, and the determination of the zero-field transition frequency. The equations can be used without prior knowledge of the molecular structure or energy levels.

Howe, D. A., Bell, H. E., Hellwig, H., DeMarchi, A., **Preliminary research and development of the cesium tube accuracy evaluation system,** *Proc. 28th Annual Symp. on Frequency Control, Fort Monmouth, N.J., May 29-31, 1974,* pp. 362-372 (Electronic Industries Association, Washington, D.C., 1974).

Key words: cavity phase shift; cesium beam tube; frequency synthesis; pulse method; Ramsey dual interaction region; second-order doppler; velocity distribution.

A method has been developed which measures the velocity distribution of the atoms in a beam tube using the Ramsey dual interaction region principle. The method involves pulsing the RF excitation signal at a period related to the atoms' time-of-flight between the interaction regions. The pulse method, with its ability to measure velocity distribution enables calculations of cavity phase shift and second-order Doppler effect. This research has motivated the development of a system, complete unto itself, for determining the accuracy of cesium beam tubes. Design goals for the system are outlined. The system development to date is discussed. Frequency synthesis is accomplished at 5.00688 MHz. This avoids frequency synthesis at X-band and thereby eliminates packaging and weight problems. A novel synthesizer design is used which incorporates a digital frequency lock of the 5.00688 MHz VCXO. A resolution of 1.4 millihertz/second is realizable; lock is within 2.8×10^{-10} at one second of a 5.0000 MHz reference with potential to better than 1×10^{-12} at one second. This synthesizer and its application to the accuracy evaluation system are discussed. Some results on the evaluation of commercial cesium beam tubes are given.

Huang, J. S., Goldburg, W. I., Moldover, M. R., **Observation of anomalously large supercooling in carbon dioxide,** *Phys. Rev. Lett.* **34,** No. 11, 639-642 (Mar. 17, 1975).

Key words: carbon dioxide; CO_2; critical point; nucleation; supercooling.

We have observed supercooling in liquid CO_2 near the critical temperature greatly exceeding that allowed by existing theories of homogeneous nucleation.

Hubbard, C. R., Swanson, H. E., Mauer, F. A., **A silicon powder diffraction standard reference material,** *J. Appl. Crystallogr.* **8,** Part 1, 45-48 (Feb. 1975).

Key words: powder diffraction standard; silicon; silicon powder diffraction standard; standard, powder diffraction; standard reference material, silicon.

A silicon powder Standard Reference Material, SRM-640, has been prepared for use as a standard in powder diffractometry. Powder diffraction measurements were performed with a tungsten internal standard and a high-angle goniometer. The measured a/λ is 3.525176. With λ(Cu $K\alpha_1$ peak) taken as 1.5405981 Å, $a=5.430880$ (35) Å, uncorrected for refraction. Comparison of a with values obtained with a single crystal from one of the boules reveals a difference of 3 parts in 10^5. This difference suggests a subtle systematic error in powder diffractometry or a change in lattice spacing near crystal boundaries. Use of the SRM should permit individual measurements of lattice parameters to be made reproducible to near 1 part in 10^5 and an absolute accuracy of at least 3 parts in 10^5.

Hubbell, J. H., McMaster, W. H., Del Grande, N. K., Mallett, J. H., **X-ray cross sections and attenuation coefficients,** Paper in *International Tables for X-Ray Crystallography, Section 2, Absorption and Scattering,* J. A. Ibers and W. C. Hamilton, Eds., **4,** Paper 2.1, 47-70 (Kynoch Press, Birmingham, England, 1974).

Key words: attenuation coefficient; compilation; Compton scattering; cross section; crystallography; photoelectric absorption; photons; Rayleigh scattering; x rays.

Tables of total cross sections (in barns/atom) for photon interaction with atoms, representing sums over the photoelectric effect, coherent (Rayleigh) scattering, and incoherent (Compton) scattering cross sections are presented for 87 elements from $Z=1$ to 94 at the 24 wavelengths from 0.4970 to 2.7496 angstroms (24.942 to 4.509 keV) which are of most use in x-ray crystallography. Corresponding tables of mass attenuation coefficients (in cm^2/g) are also given. These tables are an interpolation from a more extensive compilation (UCRL-50174 (1969) by McMaster et al) and the input data and procedures for constructing the latter compilation are described.

Hudson, R. P., Pfeiffer, E. R., **Dipolar heat capacity of CMN,** *J. Low Temp. Phys.* **16,** Nos. 3/4, 309-316 (1974).

Key words: CMN; cryomagnetism; low temperature specific heat; magnetic dipole interaction; paramagnetic salt.

The magnetic contribution to the low-temperature specific heat of cerous magnesium nitrate (CMN) was determined by the Casimir-Du Pré ac susceptibility method in the region of 1 K. The value found for the coefficient of the major (T^{-2}) term is in good agreement with that determined in this laboratory in magnetic cooling experiments. It is some 10 percent less than that calculated for the magnetic dipole interaction between the Ce^{3+} ions.

Isler, M., Grover, C., **Simplified procedures for evaluating the image quality of objective lenses for night vision devices,** *LESP-RPT-0304.00,* 16 pages (U.S. Department of Justice, Law Enforcement Assistance Administration, National Institute of Law Enforcement and Criminal Justice, Washington, D.C., May 1974).

Key words: contrast curves; low contrast resolution; night vision; objective lenses; resolution test; variable contrast resolution.

This document provides two test methods for determining the comparative image quality of objective lenses intended for use on passive portable night vision devices. The two test methods are called the low contrast resolution test and the variable contrast resolution test. The criterion for lens evaluation in both tests is the limiting resolution of the image of a three bar test pattern, as a function of the contrast of the pattern.

Jones, F. E., Quindry, T. L., Rinkinen, W. J., **Summary report on emergency vehicle sirens,** *LESP-RPT-0502.00,* 47 pages (U.S. Department of Justice, Law Enforcement Assistance Administration, National Institute of Law Enforcement and Criminal Justice, Washington, D.C., Sept. 1974).

Key words: automobile; destructive interference; directivity; emergency vehicle; insertion loss; masking noise; siren; sound power level; sound pressure level.

A test program involving 23 test automobiles: four electronic sirens and nine electromechanical sirens has been completed. Measurements have been made of the directivity and sound power level-frequency spectra of the sirens, of the insertion loss (sound attenuation) of the automobiles, of the masking noise in the automobiles while being driven over a test route of our different segments, and of the phase cancellation due to reflection for an electronic siren. Measurements of directivity were made also for a pair of electronic siren speakers in three different arrangements.

Kasa, I., **Closed-form mathematical solutions to some network analyzer calibration equations,** (Proc. 1974 Conf. on Precision Electromagnetic Measurements, London, England, July 1-5, 1974), *IEEE Trans. Instrum. Meas.* **IM-23,** No. 4, 399-402 (Dec. 1974).

Key words: calibration; sliding termination; standards.

A general evaluation procedure is described for calibration of a linear complex reflectometer (network analyzer and for two-port measurements. New closed-form formulas and procedures are given for two practical cases: 1) calibration or measurement with two known standards and a sliding termination; 2) calibration or measurement by one standard and two different sliding terminations.

The reflection coefficient magnitudes and phases of these sliding terminations need not be known.

The closed-form formulas make it possible to determine calibration constants by direct calculation without approximations or complicated multivariable iterations.

Kaufman, V., Sugar, J., **Spectrum and energy levels of five-times ionized tantalum (Ta VI),** *J. Opt. Soc. Amer.* **65,** No. 3, 302-309 (Mar. 1975).

Key words: spectra; tantalum.

The spectrum of Ta VI produced with a sliding-spark discharge was photographed in the region of ~200-2000 Å utilizing grazing-incidence and normal-incidence spectrographs. A system of seventy excited energy levels was deduced from 228 spectral lines. These arise from excitations out of both the $4f$ and $5p$ closed shells of the $4f^{14}\ 5s^2\ 5p^6$ ground configuration, giving the observed configurations $4f^{13}nl$ with $nl = 5d, 6s, 6p, 6d, 7s$ and $5p^5 nl$ with $nl = 5d, 6s, 6p$. Radial integrals were fitted for all of these configurations. A value of 785 130 ± 400 cm^{-1} for the ionization energy was derived. A graph of lowest excited levels of $4f^{13}\ 5d$ and $5p^5\ 5d$ from Lu IV to Re VIII predicts the crossing of these configurations after W VII.

Kerns, D. M., **Scattering-matrix description and nearfield measurements of electroacoustic transducers,** *J. Acoust. Soc. Amer.* **57,** No. 2, 497-507 (Feb. 1975).

Key words: acoustics; electroacoustic transducers; near-field measurements.

Recently developed and successfully applied analytical techniques for the measurement of microwave antennas at reduced distances are "translated" into corresponding techniques for the measurement of electroacoustic transducers in fluids. The basic theory is formulated in scattering-matrix form and emphasizes the use of plane-wave spectra for the representation of sound fields. This theory, in contrast to those based on asymptotic description of transducer characteristics, is suitable for the formulation and solution of problems involving interactions at arbitrary distances. Two new techniques (in particular) are described. One, utilizing deconvolution of transverse scanning data, taken with a known transducer at distances d which may be much less than the Rayleigh distance $d_R (= D^2/2)$, provides a means of obtaining complete near- and farfield characteristics, *corrected for the effects of the measuring transducer.* Applicability of a (two-dimensional, spatial) sampling theorem and of the "fast Fourier transform" algorithm, with greatly facilitate the necessary computations, is shown. The second technique provides a means of extrapolating received signal as a function of distance (observed with $d \sim d_R$) to obtain on-axis values of effective directivity. Other possible applications are indicated. These techniques rigorously utilize observed transducer output, which need not be simply related to pressure or normal velocity at a point.

Klein, R., Yates, J. T., Jr., **Nitric oxide and its decomposition on the (110) plane of tungsten,** (Proc. 2nd Int. Conf. on Solid Surfaces, Kyoto, Japan, March 25-29, 1974), *Jap. J. Appl. Phys. Suppl.* **2,** Part 2, 461-464 (1974).

Key words: decomposition; nitric oxide; tungsten.

Nitric oxide is adsorbed on the (110) plane of tungsten with a high sticking coefficient independent of coverage. Programmed thermal desorption of a W(110) surface with adsorbed NO shows no desorbed NO, but only nitrogen. Two peaks are observed in the resulting nitrogen desorption spectra. The first, appearing at low coverages of NO, shifts to lower temperatures with increasing initial coverage. The second appears at higher coverages and shifts slightly to higher temperatures with increasing coverage. The temperature region covering both states is 900-1350 K for the temperature rates employed. A simple, consistent model is developed. Work function-relative coverage measurements for NO on W(110) show an initial slow $\Delta\phi$ increase, a linear potion, and a maximum. The maximum $\Delta\phi$ is 0.85 eV and the saturated coverage value is 0.72 eV.

Klots, C. E., Sieck, L. W., **Argon sensitized formation of Xe_2^+: A new mechanism for the Jesse effect,** *Chem. Phys. Lett.* **27,** No. 1, 71-72 (July 1, 1974).

Key words: cross sections; excited states; ionization; mass spectrometry; radiation chemistry; rare gases.

Photoexcitation of the argon resonance states in the presence of xenon leads to Xe_2^+. Kinetic analysis indicates rapid near-resonant energy transfer between argon and xenon atoms. The possibility of an analogous mechanism in other rare gas systems is examined.

Komarek, E. L., Tryon, P. V., **An application of the power equation concept and automation techniques to precision bolometer unit calibration,** *IEEE Trans. Microwave Theory Tech., Part II, 1974 Symposium Issue,* **MTT-22,** No. 12, 1260-1267 (Dec. 1974).

Key words: automated measurements; bolometer unit calibration; power equation concept.

The power equation concept has been implemented into a multioctave precision bolometer unit calibration system employing automation techniques in conjunction with an automatic network analyzer (ANA) system. Using statistical methods the system is being evaluated as a calibration transfer system operating in the 2-12.4-GHz frequency range at 1-10 mW. Preliminary results reported here show a single measurement standard deviation of 0.2-1 percent from 2-10 GHz. Upon a successful evaluation, the system will be qualified as an integral part of the national measurement system.

Krauss, M., Celotta, R. J., Mielczarek, S. R., Kuyatt, C. E., **Electron impact energy loss spectra of the $1\ ^2B_2 \leftarrow \tilde{X}\ ^2A_1$ transition in NO_2,** *Chem. Phys. Lett.* **27,** No. 2, 285-288 (July 15, 1974).

Key words: electron impact; energy loss; excitation; NO_2.

Long vibrational progressions are observed in the electron impact energy loss spectrum of NO_2 in the 1.5-4.1 eV energy loss range. These progressions can be assigned to the $1\ ^2B_2 \leftarrow \tilde{X}\ ^2A_1$ transition and suggest that the $1\ ^2B_2$ state is asymmetric.

Ku, H. H., Kullback, S., **Loglinear models in contingency table analysis,** *Amer. Statist.* **28,** No. 4, 115-122 (Nov. 1974).

Key words: categorical data; contingency tables; loglinear model; minimum discrimination information; statistical analysis.

This is an expository paper on the statistical analysis of categorical data arranged in the form of contingency tables. Beginning with a 2×2 table, the estimation and testing of parameters in the loglinear model is illustrated and compared to that for the linear model in the continuous case. This is followed by detailed analysis of two examples: one for a three-way table on biomedical data, and one for a four-way table on social survey data.

Lamaze, G. P., Whittaker, J. K., Schrack, R. A., Wasson, O. A., **After-pulse suppression for 8850 and 8854 photomultipliers,** *Nucl. Instrum. Methods Letters to Editor* **123,** 403-404 (1975).

Key words: after-pulse; GaP first dynode; neutron; photoelectron; photomultiplier; resolution; suppression.

After-pulsing suppression of semiconducting first dynode photomultipliers (RCA 8850 series) has been successfully accomplished by applying a positive pulse to a wire mesh directly in contact with the tube face.

Lamotte, M., Dewey, H. J., Keller, R. A., Ritter, J. J., **Laser induced photochemical enrichment of chlorine isotopes,** *Chem. Phys. Lett.* **30,** No. 2, 165-170 (Jan. 15, 1975).

Key words: dye laser; isotope; isotope separation; photochemistry.

Chlorine isotopic abundances were significantly altered by laser induced, selective excitation of particular isotopic species of thiophosgene followed by a chemical reaction between the electronically excited thiphosgene and diethoxyethylene. The concentration of ^{35}Cl in thiophosgene was changed from 75 to 64 percent or 80 percent depending upon the isotopic species initially excited.

Leasure, W. A., Jr., Corley, D. M., Farrer, J. S., Flynn, D. R., **Truck noise—1. Peak A-weighted sound levels due to truck tires (addendum),** *DOT Report No. OST/TST-72-1,* 223 pages (Available as PB238912 from the National Technical Information Services, Springfield, Va., 22161, July 1972).

Key words: acoustics; noise measurement; noise pollution; noise (sound); sound transmission; tire noise; transportation noise; trucks; urban planning.

This report is the second in a series of reports to be published as a result of Department of Transportation sponsored truck tire research conducted by the National Bureau of Standards. In conjunction with the first report (OST-ONA-71-9) which contains details of the test design, test procedures, and all data acquired during the first period of testing, this report presents an inventory of peak A-weighted sound levels generated by typical rib, cross-bar and retread type truck tires. A test sample of nine tread designs, estimated to represent 70-80 percent (based on discussions with fleetowners) of the truck tire population on the road today, was investigated considering the following variables: wear, loading, speed, pavement surface, and tire location. Test vehicles included both single-chassis vehicles and tractor-trailers.

The results show that the A-weighted sound level increased with either an increase in load or speed. The "pocket retread" design always produced the highest level followed by the cross-bar tires and then the rib tires. This ranking held for tires in all states of wear. The influence of wear and pavement surface, however, is more complex. In general there was an increase in noise level between the new and half-worn states and a slight decrease between the half-worn and fully-worn states. The influence of pavement surface on the generated noise depends on the specific tread design, tire wear condition and the surface roughness. Tires do contribute differently to the overall noise level depending on their location on the vehicle. The data for tractor-trailor tests, for instance, would strongly indicate that the major contribution is made by the tires mounted on the drive axles of the tractor and that the relative contribution of tires mounted on either the front or rear trailer axles depends on the specific tire type and speed of the vehicle.

Future reports will broaden the data to include one-third octave band spectral data, directionality data in the form of equal sound level contours and other refined analysis of the data reported herein and in OST-ONA-71-9.

Leasure, W. A., Jr., Corley, D. M., Farrer, J. S., Flynn, D. R., **Truck noise—1. Peak A-weighted sound levels due to truck tires (final report),** *DOT Report No. OST-ONA-71-9,* 248 pages (Available as PB204188 from the National Technical Information Services, Springfield, Va., 22161, Sept. 1970).

Key words: acoustics; noise measurement; noise pollution; noise (sound); sound transmission; tire noise; transportation noise; trucks; urban planning.

This initial report presents an inventory or "catalog" of peak A-weighted sound levels measured during an extensive parametric study conducted to characterize the noise generated by typical rib, cross-bar and retread type truck tires. A test sample of nine tread designs, estimated to represent 70-80 percent (these exact designs) of the truck tire population on the road today, was investigated considering the following variables: wear, loading, speed, pavement surface, and tire location. Test vehicles included both single-chassis vehicles and a tractor-trailer.

The results show that the A-weighted sound level increased with either an increase in load or speed. The "pocket retread" design always produced the highest level followed by the cross-bar tires and then the rib tires. This ranking held for both new and half-worn tires. The influence of wear and pavement surface is more complex. For all of the tread designs except one there was an increase in noise level between the new and half-worn states. The results for different pavement surfaces are much the same as with wear in that the generated noise appears to depend on both the specific tread design and the surface roughness. Individual tires do contribute differently to the overall level depending on their location on the vehicle. In some cases, significant reductions in the noise level were observed when "noisy" tires were mounted inboard of "quieter" tires.

The report includes a discussion of the measurement and analysis techniques utilized for the establishment of this data base.

Leasure, W. A., Jr., Mathews, D. E., Rinkinen, W. J., **Truck noise 1-A: Noise evaluation tests of military truck tires (final report),** *DOT Report No. DOT-TST-74-21,* 54 pages (Available as PB234348 from the National Technical Information Services, Springfield, Va., 22161, Feb. 1974).

Key words: acoustics; military vehicles; noise; sound; tire noise; truck tires.

This report presents the A-weighted sound level and one-third octave band spectral data resulting from a study conducted to characterize the noise generated by military truck tires. The study was conducted by the National Bureau of Standards in cooperation with the U.S. Department of Transportation under the sponsorship of the U.S. Army Tank-Automotive Command. The data base established will allow for comparison of the tire noise generated by military and commercial truck tires.

The study investigated the influence of load and speed on the noise generated by tires with four different tread designs: the standard Army tire, a retread of Army design and commercial tires with rib and cross-bar type tread patterns. Army and commercial trucks were utilized as test vehicles.

In addition, the report includes a discussion of the measurement and analysis techniques utilized for the establishment of this data base.

Ledbetter, H. M., **Elastic constants of polycrystals: Equivalence of Laurent-Eudier and Voigt averaging methods,** *Phys. Status Solidi A* **26,** K67-K70 (1974).

Key words: bulk modulus; compressibility; elastic constants; elasticity Lamé constant; Poisson ratio polycrystals; shear modulus; single crystals; Young's modulus.

The equivalence of the methods of Laurent and Eudier and of Voigt for averaging cubic single-crystal elastic coefficients to obtain polycrystal elastic constants is proven and discussed. Other ways to obtain Voigt's equations are enumerated.

Lentner, K. J., **A current comparator system to establish the unit of electrical energy at 60 Hz,** *IEEE Trans. Instrum. Meas.* **IM-23,** No. 4, 334-336 (Dec. 1974).

Key words: calibration; current comparator; electrical energy unit; metrology; standard; unit; watthour meter calibration; watthour meter.

A compensated current comparator system to establish the United States legal unit of electrical energy at the National Bureau of Standards at energy levels of approximately 30 and 60 kJ is described. Analysis of the system uncertainties and experimental data indicates that the registrations of three standard type watthour meters were determined with total estimated uncertainties of about 30 ppm at unity power factor (PF) and 40 ppm at 0.5 PF. Of these uncertainties, 18 ppm represents the three standard deviation bound for the effects of random errors, and the remainder the root sum of squares of bounds to possible calibration and systematic effects. These results indicate that it should now be possible to disseminate the energy unit with uncertainties less than the presently quoted 500 ppm.

Lias, S. G., Ausloos, P., **Structure and reactivity of $C_4H_8^+$ ions formed in the radiolysis of cycloalkanes in the gas phase,** *J. Amer. Chem. Soc.* **92,** No. 7, 1840-1847 (Apr. 8, 1970).

Key words: charge transfer reactions; cycloalkanes; cyclohexane; gas phase; methylcyclopentane; parent ions.

The structure and reactivity of the $C_4H_8^+$ formed in the fragmentation of cyclohexane and methylcyclopentane parent ions has been examined ($[C_6H_{12}^+]^* \rightarrow C_2H_4 + C_4H_8^+$). It is noted that $C_4H_8^+$ consists of 1-$C_4H_8^+$, *i*-$C_4H_8^+$, and 2-$C_4H_8^+$. The relative abundances of these isomer ions depend on the energy content of the cycloalkane ion. According to the mass spectral cracking pattern of cyclohexane-1,1,2,2,3,3-d_6 the high energy parent ion splits out $C_4H_8^+$ without extensive prior rearrangement. The $C_4H_8^+$ so formed is analogous to the $C_4H_8^+$ ion produced in the photoionization or radiolysis of cyclobutane. The various $C_4H_8^+$ isomers react with the cycloalkanes by acceptance of an H_2^- entity: $C_4H_8^+ + C_6H_{12} \rightarrow C_4H_{10} + C_6H_{10}^+$. The relative reaction rates, which are determined by means of isotopic labeling experiments, differ widely with a change in the structure of both the reactant ion and the reactant molecule, with the rate of reaction being generally higher for the more exothermic process.

Lias, S. G., **Ion-molecule reactions in radiation chemistry,** (Proc. NATO Advanced Study Institute Conf. on Ion-Molecule Interactions, Biarritz, France, June 24-July 6, 1974), Paper in *Interactions Between Ions and Molecules,* P. Ausloos, Ed., pp. 541-562 (Plenum Publishing Corp., New York, N.Y., 1975).

Key words: ion-molecule reaction; ion structure; ionic fragmentation; radiation chemistry; rate constants.

This brief review presents several illustrations of how ion-molecule reactions are studied in radiation chemical experiments and also of the kinds of information about ion-molecule reactions and other ionic phenomena (such as fragmentation and isomerization) which have been obtained from such experiments. Absolute rate coefficient determinations through spectroscopic measurements in the gas and liquid phase radiolysis, as well as absolute and relative rate coefficient determinations based on chemical analysis of reaction products are described. Illustrations from radiation chemical investigations which have given unique information about mechanistic details of certain ion-molecule reactions in hydrocarbon systems are also presented. A historical review and general description of the conditions prevailing in radiation chemistry experiments are also included.

Lias, S. G., Rebbert, R. E., Ausloos, P., **Carbonium ions in radiation chemistry. II. Isomerization processes in $C_3H_7^+$ and $C_4H_9^+$ ion,** *J. Amer. Chem. Soc.* **92,** No. 22, 6430-6440 (Nov. 4, 1970).

Key words: butyl ion; carbonium ion; ion fragmentation; isomerization; propyl ion.

The structures of propyl and butyl ions formed in the gas-phase radiolysis of appropriate alkanes have been deduced from the structures of the neutral products formed in proton transfer reactions with ammonia, or from the isotopic structures of hydride (or deuteride) transfer reaction products formed in labeling experiments. *n*-Propyl ions rearrange within 10^{-10} sec to the *sec*-propyl or the protonated cyclopropane structure. Rearrangement to the *sec*-propyl ion is favored under all conditions but increases in importance with increasing internal energy content of the ion. Both isomerization reactions are reversible, but the rate constants of the reverse reactions are very low owing to the energy requirements of these processes. The isomerization of the *sec*-butyl ion to the *t*-butyl structure is observed; this rearrangement also increases in importance with increasing internal energy content of the ion. The H (or D) atoms in the secondary and tertiary carbonium ions are seen to undergo energy-dependent hydrogen-scrambling processes. The protonated cyclobutane ion formed by proton transfer to cyclobutane isomerizes mainly to the *sec*-butyl structure. The results presented here demonstrate that most of the propyl and butyl ions formed in the dissociation of butane and hexane parent ions, respectively, originate as primary carbonium ions from simple C-C cleavage processes, rather than being formed initially with the secondary structure, as they are at the threshold energies.

Lias, S. G., Viscomi, A., Field, F. H., **Chemical ionization mass spectra. XXI. Reactions in *t*-$C_5H_{11}Cl$, *t*-$C_5H_{11}Br$, *t*-$C_5H_{11}OH$, and *t*-$C_5H_{11}SH$,** *J. Amer. Chem. Soc.* **96,** No. 2, 359-364 (Jan. 23, 1974).

Key words: alcohols; alkyl halides; chemical ionization; ion-molecule reactions; mass spectrometry; mercaptans.

Mixtures of isobutane with small amounts (0.01-1%) of added *t*-$C_5H_{11}Cl$, *t*-$C_5H_{11}Br$, *t*-$C_5H_{11}OH$, and *t*-$C_5H_{11}SH$ have been studied in a high-pressure mass spectrometer as a function of total pressure, temperature, and concentration of additive. It is seen that proton transfer occurs only to *t*-$C_5H_{11}SH$, and even in this case, proton transfer is a minor process. The major reaction observed with each of the four molecules is the formation of a condensation ion which dissociates rapidly to give ($C_9H_{19}^+ + HX$) or ($C_5H_{11}^+$ + neutral products) where X is Cl, Br, OH, or SH. The formation of $C_5H_{11}^+$ is favored under all conditions, but the formation of $C_9H_{19}^+$ becomes more important as the pressure is raised or the temperature is lowered. When *i*-C_4D_{10} is substituted for *i*-C_4H_{10}, it is seen that in the mercaptan, where proton transfer may be slightly exothermic, the departing hydrogen sulfide molecule carries away a D species from the reacting *tert*-butyl ion with a high probability; conversely, in *t*-$C_5H_{11}Br$, the departing hydrogen bromide molecule has a low probability of containing a hydrogen species from the reacting *tert*-butyl ion. This result suggests that when proton transfer competes with the displacement reaction, the two reactions proceed through the same intermediate ion, a $C_9H_{20}H^+$ species, in which "internal" proton transfer has occurred. The product $C_5H_{11}^+$ ion undergoes an analogous displacement reaction with all of these molecules to form the following as products: ($C_{10}H_{21}^+ + HX$) and ($C_6H_{13}^+$ + neutral products). The $C_6H_{13}^+$ product ion also undergoes a displacement reaction with all of these molecules to form as products ($C_{11}H_{23}^+ + HX$).

Lovas, F. J., **Small silicon molecules: Possible sources of the unidentified molecular lines U81.5, U86.2, U89.2, and U90.7,** *Astrophys. J.* **193,** No. 1, 265-272 (Oct. 1, 1974).

Key words: microwave spectra; predicted spectra; radio astronomy; silicon molecules; structures; unidentified molecular lines.

Several small silicon molecules are considered as possible sources for the unidentified molecular lines: U81.5, U86.2, U89.2, and U90.7. The best spectroscopic and structural data available have been utilized to predict the lowest rotational transitions for SiO^+, SiN, SiC, HSiN, and for vibrationally excited SiO. Transitions from each of these molecules are predicted to occur close to one or more of these unidentified molecular lines. Rotational transitions which could aid the confirmation of each of the suggested assignments are also presented. In all cases, an effort has been made to estimate the uncertainties for the predicted transitions.

Mabie, C. P., Wallace, B. M., **Optical, physical and chemical properties of pineal gland calcifications,** *Calcif. Tissue Res.* **16,** 59-71 (1974).

Key words: apatite; calcospherulites; calculi; petrography; pineal.

Calcifications of the pineal gland in the form of calcospherulites have been studied by optical microscopy, electron microscopy, electron probe analysis, x-ray diffraction, thermogravimetry, and infrared and chemical analysis. Complex calcospherulite textures have been observed which have a granular substructure made up of apatite crystals averaging 218 Å in length and 38 Å in width. These apatite crystals appear to be a carbonate-containing hydroxyapatite, mineralogically similar to enamel.

Madey, T. E., Menzel, D., **Adsorption of CO on (001) ruthenium at temperatures ≥ 300 K,** (Proc. 2nd Int. Conf. on Solid Surfaces, Kyoto, Japan, March 25-29, 1974), *Jap. J. Appl. Phys. Suppl.* **2,** Part 2, 229-235 (1974).

Key words: carbon monoxide; chemisorption; defraction low energy electron; ruthenium; work function Auger spectroscopy.

The adsorption of CO on Ru(001) has been studied using a combination of techniques: LEED/Auger, Kelvin probe contact potential changes, and flash desorption mass spectrometry. Adsorption of CO is reversible at temperatures and pressures as high as 700 K and 10^{-4} torr, respectively. Two binding states of CO are identified, and isosteric heats determined both from work function changes and from LEED intensity measurements agree well with flash desorption energies. A disordering of the CO layer due to repulsive interactions between neighbors at high coverages is postulated. Electron beam-induced LEED pattern changes are characterized and found to have a high cross section ($\sim 7 \times 10^{-17}$ cm²) at ~ 110 eV.

Malloy, T. B., Jr., Lafferty, W. J., **On the barriers to planarity and the isotope effect in cyclobutane and cyclobutane-d_8,** *J. Mol. Spectrosc.* **54,** 20-38 (1975).

Key words: barriers to planarity; cyclobutane; cyclobutane-d_8; isotope effect; kinetic energy terms; potential functions.

The infrared and Raman data on the ring-puckering vibration in cyclobutane and cyclobutane-d_8 have been reexamined including the coordinate dependence of the reduced mass in the Hamiltonian. This was done for the purpose of estimating the importance of these small terms in the determination of barrier heights for four-membered rings and also on the determination of the dihedral angle corresponding to the potential minimum.

The conclusions reached are that there is an isotopic dependence of the barriers to planarity in cyclobutane and cyclobutane-d_8 yielding a difference of ~ 14 cm^{-1}, but the precise value of the difference in barrier heights is ill determined. The higher-order kinetic energy terms in the Hamiltonian can account for a spread of ~ 3 cm^{-1} in each of the barriers derived for cyclobutane and cyclobutane-d_8, depending on the details of the model used for the vibration, but not a difference of 14 cm^{-1}, which undoubtedly indicates the effects of coupling with other vibrational modes. It is also found that the derived values of the dihedral angles are quite sensitive to the details of the vibrational model, in fact, much more so than to the uncertainties in the bond distances and bond angles. A relationship between the potential constants derived for cyclobutane and cyclobutane-d_8 assuming an effective constant reduced mass and those derived for a semirigid model is demonstrated.

Manghnani, M. H., Brower, W. S., Parker, H. S., **Anomalous elastic behavior in Cu_2O under pressure,** *Phys. Status Solidi* **25,** 69-76 (1974).

Key words: cuprous oxide; elastic constants.

The elastic constants C_{ij} of single-crystal Cu_2O measured to 3 kbar show linear variation with pressure. The best-fit values of the C_{ij} and dC_{ij}/dP are: $C_{11} = 1228.8$, $C_{44} = 121.0$, $C' = (C_{11} - C_{12})/2 = 81.9$ kbar, $dC_{11}/dP = 3.62$, $dC_{44}/dP = -0.69$, and $dC'/dP = -0.63$, respectively. The elastic behavior of Cu_2O is found to be anomalous in that dC_{44}/dP and dC'/dP are both negative, and $d\mu/dP$, where μ is the isotropic shear modulus, is significantly negative (-0.67). This anomalous behavior suggests an instability of crystal structure. The high- and low-temperature limiting values of Grüneisen γ, γ_H and γ_L, computed from the dC_{ij}/dP are -1.98 and -3.59, respectively. The value of γ_H is in fairly good agreement with the reported Grüneisen γ value based on the nuclear quadrupole relaxation data. The negative Grüneisen γ values are consistent with the observed negative thermal expansion. The implication of γ_L being appreciable more negative than γ_H is that the coefficient of thermal expansion of Cu_2O should become more negative at low temperatures.

Mann, W. B., **The calibration of the National Bureau of Standards' tritium standards by microcalorimetry and gas counting,** (Proc. Tritium Symp., Las Vegas, Nev., Aug. 30-Sept. 2, 1971), Chapter 3 in *Tritium,* A. A. Moghissi and M. W. Carter, Eds., pp. 86-102 (Messenger Graphics, Las Vegas, Nev., 1971).

Key words: gas counting; microcalorimetry; tritium standards.

The calibration of the National Bureau of Standards tritium standards by microcalorimetry and gas counting will be described.

Mauer, F. A., Hubbard, C. R., Piermarini, G. H., Block, S., **Measurement of anisotropic compressibilities by a single crystal diffractometer method,** Paper in *Advances in X-Ray Analysis,* W. L. Pickles, C. S. Barrett, J. B. Newkirk, and C. O. Ruud, Eds., **18,** 437-453 (Plenum Press, New York, N.Y., 1975).

Key words: compressibility; single crystal; x-ray diffraction.

The beryllium diamond-anvil pressure cell described by Weir, Piermarini and Block has been mounted on a Bond diffractometer equipped with an orienter of the fixed-χ type. Molybdenum radiation is used to penetrate the diamonds and beryllium of which the cell is constructed, and special techniques are required to retain adequate precision in measuring cell parameters using diffraction angles in the low 2θ range. The method described provides high sensitivity in determining peak positions and eliminates the effect of centering errors on measured values of 2θ. Under favorable conditions, diffraction angles are measured with an accuracy of ± 0.001 ° in 2θ. The method has been tested by measuring the lattice parameter of vacuum float zone refined silicon. Measurements of the compressibilities of silicon and of α-Pb $(N_3)_2$ (orthorhombic) have been carried out using the method of Barnett, Block, and Piermarini to determine pressure by measuring the shift in the R-line fluorescence spectrum of ruby.

McKinney, J. E., Simha, R., **Configurational thermodynamic properties of polymer liquids and glasses. I. Poly(vinyl acetate),** *Macromolecules* **7,** No. 6, 894-901 (Nov.-Dec. 1974).

Key words: configurational; glass; glass transition; hole theory; polymer; poly(vinyl acetate); PVT; thermodynamic; liquid.

Recent experimental PVT data on poly(vinyl acetate) are analyzed using the hole theory of Simha-Somcynsky. The data were obtained at temperatures from − 30 to 100° and pressures up to 800 bars. These ranges encompass the glass transition and include large portions of the liquid and glassy regions. Three different thermodynamic histories of glass formation, all isobaric cooling at 5°C/hr, were applied. With the variable formation history the glass was formed by isobaric cooling runs at different pressures. In the two constant formation histories each of the glasses was formed by a different formation pressure, namely atmospheric and 800 bars, with subsequent temperature and pressure changes in the glass in each case. In the equilibrium state good agreement between the theoretical and experimental PVT surfaces results, in accord with earlier observations on amorphous systems. As for the transitions the theory gives the correct values of dT/dP using the assumption that the hole fraction h be constant along either of the two constant formation transition lines. Similarly, the generalization of the Ehrenfest type relation involving the single ordering parameter h results in good numerical agreement with the experimental values of dT/dP for the variable formation transition line. As previously demonstrated, H does not freeze at temperatures below the glass transition, thus a constant h does not describe the structure of the glass. Parameters which describe the extent of freezing are evaluated. The fact that these parameters are independent of formation pressure would be consistent with the existence of a single entropy surface with formation pressure, as suggested by other experimental evidence.

McLaughlin, W. L., Hjortenberg, P. E., Pedersen, W. B., **Low energy scanned electron-beam dose distributions in thin layers,** *Int. J. Appl. Radiat. Isotop.* **26,** No. 3, 95-106 (1975).

Key words: dose distributions; dosimetry; dye dosimeters; electron beams; radiation curing; radiation processing; radiochromic dyes; thin films.

Thin radiochromic dye film dosimeters, calibrated by means of calorimetry, make possible the determination of absorbed-dose distributions due to low-energy scanned electron beam penetrations in moderately thin coatings and laminar media. For electrons of a few hundred keV, calibrated dosimeters of about 30-60 μm thickness may be used in stacks or interleaved between layers of materials of interest and supply a sufficient number of experimental data points throughout the depth of penetration of electrons to provide a depth-dose curve. Depth doses may be resolved in various polymer layers on different backings (wood, aluminum, and iron) for scanned electron beams (E_{max}=400 keV) having a broad energy spectrum and diffuse incidence, such as those used in radiation curing of coatings, textiles, plastics, etc. Theoretical calculations of such distributions of energy depositions are relatively difficult to achieve.

McNesby, J. R., Hughes, E. E., **Calibration gas standards,** *Proc. Int. Instrumentation-Automation Conf. and Exhibit, New York, N.Y., Oct. 28-31, 1974, Paper 74-633, 1-5 (Instrument Society of America, Pittsburgh, Pa., 1974).*

Key words: aircraft; air pollution; automobile; standard reference materials.

Accurate measurement of emissions is best accomplished by means of specific measurement methods using instruments which are calibrated by reference to Standard Reference Materials. The National Bureau of Standards has developed a number of gas Standard Reference Materials during the past two years for the measurement of pollutant gases in automobile exhaust emissions. These Standard Reference Materials include carbon monoxide in nitrogen, propane in air, carbon dioxide in nitrogen and nitric oxide in nitrogen at concentrations relevant not only to auto exhaust emissions but also to aircraft exhaust emissions. The technical problems associated with the development of those Standard Reference Materials are discussed and a description of the ranges of concentrations available is outlined.

Meshkov, S., Rosen, S.P., **Gauge theories and M-spin conservation,** *Phys. Rev. D, Comments and Addenda* **10,** No. 10, 3520-3521 (Nov. 15, 1974).

Key words: gauge theories; lepton; muon; M-spin; scattering amplitudes; Weinberg.

M-spin conservation is shown to be a property of Salam-Weinberg gauge theories. Amplitude relations such as $A(\nu_e e^- \rightarrow \nu_e e^-) - A(\nu_\mu e^- \rightarrow \nu_\mu e^-) = A(\nu_\mu e^- \rightarrow \nu_e \mu^-)$ derived from M-spin invariance alone also hold for the gauge theories up to the breaking due to Higgs scalars.

Mielenz, K. D., **Aberrations of ellipsoidal reflectors for unit magnification,** *Appl. Opt.* **13,** No. 12, 2931-2933 (Dec. 1974).

Key words: aberrations; aspheric optics; ellipsoidal reflector; Fermat's principle; Hamiltonian point characteristic; limiting aperture; unit magnification.

Ellipsoidal reflectors are useful for the 1:1 imaging of small objects without spherical and chromatic aberration. The magnitude of the off-axis aberrations of such reflectors is computed by application of Fermat's principle to the Hamiltonian point characteristic. The limiting form of the mirror aperture for which these aberrations do not exceed a set tolerance is an ellipse whose semiaxes depend on object size and angle of incidence.

Mielenz, K. D., **Spherically corrected reflecting objective for unit magnification,** *Appl. Opt.* **13,** No. 11, 2580-2584 (Nov. 1974).

Key words: Cassegrain; reflecting objective; spectrometers; spherical aberration; third-order theory; unit magnification.

Cassegrainian-type reflecting objectives are useful as in-line imaging devices for fast spectrometer systems. They are inherently free from chromatic aberrations and may be corrected for spherical aberration. A particularly simple design, consisting of two mirrors with oppositely equal curvatures, is possible when unit magnification is desired. This system has zero third-order spherical aberration, and all other aberrations are small also. Its main disadvantage is the loss due to the central obstruction of the beam, amounting to about 28 percent exclusive of reflection losses.

Moore, L. J., Machlan, L. A., Shields, W. R., Garner, E. L., **Internal normalization techniques for high accuracy isotope dilution analyses-application to molybdenum and nickel in standard reference materials,** *Anal. Chem.* **46,** No. 8, 1082-1089 (July 1974).

Key words: isotope dilution; isotopes; mass spectrometry; molybdenum; nickel; normalization; standard reference materials; thermal ionization.

General exact equations and iteration techniques have been developed for internal normalization to eliminate the effect of thermal fractionation from isotope ratio measurements, and therefore isotope dilution analyses, by thermal ionization mass spectrometry. The techniques are applicable to more than 20 elements, and have been extensively applied to the determination of Mo in ore concentrates (55% Mo) and silicate trace standards (50 and 500 ppm M.). The standard deviations of all internally corrected Mo isotope ratio measurements were < 0.1 percent. The Mo sample size was 40 μg, but normalization techniques should apply to μg and smaller samples with a more sensitive ion detection system. Procedures are described for the chemical separation of Mo from matrix interferences and for the mass spectrometric analysis of Mo. Application of the techniques to Ni in three pollution standard reference materials is described.

Mulholland, J. D., Plotkin, H. H., Silverberg, E. C., Wilkinson, D. T., Alley, C. O., Bender, P. L., Currie, D. G., Dicke, R. H., Faller, J. E.,

Kaula, W. M., Williams, J. G., **A self-consistent set of surface coordinates for the Apollo lunar laser retroreflectors deduced from laser range measures,** (Proc. 15th Planetary Meeting of COSPAR, Madrid, Spain, May 1972), Paper in *Space Research* **XIII,** M. J. Rycroft and S. K. Runcorn, Eds., **2,** 1009-1013 (Akademie-Verlag, Berlin, Germany, Dec. 1973).

Key words: astronomy; cartography; geophysics; laser; lunar distance; moon; selenodesy.

Laser ranges from the McDonald Observatory to the three Apollo retroreflectors have been used to obtain simultaneous solutions to the selenocentric coordinates of the three arrays, using two different approaches. The original coordinates, which were obtained either from LEM orbit determination or from orbital triangulation, suffered adjustments that were compatible with their *a priori* uncertainties, which ranged up to about a kilometer. It was decided also to correct the lunar moments of inertia. The corrections thus far obtained are not definitive, since the differential residuals are still of significant size. Nonetheless, order of magnitude reductions in the differential residuals have been secured.

Niemeijer, Th., Meijer, P. H. E., **Quantum-mechanical ground state of crystals with dipole-dipole and exchange interactions,** *Phys. Rev. B* **10,** No. 7, 2962-2967 (Oct. 1, 1974).

Key words: antiferromagnetism; cerous magnesium nitrate; dipole-dipole interaction; ferromagnetism; ground state; magnetic; permutation group; quantum mechanics.

The general quantum-mechanical extension of Luttinger and Tisza's approach to the ground state of crystals with dipole-dipole and exchange interactions is given. It is shown that within this approach the ground state can only be ferro- or antiferromagnetic if the unit cell contains only one or two magnetically equivalent atoms or ions.

O'Connell, J. S., Lightbody, J. W., Jr., **Momentum transfer sum rules in electron scattering,** *Nucl. Phys.* **A237,** 309-318 (1975).

Key words: charge density; Coulomb energy; Coulomb excitation; electron scattering; form factors; sum rules; transition charge.

The integral properties of elastic and inelastic Coulomb form factors are examined. Relations are given for the nuclear Coulomb energy, central charge density, transition charge, radial moments, and squared density integral.

Olsen, P. T., Williams, E. R., **A more accurate determination of γ_p' through improved dimensional measurement techniques,** *IEEE Trans. Instrum. Meas.* **IM-23,** No. 4, 302-305 (Dec. 1974).

Key words: automated measurement systems; gyromagnetic ratio; magnetic field; protons; solenoid.

An increase in the accuracy of the gyromagnetic ratio of the proton can be achieved by determining the magnitude of a calculable magnetic field to higher accuracy. Such an increase requires dimensional measurements of a physical object to an absolute accuracy of a few parts in ten million. A unique computer-controlled automated measurement system for carrying out such measurements has been developed at the U.S. National Bureau of Standards and is currently in operation at its nonmagnetic facility. This measurement system provides an order of magnitude improvement over all previous measurements.

Olson, W. B., Maki, A. G., Sams, R. L., **Infrared measurements on arsine: ν_1 and ν_3 bands, perturbation-allowed transitions, equilibrium structure,** *J. Mol. Spectrosc.* **55,** Nos. 1-3, 252-270 (1975).

Key words: arsine; infrared high resolution; perturbation-allowed transitions; resonances; secular determinants; spectra; structure.

High resolution infrared measurements are reported on arsine (AsH_3) from 2260 to 1960 cm^{-1}. Numerous perturbation-allowed transitions have been found and are used to determine the C_0 rotational constant. Ten ground state rotational constants are determined including one that describes the splitting of the $k=3$ levels. A complete equilibrium structure is determined. A total of 26 upper state constants are determined by means of a computer program which simultaneously fits both ν_1 and ν_3 bands and includes many off-diagonal matrix elements. This analysis will fit transitions through $J=K=12$ to within experimental error, but it is concluded that to fit higher rotational transitions the perturbing effects of $2\nu_4$ must be taken into account explicitly.

Olver, F. W. J., **Legendre functions with both parameters large,** *Phil. Trans. Roy. Soc. London* **278,** No. 1279, 175-185 (Mar. 20, 1975).

Key words: asymptotic approximations; error bounds; Legendre functions; parabolic cylinder functions; turning points; Weber functions.

By application of the theory for second-order linear differential equations with two turning points developed in the preceding paper, some new asymptotic approximations are obtained for the associated Legendre functions when both the degree n and order m are large. The approximations are expressed in terms of parabolic cylinder functions, and are uniformly valid with respect to $x\epsilon(-1,1)$ and $m/(n+1/2)\ \epsilon[\delta, 1+\Delta]$, where δ and Δ are arbitrary fixed numbers such that $0<\delta<1$ and $\Delta>0$. The values of m and $n+1/2$ are either both real, or both purely imaginary. In all cases explicit bounds are supplied for the error terms associated with the approximations.

Olver, F. W. J., **Second-order linear differential equations with two turning points,** *Phil. Trans. Roy. Soc. London* **278,** No. 1279, 137-174 (Mar. 20, 1975).

Key words: asymptotic approximations; connection formulas; error bounds; ordinary differential equations; parabolic cylinder functions; turning points; wave scattering; Weber functions.

Differential equations of the form

$$d^2w/dx^2 = \{u^2f(u,a,x) + g(u,a,x)\}w$$

are considered for large values of the real parameter u. Here x is a real variable ranging over an open, possibly infinite, interval (x_1, x_2), and a is a bounded real parameter. It is assumed that $f(u,a,x)$ and $g(u,a,x)$ are free from singularity within (x_1, x_2), and $f(u,a,x)$ has exactly two zeros, which depend continuously on a and coincide for a certain value of a. Except in the neighbourhoods of the zeros, $g(u,a,x)$ is small in absolute value compared with $u^2f(u,a,x)$.

By application of the Liouville transformation, the differential equation is converted into one of four standard forms, with continuous coefficients. Asymptotic approximations for the solutions are then constructed in terms of parabolic cylinder functions.

Parrish, W. R., Hiza, M. J., **Liquid-vapor equilibria in the nitrogen-methane system between 95 and 120 K,** (Proc. 1973 Cryogenic Engineering Conf., Atlanta, Ga., Aug. 8-10, 1973), Paper H-2 in *Advances in Cryogenic Engineering* **19,** 300-308 (Plenum Press, New York, N.Y., 1974).

Key words: binary mixture; excess Gibbs energy; experimental phase equilibria data; heat of mixing; liquid-vapor equilibria; nitrogen-methane system.

A study was undertaken to obtain liquid-vapor equilibria data for the nitrogen-methane system at uniform temperature increments between the triple point of methane and the critical point of nitrogen. The measured liquid and vapor phase equilibrium compositions and the derived excess Gibbs energy values for six isotherms from 95 to

120 K are compared with the corresponding values taken from other investigations. The excess Gibbs energy for the equimolar mixture exhibits a zero to slightly positive temperature dependence, in qualitative agreement with calculations based on the Snider-Herrington hard sphere model. This temperature dependence of the excess Gibbs energy also suggests that the excess enthalpy (heat of mixing) must be equal to or slightly less than the excess Gibbs energy.

Phaneuf, R. A., Crandall, D. H., Dunn, G. H., **Production of D*($n=4$) from electron-D_2^+ dissociative recombination,** *Phys. Rev.* ***A11,*** No. 2, 528-535 (Feb. 1975).

Key words: cross sections; D_2^+; dissociative recombination; product $D^*(n=4)$.

Crossed beams of electrons and D_2^+ ions were used to measure absolute cross sections for the dissociative recombination process, $e + D_2^+(X^2\Sigma_u^+) \rightarrow D + D^*(n=4)$ over a range of electron energies extending from 0.6 to 7 eV. The process was monitored by detecting a known portion of the 485.9-nm emission resulting from radiative decay of the product $D^*(n=4)$ atoms. The cross sections, which correspond to a known vibrational-state distribution of the target ions, exhibit the same dependence on electron energy as recent measurements of the total dissociative recombination cross section reported by Peart and Dolder, and have a magnitude of about 10 percent of the total cross section, suggesting that the product D atoms are formed in excited states with a variety of principal quantum numbers. Systematic measurement uncertainties at high confidence are about 14 percent, and random uncertainties are at the 25 percent (standard deviation) level. The calculation of cross sections from the observed light intensities depends on the mean lifetimes and branch ratios for 485.9-nm emission, whose evaluation in turn requires assumptions concerning the recombination process. The situation is complicated by the presence of an electron-beam-confining magnetic field in the collision volume, which causes the incident ions and product atoms to experience a transverse motional electric field. A time-independent perturbation calculation of the weak-field Stark and Zeeman effects was performed and mean lifetimes and branch ratios were estimated under different assumptions concerning the recombination process. Assuming that all perturbed product $n=4$ states are equally populated by dissociative recombination yields an experimental cross section of 1×10^{-16} cm² at 0.7 eV, decreasing to 3.3×10^{-17} cm² at 3 eV, and to 1×10^{-17} cm² at 7 eV. Assuming that only the perturbed 4*s* states are intitially populated results in cross sections larger by some 50 percent.

Phelps, A. V., **Applications of gaseous electronics to laser technology,** Chapter 3 in *Gaseous Electronics, Some Applications,* J. W. McGowan and P. K. John, Eds., pp. 25-46 (North-Holland Publishing Co., Amsterdam, The Netherlands, 1974).

Key words: atoms; electron excitation; excitation transfer; gaseous electronics; lasers; molecules.

Applications of the results of research in the physics of gaseous electronics to recent laser technology are illustrated. Excitation transfer, charge exchange, metastable atom production and destruction are dominant processes in the HeNe laser and the metal ion lasers. Rather extensive data on cross sections for elastic and inelastic scattering, attachment and ionization in gases such as N_2 and CO_2 make possible fairly accurate predictions of the gain, efficiency, etc., of CO_2-N_2-He lasers. The new class of ground state dissociation lasers is discussed in terms of a proposed laser utilizing stimulated emission between the bound excited state and the dissociating ground state of the LiXe molecule.

Plummer, E. W., Waclawski, B. J., Vorburger, T. V., **Photoelectron spectra of the decomposition of ethylene on (110) tungsten,** *Chem. Phys. Lett.* **28,** No. 4, 510-515 (Oct. 15, 1974).

Key words: C_2H_4 decomposition; chemisorption bonds; LEED; photoelectron spectra; tungsten; work function.

Photoelectron spectra, LEED patterns, and work function changes were obtained for ethylene adsorbed on (110) tungsten at room temperature, and with subsequent heat treatment. For saturated adsorption of C_2H_4 on (110)W at room temperature, features in the photoelectron spectrum were observed which are believed to be due to the C–H, C–C, and C–metal bonds in an adsorbed species of the form C_2H_2. The work function decreased by 1.2 eV at saturation, but LEED showed no change from the clean surface pattern. Upon heating to ≈500 K, where hydrogen is known to desorb, the C–H bond was broken, whereas the C–C and C–metal bonds remained. The work function increased, from saturation, by ≈0.6 eV and the LEED pattern exhibited a large diffuse background with no new spots. Upon heating to ≈1100 K the C–C bond broke and the LEED pattern ordered into the characteristic carbon contamination pattern.

Prince, E., Dickens, B., Rush, J. J., **A study of one-dimensional hindered rotation in NH_3OHClO_4,** *Acta Crystallogr.* **B30,** Part 5, 1167-1172 (May 1974).

Key words: constrained refinement; hindered rotation; hydrogen bonds; hydroxylammonium; neutron diffraction; perchlorates; thermal motion; torsional oscillation.

The structure of the phase of hydroxylammonium perchlorate, NH_3OHClO_4, which is stable at 25 °C has been refined from 3-dimensional neutron diffractometer data. The structure has space group $P2_1cn$, cell dimensions $a = 7.52$ (2), $b = 7.14$ (1), $c = 15.99$ (2) Å, and 8 formula units per unit cell. There are very large thermal motions of the hydrogen atoms, and the environment of the two crystallographically different NH_3OH^+ ions suggests hindered rotation of each NH_3 group around the axis defined by the N–O bond. Therefore the structure was refined using a model in which the perchlorate groups and the hydroxyl hydrogens were given conventional anisotropic temperature factors, but the ONH_3 groups were treated as rigid bodies, each with an isotropic translation, and isotropic libration of the group as a whole, and a torsional oscillation of the NH_3 group. The final weighted R for 684 observed reflections was 0.051. There are 12 hydrogen bonds between the NH_3OH^+ ions and the ClO_4^- ions, and one hydrogen bond between NH_3OH^+ ions. The apparent r.m.s. amplitude of torsional oscillation of the NH_3–O groups about the N–O vector, as derived from the structural refinement, is ~25°, and is therefore consistent with frequent reorientation of the NH_3 parts of the NH_3OH^+ ions. Other apparent r.m.s. amplitudes in the structure are only slightly higher than normal values. The NH_3OH^+ ions are in staggered conformations and the ClO_4^- ions are essentially regular tetrahedra.

Prosen, E. J., Goldberg, R. N., Staples, B. R., Boyd, R. N., Armstrong, G. T., **Microcalorimetry applied to biochemical processes,** (Proc. U.S. Japan Joint Seminar, Akron, Ohio, April, 8-12, 1974), Paper in *Thermal Analysis: Comparative Studies on Materials,* H. Kambe and P. D. Garn, Eds., pp. 253-289 (Kodansha Ltd. and John Wiley and Sons, Tokyo and New York, 1974).

Key words: analysis; assay in serum; bacterial growth calorimetry; enzyme catalyzed processes; glucose; microcalorimetry; serum thermochemistry of enzyme processes.

A single-reaction-vessel, batch-type, conduction microcalorimeter is described, having a volume of about 0.3 ml. The sensitivity in terms of electrical output voltage per unit of heat transfer power is 60 mV · W^{-1}, the lower limit of detectable thermal power is about 0.1 μW, and the lower limit of total heat that can be measured is < 0.2 mJ. The calorimeter is calibrated electrically and by known chemical reactions such as the neutralization of HCl by NaOH in solution. The calorimeter has been applied to the measurement of enzyme catalyzed biochemical processes. On the basis of measurements made in aqueous buffer solutions, the *hexokinase* catalyzed phosphorylation of glucose has been used to assay glucose in the complex media human serum and blood plasma, with results that correlate well with customary clinical laboratory procedures. The growth of *Enterobacter cloacae, Proteus rettgeri,* and *Klebsiella pneumoniae* in the calorime-

ter under controlled conditions show characteristic energy evolution patterns. In a somewhat larger reaction cell, the fertilization and growth of *Arbacia punctulata* eggs were observed.

Rains, T. C., **Atomic absorption spectrometry—general considerations for the application of experimental techniques,** *Amer. Soc. Testing Mater. Spec. Tech. Publ.* **564,** pp. 50-66 (1974).

Key words: accuracy; atomic spectroscopy; atomic vapor; chemical analysis; evaluation; interferences; light sources; precision.

In applying atomic absorption spectrometry to an analytical problem, the analyst must have an understanding of the basic instrumental components. The essential components of an atomic absorption instrument consist of a primary source of radiation, a means of producing atomic vapor from the analyte, wavelength selection, signal detection, and readout. While several types of radiation sources are available, hollow cathode lamps are the primary choice for most workers in the field.

The production of atomic vapor of the analyte is probably the most important parameter in atomic absorption spectrometry. The selection of the oxidant-fuel or nonflame method of producing neutral atoms will depend upon the concentration of analyte and the matrices. While the analyst has a wide choice of methods at his disposal, an understanding of the problems related to the production of atomic vapor is essential to obtain the maximum precision and accuracy. Also, interferences, sample preparation, and methods for evaluation of data are discussed.

Rains, T. C., Menis, O., **Determination of aluminum by flame emission spectrometry with repetitive optical scanning,** *Anal. Lett.* **7,** No. 11, 715-727 (1974).

Key words: aluminum; flame emission spectrometry; interferences; repetitive optical scanning.

The distribution of atomic aluminum emission in the nitrous oxide-acetylene flame was investigated by means of repetitive optical scanning in the derivative mode. In this system, the difficulties encountered with this source from the CN, CH, and C_2 band systems were overcome. This technique which doesn't require a separation or preconcentration step was applied to the determination of aluminum in various types of ferrous materials. The results were compared with other classical methods. By the proposed method aluminum was also determined in a high-purity iron at the 5 μg/g level with a relative standard deviation of 10 percent.

Reader, J., **Spectrum and energy levels of singly ionized rubidium (Rb II),** *J. Opt. Soc. Amer.* **65,** No. 3, 286-301 (Mar. 1975).

Key words: rubidium; spectra; ultraviolet; wavelengths.

The spectrum of Rb II has been observed in a pulsed radio-frequency discharge with the NBS 10.7-m normal-incidence vacuum spectrograph, the NBS 10.7 m Eagle spectrograph in air, and the NBS 3.34 m plane-grating spectrograph in air. The observations cover the regions 1489-2661 Å and 4380-10 081 Å. The wavelengths of the strong resonance lines in the 530-741 Å region were accurately measured in the 3rd and 4th orders with a sliding-spark discharge. Analysis of the spectrum has provided the positions of the previously missing levels of the $4p^5$ 4*d*, 4*f*, and 6*d* configurations. The energy-level system has been extended to include the complete $4p^5$ 5*f*, 5*g*, 6*f*, and 6*g* configurations, most of the levels of the $4p^5$ 6*p*, 7*f*, 7*g*, 8*s*, and 9*s* configurations, and parts of the $4p^5$ 7*d*, 8*d*, 8*f*, 8*g*, 9*d*, and 9*f* configurations. 600 lines are classified as transitions between 165 levels. Most of the observed configurations have been theoretically interpreted. The energy parameters determined from least-squares fits to the observed levels are compared with Hartree-Fock calculations. The ionization energy, derived from the $4p^5nf\ 3/2[9/2]_5$, $n=4-7$, and $4p^5ng\ 3/2[11/2]_6$, $n=5-8$, series, is 220 105.0 ± 0.5 cm^{-1} (27.2898 ± 0.0001 eV).

Rowe, J. M., Rush, J. J., Smith, H. G., **"In-band" modes of vibration of $PdH_{0.03}$,** *Phys. Rev. B* **8,** No. 12, 6013-6014 (Dec. 15, 1973).

Key words: crystal; fermi surface; interstitial hydrogen; lattice dynamics; palladium hydride; phonons.

The [110] transverse branch of the phonon dispersion relation in a single crystal of $PdH_{0.03}$ has been measured and compared to the results for pure Pd. A limited amount of data has been taken for other branches, and the mean frequency ratio ($PdH_{0.03}$/Pd) observed for all measurements is 0.995. No change was observed in the shape or strength of the anomaly in the $[110]T_1$ branch.

Ruthberg, S., **Pressure measurements for the range 1 kPa to 100 μPa,** Chapter 4 in *Experimental Thermodynamics, Vol. II. Experimental Thermodynamics of Non-Reacting Fluids,* B. Le Neindre and B. Vodar, Eds., Part 6, pp. 229-271 (Butterworth and Co., London, England, 1975).

Key words: capacitance-diaphragm gauge; Knudsen radiometer; McLeod gauge; micromanometry; quartz Bourdon gauge; static expansion; thermal transpiration; vapor-stream pumping; viscosity gauge.

Methods of measurement and calibration are analyzed for the range 1 kPa to 100 μPa (nominally 10 torr to 10^{-6} torr). Those procedures are considered for which measurements data, uncertainty analyses, and history exist in sufficient amount to allow for a reasonable confidence in their use. Precision liquid column micromanometers of the point contact and interferometric principles are assessed. Capillarity, density, leveling, sorption and leakage, and length measurement uncertainties are derived. McLeod gauge operation and uncertainties are derived including thermal transpiration and vapor-stream pumping effects at the cold trap. Viscosity manometers of the oscillating vane and spinning disc are described. The Knudsen radiometer manometer is considered. Uncertainties are detailed for the volumetric pressure divider-static expansion calibration procedure. The precision of transfer gauges is included.

Saxena, A. N., Weisberg, L. R., Mann, W. B., Schima, F. J., **Implantation of $^{14}N^+$ into monocrystalline GaN films,** *Int. J. Appl. Radiat. Isotop. Tech. Note* **26,** 33-34 (Jan. 1975).

Key words: *p*-type GaN; Schottky barrier diode; single crystal GaN; $^{14}N^+$ implantation.

A rectifying Schottky barrier diode has been prepared in a thin film single crystal of GaN. Surface N-vacancy concentration was reduced by means of $^{14}N^+$ implantation.

Schroeder, L. W., Prince, E., Dickens, B., **Hydrogen bonding in $Ca(H_2PO_4)_2 \cdot H_2O$ as determined by neutron diffraction,** *Acta Crystallogr.* **B31,** Part 1, 9-12 (Jan. 1975).

Key words: hydrate; hydrogen bonding; monocalcium phosphate; monohydrate; neutron diffraction; phosphate; water molecule.

The hydrogen positions in $Ca(H_2PO_4)_2 \cdot H_2O$ have been determined and the structure refined to $R_w = 0.068$ and $R = 0.055$ using 1045 neutron data. No evidence is found for any disorder of the protons. The two crystallographically distinct $H_2PO_4^-$ ions are hydrogen bonded to each other and to the water molecule. The oxygen atom of the water coordinates to a calcium ion and a hydrogen atom from $H_2PO_4^-$ along its lone-pair orbital directions with distances $Ca...O_w = 2.479$ Å and $H...O_w = 1.679$ Å. One of the hydrogen atoms of the water molecule is 2.106 and 2.315 Å from two oxygen atoms, with $O_w - H...O$ angles of 110.9 and 147.5°. The distances and angles indicate that only the stronger of these two interactions is structurally significant. The other hydrogen atom of the water molecule is involved in a hydrogen bond with $H_w...O = 1.823$ Å and the angle $O_w - H...O = 160.4°$.

Sengers, J. M. H. Levelt, **Thermodynamic properties near the critical state,** Chapter 14 in *Experimental Thermodynamics, Vol.*

II. Experimental Thermodynamics of Non-Reacting Fluids, B. Le Neindre and B. Vodar, Eds., pp. 657-724 (Butterworth and Co., London, England, 1975).

Key words: critical region; dielectric constant; equation of state; homogeneity; light scattering; power laws; refractive index; scaling; Schlieren method; specific heat; speed of sound; x-ray scattering.

A review is given of experimental methods for the determination of thermodynamic properties in the critical region of gases. The typical experimental difficulties: near-instability of the system, long equilibrium times and gravity effects, are discussed. Optical and dielectric measurements for the determination of density and of density gradients, are emphasized. A survey of the potential of light and x-ray scattering experiments is given. Other topics covered are constant-volume specific heat, conventional P-V-T, coexistence curve and speed of sound determinations. The discussion of experimental methods is preceded with a summary of the present state of critical region thermodynamics; power laws, gas-liquid symmetry, homogeneity, scaling and extended scaling are discussed.

Shields, J. Q., **Measurement of four-pair admittances with two-pair bridges,** *IEEE Trans. Instrum. Meas.* **IM-23,** No. 4, 345-352 (Dec. 1974).

Key words: Ac DRRS; coaxial cable effects; coaxial star connectors; extrapolation techniques; four-pair admittances; permutation techniques; precision admittance standards; precision capacitance measurements; transformer bridges; transformer ratio measurements; two-pair admittances.

The purpose of this paper is twofold: 1) to show how extrapolation techniques can be used to obtain well-defined and versatile measuring systems; and 2) to apply such techniques to the measurement of four-pair admittances with two-pair bridges. When four-pair admittances are large, measurements with two-pair bridges have limited precision, but with reasonably small admittances, measurement precision is essentially equal to that attained with four-pair ridges.

Shine, R. A., Linsky, J. L., **Physical properties of solar chromospheric plages. II. Chromospheric plage models,** *Solar Phys.* **39,** No. 1, 49-77 (Nov. 1974).

Key words: radiative transfer; solar active regions; solar chromosphere; spectral line formation.

We propose chromospheric models of plages to explain profiles of the Ca II H, K, λ8498, λ8542, and λ8662 lines described in Paper I. These models are consistent with boundary conditions imposed by the photosphere and the Lyman continuum. We find that increasing emission in these lines is consistent with a picture of increasing temperature gradient in the low chromosphere and the resulting increase in pressure and electron density at similar line optical depths. With this picture we suggest how to empirically determine the distribution of chromospheric parameters across the solar disk directly from Ca II filtergrams. We also propose that the high density aspects of solar activity are produced by steep temperature gradients in the low chromosphere and thus by the enhanced heating mechanisms that steepen these gradients.

Sieck, L. W., Gorden, R., Jr., Lias, S. G., Ausloos, P., **Ionic polymerization of vinyl halides initiated by photoionization using photons with energies near the ionization threshold,** *Int. J. Mass Spectrom. Ion Phys.* **15,** 181-196 (1974).

Key words: ion-molecule reactions; mass spectrometry; photoionization; rate constants; reaction mechanisms; vinyl halides.

Thermal bimolecular rate coefficients have been obtained for the reactions of the parent monomer ions in the vinyl halides with the respective neutral molecules when the ions are formed by photoionization at or very near the ionization thresholds. The values obtained are as follows: $C_2H_3F^+$, 0.27 eV above threshold, $k = 3.2 \times 10^{-10}$ cm^3 molecule^{-1} s^{-1}, $C_2H_3Cl^+$, within kT of threshold, $k = 1.78 \times 10^{-10}$ cm^3 molecule^{-1} s^{-1}, and $C_2H_3Br^+$, 0.2 eV above threshold, $k = 1.25 \times 10^{-10}$ cm^3 molecule^{-1} s^{-1}. An increase in photon energy drastically lowers the values of these coefficients. The reactions of $C_2H_3F^+$ and $C_2H_3Cl^+$ were also investigated at high pressures in order to elucidate certain aspects of the cationic polymerization scheme. The formation of $(C_2H_3Cl)_2^+$ and $(C_2H_3Cl)_3^+$ is reported for the first time. The factors controlling the relative importances of various modes of dissociation of the vinyl halide dimer ions are discussed in terms of thermodynamic and structural considerations.

Sindt, C. F., **Heat transfer to slush hydrogen,** (Proc. 1973 Cryogenic Engineering Conf., Atlanta, Ga., Aug. 8-10, 1973), Paper K-3 in *Advances in Cryogenic Engineering* **19,** 427-436 (Plenum Press, New York, N.Y., 1974).

Key words: boiling heat transfer; convective heat transfer; heat transfer; liquid hydrogen; slush hydrogen.

Heat transfer to slush hydrogen was measured at one atmosphere and at triple-point pressure. The data were compared with those for heat transfer to liquid hydrogen, and to classical heat transfer correlations for nucleate boiling. The slush data fit convective heat transfer correlations quite well. In general, the data show that for a given heat flux, the temperature difference between the wall and the bulk liquid is not as highly influenced by pressure as predicted by the correlation for nucleate boiling.

Souders, T. M., **An audio-frequency four-terminal resistance bridge,** *IEEE Trans. Instrum. Meas.* **IM-23,** No. 4, 342-345 (Dec. 1974).

Key words: audio-frequency; bridge; four-terminal resistance; high current; operational amplifier; phase angle; resistance; transformer-ratio-arm.

The design and performance of an audio-frequency four-terminal resistance bridge is described which compares resistors from 1 to 0.001 Ω over a frequency range of 50 Hz-10 kHz.

Current scaling establishes equal voltage across the resistors, permitting the standard to have the larger value and most optimum design while dissipating less power than the unknown. An amplifier-aided two-stage current transformer forms the ratio arms. Ratios of 1, 2, 4, 5, 10, and 20 are available, and a maximum applied current of 200 A is accommodated. Bridge ratio errors are less than 2×10^{-6} in both magnitude and phase at frequencies up to 1 kHz, increasing to 2×10^{-5} at 10 kHz.

Simple transformer scaling techniques are described for producing accurate and stable resistance standards at the 0.001-Ω level.

Stevens, W. J., Das, G., Wahl, A. C., Krauss, M., Neumann, D., **Study of the ground state potential curve and dipole moment of OH by the method of optimized valence configurations,** *J. Chem. Phys.* **61,** No. 9, 3686-3699 (Nov. 1, 1974).

Key words: dipole moment function; dissociation energy; electronic structure; hydroxyl radical; potential curve; self-consistent-field.

Accurate theoretical potential and dipole moment curves are presented for the $X\,^2\Pi_i$ state of the hydroxyl radical. The theoretically determined dissociation energy is 4.53 eV as compared to the experimental value of 4.63 eV. The computed dipole moment at the experimental equilibrium internuclear separation is 1.674 D, which is in excellent agreement with the most reliable experimental value of 1.66 ± 0.01 D. A detailed, general prescription for constructing optimized valence configuration wavefunctions for diatomic hydrides is presented with OH as a specific example.

Stewart, S. L., **STAPLE, an experimental structured programming language,** *Comput. Languages* **1,** No. 1, 61-71 (Jan. 1975).

Key words: block structure; control flow; GOTO-less programming; language design; precompiler; quality software; structural programming.

STAPLE is a structured programming language with nested block structure in the source language to indicate flow of control. The semantics of the non-control structures are essentially the same as FORTRAN. The design goals were an easily implemented, easily modified tool for experiments and demonstrations of structured versus unstructured programming techniques.

Sullivan, D. B., Dziuba, R. F., **A low-temperature direct-current comparator bridge,** *IEEE Trans. Instrum Meas.* **IM-23,** No. 4, 256-260 (Dec. 1974).

Key words: current comparator; low temperature electrical measurement; quartum interference device; ratio transformer; resistive divider; superconductivity.

The application of superconducting direct-current comparators to the measurement of resistance ratios is described. One comparator consists of a binary set of ratios between 1:1 and 160:1 providing for self-calibration by a buildup procedure. A second comparator exhibiting discrete ratios of 1:1, 10:1, and 100:1 is also described. Ratio uncertainty of less than 1 part in 10^9 is achieved by enclosing the ratio windings in overlapping toroidal superconducting shields. Superconducting quantum interference devices (SQUID's) serve as flux sensors for the comparators. One of these current comparators is used to calibrate a 100-Ω:1-Ω resistive divider, which at a current of 10 mA exhibits a self-heating error of 0.0023 ppm.

Taggart, H. E., Nelson, R. E., Scott, W. W., Shafer, J. F., Tary, J. J., Workman, J. L., Treado, M. J., **Mobile FM transmitters,** *NILECJ-STD-0202.00,* 18 pages (U.S. Department of Justice, Law Enforcement Assistance Administration, National Institute of Law Enforcement and Criminal Justice, Washington, D.C., Oct. 1974).

Key words: communications; law enforcement; mobile transceiver; performance standard; transceiver; transmitter.

This standard for law enforcement communications transmitters specifies minimum performance requirements for mobile transmitters. Frequency ranges over which the standard applies are 25-50 MHz, 150-174 MHz, and 400-512 MHz.

Tilford, S. G., Simmons, J. D., **Reexamination of the vacuum ultraviolet emission spectrum of CO in the 950-1200 Å region,** *J. Mol. Spectrosc.* **53,** 436-442 (1974).

Key words: band assignments; carbon monoxide; electronic spectrum; emission spectrum; high resolution spectrum; vacuum ultraviolet region.

New spectrograms of CO below 1200 Å reveal that emission bands terminating on the high energy $E_0\,{}^1\Sigma^+$ and $^1\Pi$ states plus most of the previously reported unidentified emission bands of CO actually originate from molecular nitrogen. Four new emission band systems in CO, tentatively identified as $V\,{}^1\Pi - X\,{}^1\Sigma^+$, $W\,{}^1\Pi - X\,{}^1\Sigma^+$, $Y\,{}^1\Sigma^+ - X\,{}^1\Sigma^+$, and $Z\,{}^1\Sigma^+ - X\,{}^1\Sigma^+$, have been observed. The corresponding T_{v0}'s are 98917, 102804, 99963, and 105724 cm^{-1}, respectively.

Turgel, R. S., **Digital wattmeter using a sampling method,** *IEEE Trans. Instrum. Meas.* **IM-23,** No. 4, 337-341 (Dec. 1974).

Key words: analog-to-digital conversion; digital; electricity; electric power; measurement; sampling; wattmeter.

Average electric power can be measured by a system that samples voltages and currents at predetermined intervals. The sampled signals are digitized and the result is computed by numerical integration. The response of the system agrees with that of a standard electrodynamic wattmeter within 0.02 percent from dc to 1 kHz, with the possible exception of zero power factor measurements. Measurements up to 5 kHz can be made with somewhat greater uncertainties.

Utton, D. B., **Proton spin-lattice relaxation in cerous magnesium nitrate hydrate,** *J. Chem. Phys.* **62,** No. 2, 670-674 (Jan. 15, 1975).

Key words: cerous magnesium nitrate hydrate; lattice; proton; relaxation; spin; 65-335 K.

The proton spin-lattice relaxation in powdered $Ce_2Mg_3(NO_3)_{12} \cdot 24H_2O$ has been measured in the temperature range 65-335 K. In contrast to other paramagnetic salts it has been found that the nuclear relaxation due to nuclear dipole-dipole interactions is comparable in magnitude with the relaxation due to the electronic moments on the paramagnetic ions in this temperature range. Below 160 K the relaxation times are independent of the resonance frequency and have a temperature dependence given by $\tau_1 = 0.375 \exp(-182/T)$ sec. This is attributed to relaxation via the Ce^{3+} ions and hence makes it possible to calculate a value for their relaxation times. It is also concluded that the second excited doublet of the Ce^{3+} ions is at an energy of 200 ± 18 K. At higher temperatures two relaxation time minima are observed. At 14 MHz the minimum values are 71 and 69 msec at 244 and 303 K, respectively. The weak temperature dependence of the NMR second moment indicates that 180° flips of the water molecules provide the relaxation mechanism in this temperature range. Calculated values of τ_1, using the published crystallographic data, and assuming that there are two types of water molecule, are in reasonable agreement with experiment. The observed activation energies are approximately 6.8 and 9.5 kcal/mole.

Wachtman, J. B., Jr., **Highlights of progress in the science of fracture of ceramics and glass,** *J. Amer. Ceram. Soc.* **57,** No. 12, 509-519 (Dec. 12, 1974).

Key words: ceramics; fracture; fracture mechanics; glass; impact damage; strength; thermal shock; time to failure.

Rapid, catastrophic propagation of cracks is described in terms of stress concentration and energy balance conditions from a fracture-mechanics viewpoint. Slow crack propagation by stress corrosion or other mechanisms is also presented in fracture-mechanics terms. Data on slow crack propagation and accompanying acoustic emission in a variety of ceramics and glasses are reviewed. A survey is presented of the application of these results to the quantitative treatment of strength, dependence of strength on loading rate, time to failure, proof testing, acoustic emission monitoring, thermal shock, impact damage, and erosive machining. Some limitations in the application of fracture mechanics to ceramics are discussed.

Wainwright, A. E., Walls, F. L., McCaa, W. D., **Direct measurements of the inherent frequency stability of quartz crystal resonators,** *Proc. 28th Annual Symp. on Frequency Control, Fort Monmouth, N.J., May 29-31, 1974,* pp. 177-180 (Electronic Industries Association, Washington, D.C., 1974).

Key words: Allan variance; flicker of frequency modulation; Johnson noise; linewidth; random walk frequency modulation; spectral density of frequency fluctuations $S_y(f)$; white phase modulation.

A technique is presented that allows one to measure directly the fluctuations of the natural resonant frequency of quartz crystal resonators in a passive circuit. This technique greatly aids in modeling the noise in both crystal resonators and crystal controlled oscillator circuits. Definite changes of slope in the spectral density of the frequency fluctuations, as a function of frequency offset from the natural resonant frequency of the crystals indicate that several mechanisms are contributing to the frequency instabilities in crystals. Our measurements also indicate that the electronics in the oscillators seriously degrade the frequency stability for sample times

less than 100 s. The effects are especially dramatic for times less than 1 s.

Wasik, S. P., **Determination of hydrocarbons in sea water using an electrolytic stripping cell,** *J. Chromatogr. Sci.* **12,** 845-848 (Dec. 1974).

Key words: aromatic hydrocarbons; gas chromatography; hydrocarbon analysis; partition coefficient; sea water; stripping cell.

A stripping cell is described which can be used to analyze and to measure partition coefficients of hydrocarbons in sea water. Small hydrogen bubbles evolved electrolytically from a gold electrode are allowed to rise up a cylindrical cell containing a known amount of sea water. The dissolved hydrocarbons in the sea water are equilibrated with the hydrogen bubbles. The hydrocarbon concentration in the headspace is determined by gas chromatography. The partition coefficient and hydrocarbon concentration in the sea water are determined from the volume of sea water and the hydrocarbon concentration in the headspace after a given volume of hydrogen has bubbled through the cell.

Weisman, I. D., Bennett, L. H., McAlister, A. J., Watson, R. E., **$LaNi_{5-x}Pt_x$: NMR investigation of structural and electronic properties,** *Phys. Rev. B* **11,** No. 1, 82-91 (Jan. 1, 1975).

Key words: alloys; contact term; core polarization; exchange enhancement; Knight shifts; $LaNi_5$; $LaNi_{5-x}Pt_x$; $LaPt_5$; NMR; ordering; relaxation times; solid solutions.

Pt-site Knight shifts κ, relaxation times, and crystallographic data have been obtained for the $LaNi_{5-x}$ Pt_x ($0 \leq x \leq 5$) system. There are two transition-metal sites: one, *A*, in a La layer and one, *B*, between La layers; different κ's are observed for each site. The system is found to be completely miscible and NMR intensities and crystallographic results show that Pt prefers the *B* site and that considerable ordering occurs for $x \lesssim 4$. The ^{195}Pt κ's are ~ 1 percent and ~ 0 percent for the *A* and *B* sites, respectively, in $LaPt_5$; the *A*-site κ is approximately 0 at $LaNi_4Pt$ and the *B*-site κ reaches -2 percent in $LaNi_{4.75}Pt_{0.25}$. The shifts, taken together with relaxation times, indicate that *s*-band effects dominate, particularly for the *A*-site, in $LaPt_5$ and that the Pt atoms on both sites become more transition-metal-like with increasing *x*. Exchange enhancement is shown to be an essential factor at the Ni-rich end. Variations in chemical activity, as in hydride formation, are discussed in light of these electronic differences between $LaNi_5$ and $LaPt_5$.

West, E. D., Case, W. E., **Current status of NBS low-power laser energy measurement,** (Proc. 1974 Conf. on Precision Electromagnetic Measurements, London, England, July 1-5, 1974), *IEEE Trans. on Instrumentation and Measurements,* **IM-23,** No. 4, 422-425 (Institute of Electrical and Electronics Engineers, New York, N.Y., Dec. 1974).

Key words: laser calorimeter; laser energy; laser power.

A set of four electrically calibrated calorimeters is currently in use at the Boulder Laboratories of the National Bureau of Standards to calibrate and test devices for measuring average laser power in the range from 100 μW to 1 W and energies in the range 0.03 to 10 J. Laser sources used with these calorimeters are argon, krypton, helium-neon and neodymium-doped YAG, all CW, and pulsed YAG with pulse energies about 0.1 J and pulsewidths of about 200 μs and 30 ns.

The calorimeters have been intercompared as a check on systematic errors. The national standard is taken as the average for three of the calorimeters of the current C4 design, because these were designed to permit better measurements of the absorptance and window transmittance. Deviations from the group average are -0.12, -0.01, and $+0.13$ percent. The earlier standard C3-1 differs from the group average by $+0.21$ percent.

Westfall, M., Hurley, C. W., Eliason, L. K., **Metallic handcuffs,** *NILECJ-STD-0307.00,* 8 pages (U.S. Department of Justice, Law Enforcement Assistance Administration, National Institute of Law Enforcement and Criminal Justice, Washington, D.C., Oct. 1974).

Key words: ace type pin tumbler lock; cheek plate tamper resistance; salt spray corrosion resistance; warded lock.

This standard establishes minimum performance requirements and test methods for metallic handcuffs intended to be used to restrict the physical movement of apprehended persons. Specific tests are described including visual inspection, dimensional measurements, test loading of handcuffs, test loading of locking mechanism, cheek plate tamper resistance, dust and salt spray corrosion resistance.

Williams, E. R., Olsen, P. T., Field, B. F., **Standard cell calibration via current transfer,** *IEEE Trans. Instrum. Meas.* **IM-23,** No. 4, 299-302 (Dec. 1974).

Key words: gyromagnetic ratio of the proton; fine structure constant; volt transfer.

The EMF's of standard cells are now being transferred between laboratories over a 1 1/2-km cable with a precision of 4 parts in 10^8 to provide an instantaneous comparison of the $2e/h$ and γ_p' experiments being carried out at the two facilities. This is accomplished by transferring a constant current that produces a 1-V drop across standard resistors located at both ends of the cable.

Wood, L. A., **Physical constants of different rubbers,** Paper in *Polymer Handbook, 2nd Edition,* J. Brandrup and E. H. Immergut, Eds., pp. V-7—V-12 (John Wiley & Sons, Inc., New York, N.Y., 1975).

Key words: butyl rubber; constants; natural rubber; neoprene; physical constants; polymers; properties; rubbers; styrene-butadiene rubbers.

Selected values from 65 published literature references are tabulated for about 30 physical constants (mechanical, optical, thermal, etc.) for natural rubber, styrene-butadiene rubber (SBR), butyl rubber (IIR), and polychloroprene rubber (CR or neoprene). This is revision and extension of the tables published in 1966 in the first edition of the Polymer Handbook, J. Brandrup and E. H. Immergut, ed.

Wu, Y-C., **Thermodynamics of mixtures of aqueous electrolyte solutions—a viewpoint on the structure of electrolyte solutions,** (Proc. Int. Symp. on Structure of Water and Aqueous Solutions, Marburg, West Germany, July 1973), Chapter II, Section 6, in *Structure of Water and Aqueous Solutions,* W. A. P. Luck, Ed., pp. 189-206 (Verlag Chemie and Physik Verlag, Weinheim/Bergstr., Germany, 1974).

Key words: electrolyte solutions; ionic cosphere; structure of solutions; thermodynamics of mixture.

The structural effect of water on aqueous ionic solutions is best interpreted by the concept of ion-solvent cosphere overlapping, developed by Gurney and Frank. Friedman has advanced a theory which includes the overlapping effect. The success of the theory to fit experimental data for several 1-1 electrolytes up to 1 molal concentration has proven the existence of the overlapping effect.

Experimentally, one of the best methods of differentiating the ionic cosphere overlapping effect seems to be the study of mixed electrolyte solutions. The excess function of mixing, $\Delta\mu Q^E$, is a measure of the difference of the excess function of the mixture from those of the pure binary electrolyte solutions. In the common ion mixture, this difference has been shown from the same charge ion interactions. Recently, Robinson, Wood, and Reilly have derived theoretically that the same effects are specific. The specificity of the same charge ion interactions appears to rise from the cosphere overlapping effect. Gurney postulated a rule that the mean activity coefficients, based on

the order-disorder character of each ionic cosphere, go "from dissimilar character downward to similar character." The ionic cosphere overlapping effects on the thermodynamics of mixtures to parallel the same rule.

Yakowitz, H., **Electron-probe microanalysis—a capsule survey,** *J. Vac. Sci. Technol.* **11,** No. 6, 1100-1104 (Nov./Dec. 1974).

Key words: electron probe microanalyzer; microanalysis; qualitative analysis; quantitative analysis; specimen preparation; x rays.

A brief overview of the way in which electron-probe microanalysis can be used to obtain information from microvolumes comprising 10^{-12} g or less of specimen material is presented. Elemental identification, distribution, and quantitative analytical procedures are outlined. Energy-resolving detectors and wavelength-dispersive spectrometers are compared; analysis of elements with atomic number < 11 is also briefly considered in this context. An example of the solution of a service failure by means of elemental-distribution mapping is offered. Finally, an indication is given of the accuracy which can be expected from quantitative electron-probe microanalysis.

Yakowitz, H., **Role of the divergent beam (Kossel) x-ray technique in scanning electron microscopy,** (Proc. Seminar on Quantitative Scanning Electron Microscopy, London, England, Sept. 13-15, 1972), Chapter 13 in *Quantitative Scanning Electron Microscopy,* M. D. Muir, E. M. Boswarba and D. B. Holt, Eds., pp. 451-486 (Academic Press, London, England, Dec. 1974).

Key words: channelling of electrons; crystal orientation; Kossel; lattice spacing determination; microdiffraction; scanning electron microscopy; strain analysis; x ray.

The Kossel method is a divergent beam x-ray diffraction technique which requires a point source of x rays for optimum application. The scanning electron microscope provides the investigator with an almost ideal point source of x rays as well as a means for viewing the actual region irradiated.

Using Kossel patterns, one can study regions about 15 μm in size or larger. In particular, precise lattice spacing data from small crystal regions can be obtained. Furthermore, orientation information of microcrystals or crystal-line inclusions can be obtained within 1/4 to 1/2° of arc. Complete elastic stress-strain analysis of crystals can also be carried out. The method can also be combined with x-ray topographic methods to provide basic perfection data.

Methods for determining lattice spacings are critically compared. The most satisfactory general method—the regressive analysis of the conic equation (RACE) method is fully discussed. Information obtainable from the stress-strain analysis will be outlined, and the reliability limits of the computed strains is discussed using Fe-3 1/4 PCT.Si as an example. Instrumental requirements indicated by the results of the reliability analysis are described. Finally, some of the newer possibilities such as comparison with channelling pattern results are taken up.

Zobrist, D. W., Fassbender, P., Bearden, F. E., Costrell, L., **Software standards and CAMAC,** *Instrum. Technol.* **22,** No. 3, 33-38 (Mar. 1975).

Key words: CAMAC; computer systems; control systems; industrial control; software; standards.

One month prior to a meeting of the International Purdue Workshop on Industrial Computer Systems, the idea was conceived to demonstrate software transportability, using ANSI X3.9-1966 Standard FORTRAN and ISA-S61.1 external procedures for process control, and the demonstration was to point out the need and potential of standards in other areas. Two complete computer systems, including peripherals and CAMAC interfaces, and process instrumentation, were borrowed from a dozen scattered sources. The systems were hooked up and running in about two days. This article describes the demonstration project, the many obstacles encountered, and lessons learned.

U. S. GOVERNMENT PRINTING OFFICE : 1975 O - 578-011

NBS TECHNICAL PUBLICATIONS

PERIODICALS

JOURNAL OF RESEARCH reports National Bureau of Standards research and development in physics, mathematics, and chemistry. It is published in two sections, available separately:

• **Physics and Chemistry (Section A)**

Papers of interest primarily to scientists working in these fields. This section covers a broad range of physical and chemical research, with major emphasis on standards of physical measurement, fundamental constants, and properties of matter. Issued six times a year. Annual subscription: Domestic, $17.00; Foreign, $21.25.

• **Mathematical Sciences (Section B)**

Studies and compilations designed mainly for the mathematician and theoretical physicist. Topics in mathematical statistics, theory of experiment design, numerical analysis, theoretical physics and chemistry, logical design and programming of computers and computer systems. Short numerical tables. Issued quarterly. Annual subscription: Domestic, $9.00; Foreign, $11.25.

DIMENSIONS/NBS (formerly Technical News Bulletin)—This monthly magazine is published to inform scientists, engineers, businessmen, industry, teachers, students, and consumers of the latest advances in science and technology, with primary emphasis on the work at NBS. The magazine highlights and reviews such issues as energy research, fire protection, building technology, metric conversion, pollution abatement, health and safety, and consumer product performance. In addition, it reports the results of Bureau programs in measurement standards and techniques, properties of matter and materials, engineering standards and services, instrumentation, and automatic data processing.

Annual subscription: Domestic, $9.45; Foreign, $11.85.

NONPERIODICALS

Monographs—Major contributions to the technical literature on various subjects related to the Bureau's scientific and technical activities.

Handbooks—Recommended codes of engineering and industrial practice (including safety codes) developed in cooperation with interested industries, professional organizations, and regulatory bodies.

Special Publications—Include proceedings of conferences sponsored by NBS, NBS annual reports, and other special publications appropriate to this grouping such as wall charts, pocket cards, and bibliographies.

Applied Mathematics Series—Mathematical tables, manuals, and studies of special interest to physicists, engineers, chemists, biologists, mathematicians, computer programmers, and others engaged in scientific and technical work.

National Standard Reference Data Series—Provides quantitative data on the physical and chemical properties of materials, compiled from the world's literature and critically evaluated. Developed under a world-wide program coordinated by NBS. Program under authority of National Standard Data Act (Public Law 90-396).

NOTE: At present the principal publication outlet for these data is the Journal of Physical and Chemical Reference Data (JPCRD) published quarterly for NBS by the American Chemical Society (ACS) and the American Institute of Physics (AIP). Subscriptions, reprints, and supplements available from ACS, 1155 Sixteenth St. N. W., Wash. D. C. 20056.

Building Science Series—Disseminates technical information developed at the Bureau on building materials, components, systems, and whole structures. The series presents research results, test methods, and performance criteria related to the structural and environmental functions and the durability and safety characteristics of building elements and systems.

Technical Notes—Studies or reports which are complete in themselves but restrictive in their treatment of a subject. Analogous to monographs but not so comprehensive in scope or definitive in treatment of the subject area. Often serve as a vehicle for final reports of work performed at NBS under the sponsorship of other government agencies.

Voluntary Product Standards—Developed under procedures published by the Department of Commerce in Part 10, Title 15, of the Code of Federal Regulations. The purpose of the standards is to establish nationally recognized requirements for products, and to provide all concerned interests with a basis for common understanding of the characteristics of the products. NBS administers this program as a supplement to the activities of the private sector standardizing organizations.

Federal Information Processing Standards Publications (FIPS PUBS)—Publications in this series collectively constitute the Federal Information Processing Standards Register. Register serves as the official source of information in the Federal Government regarding standards issued by NBS pursuant to the Federal Property and Administrative Services Act of 1949 as amended, Public Law 89-306 (79 Stat. 1127), and as implemented by Executive Order 11717 (38 FR 12315, dated May 11, 1973) and Part 6 of Title 15 CFR (Code of Federal Regulations).

Consumer Information Series—Practical information, based on NBS research and experience, covering areas of interest to the consumer. Easily understandable language and illustrations provide useful background knowledge for shopping in today's technological marketplace.

NBS Interagency Reports (NBSIR)—A special series of interim or final reports on work performed by NBS for outside sponsors (both government and non-government). In general, initial distribution is handled by the sponsor; public distribution is by the National Technical Information Service (Springfield, Va. 22161) in paper copy or microfiche form.

Order NBS publications (except NBSIR's and Bibliographic Subscription Services) from: Superintendent of Documents, Government Printing Office, Washington, D.C. 20402.

BIBLIOGRAPHIC SUBSCRIPTION SERVICES

The following current-awareness and literature-survey bibliographies are issued periodically by the Bureau:

Cryogenic Data Center Current Awareness Service

A literature survey issued biweekly. Annual subscription: Domestic, $20.00; foreign, $25.00.

Liquefied Natural Gas. A literature survey issued quarterly. Annual subscription: $20.00.

Superconducting Devices and Materials. A literature survey issued quarterly. Annual subscription: $20.00. Send subscription orders and remittances for the preceding bibliographic services to National Technical Information Service, Springfield, Va. 22161.

Electromagnetic Metrology Current Awareness Service Issued monthly. Annual subscription: $100.00 (Special rates for multi-subscriptions). Send subscription order and remittance to Electromagnetics Division, National Bureau of Standards, Boulder, Colo. 80302.

U.S. DEPARTMENT OF COMMERCE
National Bureau of Standards
Washington, D.C. 20234

OFFICIAL BUSINESS
Penalty for Private Use, $300

POSTAGE AND FEES PAID
U.S. DEPARTMENT OF COMMERCE
COM-215

SPECIAL FOURTH-CLASS RATE
BOOK

JOURNAL OF RESEARCH of the National Bureau of Standards
A. Physics and Chemistry

Vol. 79A, No. 4 July–Aug. 1975

Page

Contents

Radiance temperature (at 653 nm) of iron at its melting point. A. Cezairliyan and J. L. McClure. 541

Precision measurements of the dimensional stability of four mirror materials. B. Justice. 545

A correlation for the second interaction virial coefficients and enhancement factors for moist air. R. W. Hyland. 551

The enthalpies of combustion and formation of thianthrene. W. H. Johnson. 561

Unbound water content from application of adsorption theory. William V. Loebenstein. 565

Publications of the National Bureau of Standards. 577

SJRA UNIVE300UA R
UNIVERSITY MICROFILMS INC
ATTN SERIALS SECTION
300 NORTH ZEEB RD
ANN ARBOR MI 48106

Library of Congress Catalog Card Number: 62-37059

For sale by the Superintendent of Documents, U.S. Government Printing Office, Washington, D.C. 20402. (Order by SD Catalog No. C13.22/sec.A:79/(4). Single copy price varies. Subscription price: $17.00 a year; $4.25 additional for foreign mailing.

UNITED STATES GOVERNMENT PRINTING OFFICE, WASHINGTON : 1975